

**Switchable biological ligand systems: investigation of adhesion
and inhibition by multivalent polymer materials**

Inaugural-Dissertation

to obtain the academic degree

Doctor rerum naturalium (Dr. rer. Nat)

of the Faculty of Mathematics and Natural Sciences

at the Heinrich-Heine-University Düsseldorf

submitted by

Dimitri Wilms

from Nowosibirsk

Düsseldorf, den 03.05.2022

From the Institute of Organic Chemistry and Macromolecular Chemistry at the
Heinrich-Heine-University Düsseldorf

Published by permission of the
Faculty of Mathematics and Natural Sciences at
Heinrich-Heine-University Düsseldorf

Supervisor: Jun. Prof. Dr. Stephan Schmidt

Co-supervisor: Prof. Dr. Matthias Karg

Date of oral examination: 09.08.2022

The work presented in this thesis was accomplished in a period between August 2018 and February 2022 at the Chair of Macromolecular Chemistry at the Institute of Organic Chemistry and Macromolecular Chemistry at the Heinrich-Heine-University Düsseldorf under the supervision of Jun. Prof. Dr. Stephan Schmidt.

Declaration of authorship

I hereby declare that the thesis submitted is my own work without making use of impermissible aids, considering the “Rules on the Principles for Safeguarding Good Scientific Practice at the Heinrich-Heine-University Düsseldorf”. All direct or indirect sources are acknowledged in the bibliography as references. I further declare that I have not submitted this nor a similar thesis at any other examination board in order to obtain a degree.

Düsseldorf, 03.05.2022

(Dimitri Wilms)

„Don't become a mere recorder of facts, but try to penetrate the mystery of their origin.”

- Ivan Pavlov

Table of contents

Abstract	III
Zusammenfassung	V
List of Publications	VIII
Peer reviewed publications included in this thesis	VIII
Peer reviewed publications not included in this thesis	VIII
Oral and poster presentations	X
1. General Introduction	1
1.1. Lectins	2
1.2. Lectin-carbohydrate interactions	2
1.3. Plant lectins	4
1.3.1. Concanavalin A	5
1.4. Lectins in microorganisms	6
1.4.1. Escherichia coli	7
1.5. Anti-adhesion therapy	7
1.6. Synthetic approaches toward mimicking multivalent cellular glycan structures and anti-adhesin drugs	9
1.7. Microgels	12
1.7.1. Synthesis	12
1.7.2. Microgels from <i>N</i> -isopropylacrylamide	16
1.7.3. Microgels from oligo(ethylene glycol methacrylate)	16
1.8. Methods	17
1.8.1. Atomic Force Microscopy	17
1.8.2. Force-distance mode	17
1.8.3. Scanning mode	17
1.8.4. Optical microscopy	18
1.8.5. Stochastic Optical Reconstruction Microscopy (dSTORM)	19
1.8.6. Dynamic Light Scattering (DLS)	20
2. Aims and Outline	22
3. Conclusion and Perspectives	25
4. Publications	27
4.1. Switchable Adhesion of <i>E. coli</i> to Thermosensitive Carbohydrate-Presenting Microgel Layers: A Single-Cell Force Spectroscopy Study	27
4.2. Elastic modulus distribution in poly(<i>N</i> -isopropylacrylamide) and oligo(ethylene glycol methacrylate)-based microgels studied by AFM	51

4.3. Specific binding of ligand-functionalized thermoresponsive microgels: Effect of microgel architecture, ligand density, and ligand hydrophobicity	63
6. Citations	91
7. List of abbreviations	101
8. Acknowledgements	103

Abstract

The adhesion of cells and microorganisms fundamentally depends on carbohydrate-receptor interactions. Examples where such bonds play a major role are cell-cell communications, fertilization or infections by pathogenic bacteria. The focus of this work is the study of such interactions in a controlled manner to support development of future compounds which might have antiadhesive and antibiotic effects. To mimic the composition of biological membranes, a fitting scaffold must be chosen to allow adjustments in multivalency, physical and chemical behavior. In this work, microgels are used as they have proven to have a great versatility and tunability. Synthesized from smart polymeric materials, the colloids are combined with carbohydrates or proteins as common biological motifs. The resulting responsive and bio-conjugated microgels represent a great tool for investigation of ligand-receptor interaction with an additional possibility for external control. Synthesis, functionalization and deposition, is straightforward and adjustments of physicochemical properties can be made in order to obtain all necessary functions allowing for easy remote control through changes in temperature or pH of the solvent. Additionally, the physical properties of microgel particles are very close to many biological gel-like equivalents in terms of high water content and softness, qualifying the system for biomimetic application. As interactions between cells or microorganisms are a complex overlay of several processes, it is challenging to perform *in-vivo* studies with microorganisms. Therefore, the extensive control of functionalization, size, stiffness and responsivity opens up a possible way to mimic and study biological interactions on a cellular level and transfer the results to industrial or medicinal applications.

This work aims to investigate how carbohydrate ligands interact with lectins and how non-specific interactions and properties of the scaffold can influence binding. First, the adhesion of *E. coli* to a mannose functionalized microgel monolayer is quantified via single-cell force spectroscopy (SCFS). The aim of this work is to investigate the ability of carbohydrate-presenting responsive microgels to bind specific bacteria controlled by a remote trigger. In this case, the trigger is a temperature change above or below the microgels volume phase transition temperature (VPTT) where the scaffold polymer undergoes a change in solubility from hydrophilic to hydrophobic. This results in collapse or swelling of the microgels and a drastic change in volume and surface area. This process is used to change the mannose density as the ligands are distributed further apart in the swollen state and close together in the collapsed state, changing the avidity and specific binding strength of the mannose units. For the measurements, a single *E. coli* bacteria was attached to a glass bead on the tip of a AFM cantilever. The fixation

of the bacteria was done via poly-dopamine, a non-invasive wet adhesive, to ensure viability over the course of the experiments. The immobilized *E. coli* is pressed against a monolayer of mannose functionalized poly(*N*-isopropylacrylamide) (pNIPAM) and poly(OEGMA-co-MEO₂MA) (pOEGMA) microgels, which are deposited on a hard surface via drop-casting. Upon retraction adhesion specific values, such as adhesion force, work of adhesion and retraction distance for separation can be obtained.

Throughout the experiments, microgels with different compositions regarding monomer and crosslinker showed great variability in potential for switchable binding, therefore in the next article the structural properties of this type of microgels were investigated. It is well known that crosslinker amount and type changes elastic properties of microgels, which in turn affect adhesion of cells and organisms. To characterize our microgel systems in greater detail, we implemented high resolution force mapping in solution. Reducing the crosslinker content leads to decreased stiffness, and an increased swelling degree and thus a higher impact on adhesion upon volume phase transition. Therefore, we studied the spatial elastic modulus distribution of pNIPAM and pOEGMA microgels in presence and absence of bifunctional crosslinker. The microgels were deposited on glass and immersed in water prior to recording high resolution maps at 25 °C. The distribution of polymer of a single microgel as well as the elastic modulus are important factors for the microgel's ability to bind and release pathogens.

The final part focuses on binding studies of *E. coli* bacteria by ultra-low crosslinked carbohydrate presenting microgels in solution with the aim of gentle capture and release controlled by a temperature switch. Such catch and release devices could be useful for detecting and cultivating certain sugar-binding cells, such as cancer cells. Here the *E. coli* was used as a well-controlled model system for testing the capture and release of sugar-binding cell. Microgels synthesized in absence of bifunctional crosslinker show the lowest elastic modulus, a relatively smooth surface structure at room temperature and in sum the greatest potential for controlled capture and release of mannose binding bacteria. So for the experiments, *E. coli* bacteria are mixed with either mannose bearing ultra-low crosslinked p(NIPAM) or p(OEGMA) microgels and incubated at 37 °C. After the formation of visible clusters, the solution is cooled down back to room temperature unit cluster dissolution is completed. Additionally, cluster formation and dissolution are tracked with optical microscopy throughout heating and cooling. Overall, this work showed how to construct microgels for the efficient capture and release of sugar binding cells.

Zusammenfassung

Die Adhäsion von Zellen und Mikroorganismen hängt grundlegend von Kohlenhydrat-Rezeptor-Wechselwirkungen ab. Beispiele, bei denen solche Bindungen eine wichtige Rolle spielen, sind die Zell-Zell-Kommunikation, die Befruchtung einer Eizelle durch ein Spermium oder Infektionen durch Pathogene, wie Bakterien oder Viren. Der Schwerpunkt dieser Arbeit liegt auf der Untersuchung solcher Wechselwirkungen unter kontrollierten Bedingungen, um die Entwicklung künftiger Verbindungen zu unterstützen, die antiadhäsive und antibiotische Wirkungen haben könnten. Um die Zusammensetzung biologischer Oberflächen zu imitieren, muss ein geeignetes Gerüst gewählt werden, welches Anpassungen in Bezug auf Multivalenz, physikalisches und chemisches Verhalten ermöglicht. In dieser Arbeit werden Mikrogele verwendet, da sie sich als sehr vielseitig einsetzbar erwiesen haben. Die aus intelligenten polymeren Materialien synthetisierten Kolloide werden mit Kohlenhydraten oder Proteinen als gängigen biologischen Motiven kombiniert. Die daraus resultierenden schaltbaren und bio-konjugierten Mikrogele sind ein hervorragendes Instrument zur Untersuchung der Ligand-Rezeptor-Wechselwirkungen mit der zusätzlichen Möglichkeit zur externen Schaltbarkeit. Die Synthese, Funktionalisierung und Immobilisierung ist einfach und die physikochemischen Eigenschaften können angepasst werden, um alle Anforderungen zu erfüllen, und ermöglichen eine einfache Fernsteuerung durch Änderung der Temperatur oder des pH-Werts des Lösungsmittels. Darüber hinaus kommen die physikalischen Eigenschaften der Mikrogelpartikel vielen biologischen Gel-ähnlichen Äquivalenten sehr nahe, was den hohen Wassergehalt und die Elastizität betrifft, was das System für biomimetische Anwendungen qualifiziert. Da die Interaktionen zwischen Zellen oder Mikroorganismen eine komplexe Überlagerung mehrerer Prozesse darstellen, ist es eine Herausforderung, in-vivo-Studien mit Mikroorganismen durchzuführen. Daher eröffnet die umfassende Kontrolle von Funktionalisierung, Größe, Elastizität und Schaltbarkeit eine Möglichkeit, biologische Interaktionen auf zellulärer Ebene nachzuahmen und zu untersuchen und die Ergebnisse auf industrielle oder medizinische Anwendungen zu übertragen.

In dieser Arbeit soll untersucht werden, wie Kohlenhydratliganden mit Lektinen interagieren und wie unspezifische Wechselwirkungen und Eigenschaften des Gerüsts die Bindung beeinflussen können. Zunächst wird die Adhäsion von *E. coli* an eine mit Mannose funktionalisierte Mikrogel-Monolage mittels Einzelzell-Kraftspektroskopie (SCFS) quantifiziert. Ziel dieser Arbeit ist es, die Fähigkeit von kohlenhydratpräsentierenden schaltbaren Mikrogelen zu untersuchen, spezifische Bakterien zu binden, die durch einen

„Stimulus“ gesteuert werden. In diesem Fall ist der Stimulus eine Temperaturänderung, da bei Verändern der Temperatur oberhalb oder unterhalb der Volumen-Phasen-Übergangstemperatur (VPTT) des Mikrogels das Polymer seine Löslichkeit von hydrophil zu hydrophob und umgekehrt ändert. Dies führt zum Kollabieren oder Anschwellen der Partikel, was mit einer drastischen Veränderung von Volumen und Oberfläche einhergeht. Dieser Prozess wird genutzt, um die Mannosedichte zu steuern, da die Liganden im gequollenen Zustand weiter auseinander und im kollabierten Zustand eng beieinander liegen, was die Avidität und die spezifische Bindungsstärke der Mannoseliganden verändert. Für die Messungen wurde ein einzelnes *E. coli* Bakterium an eine Glaskugel an der Spitze eines AFM-Cantilevers angebracht. Die Fixierung des Bakteriums erfolgte mit Poly-Dopamin, einem nicht-invasiven Adhäsiv, um die Lebensfähigkeit während der Experimente zu gewährleisten. Die immobilisierten *E. coli* werden gegen eine Monoschicht aus mit Mannose funktionalisiertem poly(*N*-Isopropylacrylamid) (pNIPAM) und poly(OEGMA-co-MEO₂MA) (pOEGMA) Mikrogelen gepresst, die im „drop-casting“ Verfahren auf eine harte Oberfläche aufgebracht werden. Bei Retraktion des Bakteriums lassen sich mehrere adhäsionsspezifische Werte wie Adhäsionskraft, -energie und -arbeit sowie die maximale Distanz bis zur vollständigen Ablösung ermitteln.

Bei den Experimenten zeigten Mikrogele mit unterschiedlichen Zusammensetzungen in Bezug auf Monomer und Vernetzer eine große Variabilität in Bezug auf das Potenzial für eine schaltbare Bindung, weshalb im nächsten Artikel die strukturellen Eigenschaften dieser Art von Mikrogelen untersucht wurden. Es ist bekannt, dass Menge und Art des Vernetzers die elastischen Eigenschaften von Mikrogelen verändern, was wiederum die Adhäsion von Zellen und Organismen beeinflusst. Um die Mikrogelsysteme genauer zu charakterisieren, wurde ein hochauflösendes AFM Force Mapping in Lösung durchgeführt. Eine Verringerung des Vernetzergehalts führt zu einer geringeren Steifigkeit und einem höheren Quellungsgrad und damit zu einer stärkeren Auswirkung auf die Adhäsion beim Volumenphasenübergang. Daher untersuchten wir die räumliche Verteilung des Elastizitätsmoduls von pNIPAM- und pOEGMA-Mikrogelen in Gegenwart und Abwesenheit von bifunktionellem Vernetzer. Die Mikrogele wurden auf Glas immobilisiert und in Wasser getaucht, bevor hochauflösende Kraftkurvenraster bei 25 °C aufgenommen wurden. Die Verteilung des Polymers in einem einzelnen Mikrogele sowie der Elastizitätsmodul sind wichtige Faktoren für die Fähigkeit der Mikrogele, Krankheitserreger zu binden und freizusetzen.

Der letzte Teil konzentriert sich auf die Untersuchung der Bindung von *E. coli*-Bakterien durch ultraniedrig vernetzte, kohlenhydratpräsentierende Mikrogele in Lösung mit dem Ziel eines

schonenden, durch eine Temperaturänderung gesteuerten Einfangen und einer Freisetzung. Solche Einfang- und Freisetzungsanwendungen könnten für den Nachweis und die Kultivierung bestimmter zuckerbindender Zellen, wie z. B. Krebszellen, genutzt werden. Hier wurde *E. coli* als kontrollierbares Modellsystem verwendet, um das Einfangen und Freisetzen von zuckerbindenden Zellen zu testen. Mikrogele, die ohne bifunktionellen Vernetzer synthetisiert wurden, zeigen das niedrigste Elastizitätsmodul, eine relativ glatte Oberflächenstruktur bei Raumtemperatur und insgesamt das größte Potenzial für das kontrollierte Einfangen und Freisetzen von Mannose bindenden Bakterien. Für die Experimente werden daher *E. coli*-Bakterien entweder mit Mannose funktionalisierten, ultraniedrig vernetzten p(NIPAM)- oder p(OEGMA)-Mikrogelen gemischt und bei 37 °C inkubiert. Nachdem sich sichtbare Cluster gebildet haben, wird die Lösung auf Raumtemperatur abgekühlt, bis die Auflösung der Cluster abgeschlossen ist. Zusätzlich wird die Bildung und Auflösung von Clustern während des Erhitzens und Abkühlens mit dem Lichtmikroskop verfolgt.

List of Publications

Peer reviewed publications included in this thesis

Switchable Adhesion of *E. coli* to Thermosensitive Carbohydrate-Presenting Microgel Layers: a Single-Cell Force Spectroscopy Study

D. Wilms, F. Schröer, T. J. Paul and S. Schmidt

Langmuir **2020**, 36, 12555-12562

Elastic modulus distribution in poly(N-isopropylacrylamide) and oligo(ethylene glycol methacrylate)-based microgels studied by AFM

D. Wilms, Y. Adler, F. Schröer, L. Bunnemann and S. Schmidt

Soft Matter, **2021**, 17, 5711

Specific binding of ligand-functionalized thermoresponsive microgels: Effect of microgel architecture, ligand density, and ligand hydrophobicity

D. Wilms, A. Urach, F. Schröer, S. Schmidt

Manuscript to be submitted for peer review

Peer reviewed publications not included in this thesis

The effect of PEGylation on receptor anchoring and steric shielding at interfaces: an adhesion and surface plasmon resonance study with precision polymers

F. Jacobi, D. Wilms, T. Seiler, T. Queckbörner, M. Tabatabai, L. Hartmann and S. Schmidt

Biomacromolecules, **2020**, 21 (12), 4850-4856

Biomimetic estrogen sensor based on soft colloidal probes

D. Rettke, F. Seufert, J. Döring, K. Ostermann, D. Wilms, S. Schmidt and T. Pompe

Biosensors and Bioelectronics, **2021**, 192, 113506

Synthesis and Self-assembly of Amphiphilic Precision Glycomacromolecules

VIII

A. Banger, J. Sindram, M. Otten, J. Kania, D. Wilms, A. K. Strzelczyk, S. Miletic, T. C. Marlovits, M. Karg and L. Hartmann

Polymer Chemistry, **2021**, 12, 4795-4802

Selective Adhesion and Switchable Release of Breast Cancer Cells via Hyaluronic Acid Functionalized Dual Stimuli-Responsive Microgel Films

M. Schmidt, A. Franken, D. Wilms, T. Fehm, H. J. Neubauer and S. Schmidt

ACS Applied Bio Materials, **2021**, 4, 8, 6371-6380

Lectin and *E. coli* binding to carbohydrate functionalized poly(oligo(ethylene glycol))-based microgels: Effect of elastic modulus, crosslinker and carbohydrate density

F. Schröer, T. J. Paul, D. Wilms, T. H. Saatkamp, N. Jäck, J. Müller, A. K. Strzelczyk and S. Schmidt

Molecules, **2021**, 26(2):263

Oral and poster presentations

Study of bacterial adhesion inhibition by multivalent polymeric compounds via single cell force spectroscopy and optical microscopy

D. Wilms, T. J. Paul and S. Schmidt

15th Zsigmondy Colloquium of the German Colloid Society, **2019**

Adhesion of Mannose Binding Bacteria to Soft Functionalized Microgel Layers in a Single Cell Force Spectroscopy Study

D. Wilms, T. J. Paul, A. K. Strzelczyk, F. Schröer and S. Schmidt

16th Zsigmondy Colloquium of the German Colloid Society, **2020**

Temperature switchable adhesion of *E. coli* to Mannose functionalized microgel layers

D. Wilms, F. Schröer, T. J: Paul, A. K. Strzelczyk and S. Schmidt

ACS Spring, **2021**

Temperature Switchable Adhesion of *E. coli* to Mannose Functionalized Microgel Layers

D. Wilms, F. Schröer, T. J: Paul, A. K. Strzelczyk and S. Schmidt

Virtual Symposium on Microgels, **2021**

1. General Introduction

On the cellular level adhesion is controlled by ligand-receptor binding. This interaction is largely mediated by surface-exposed carbohydrates which are targeted by specifically carbohydrate binding proteins, *e.g.* lectins. Several processes such as cell-cell communication, fertilization or infection by pathogens rely on such specific binding to occur to take place. The most important carbohydrate presenting entity on the cellular scale is the glycocalyx, located on the outside of all eucaryotic cells. As the glycocalyx is the gateway for the above listed biological processes the variety and structural complexity of carbohydrates on the glycocalyx is great. The lectin-carbohydrate bond is considered relatively weak compared to covalent or electrostatic interactions, this is countered by multivalent binding.

By combining a large number of individually weak binding events, the overall adhesion is increased. Additionally, the statistical probability of re-binding occurring is maximized as dissociated moieties are kept in proximity to the lectin by its neighbors. This statistical rebinding is one of four effects occurring in multivalent presentation of ligands and receptors the others being the clustering and chelate effects as well as sterical repulsion.

A well-known and typical example of a lectin is concanavalin A (ConA), which presents several binding sites in its tetramer state enabling the chelate effect to apply. If more than one ligand is presented to such a lectin any subsequent binding event is favored due to entropic reasons. The natural prerequisite is the possibility for each ligand to reach the corresponding binding site, through an appropriate architecture of the scaffold.

If the ligands are presented in a way to allow binding to several receptor bearing subunits, it may result in a clustering effect. The accumulation of bridging ligands leads to a stabilization of such clusters, which in turn can lead to larger agglomerates. These are then stable enough to be isolated by sedimentation or filtration in the bound state.

In the previous cases, the architecture of the scaffold accommodates availability of the ligand to the receptor. The architecture has an additional influence on the binding efficiency as the backbone can shield the binding site from competing ligands or enable a matching geometry for chelate-like binding.

1.1. Lectins

The term "lectin" was introduced in 1954 by Boyd and Shapeleigh, who derived it from the Latin "*legere*", to select. At that time, it referred to a heterogeneous group of proteins and glycoproteins, mainly of plant origin, which have the property of clumping erythrocytes (hem agglutination). However, lectins were the subject of scientific studies long before. For example, the hem agglutinating property of various snake venoms was described as early as 1860. In 1888, Hermann Stillmark succeeded in isolating the lectin ricin for the first time from the seeds of *Ricinus communis*. In 1950, it was shown that lectin-mediated erythrocyte agglutination was based on multivalent binding of surface-exposed sugars or glycoconjugates, *e.g.* glycoproteins, glycolipids, and other carbohydrate structures. It was also at this time that the first bacterial lectins were discovered that mediated carbohydrate-specific adhesion of bacteria to surface-exposed glycoconjugates of host cells and were localized to the pili and fimbriae¹⁻³. Because of the presumed close relationship between lectins and antibodies, the science of lectins initially developed as part of immunology⁴. Later, lectins were defined as carbohydrate-binding proteins and glycoproteins of no immunogenic origin that agglutinate cells and/or precipitate glycoconjugates to distinguish them from antibodies^{5, 6}. However, because this interpretation required the presence of at least two sugar-binding sites per molecule⁷ and because agglutinating or precipitating activity was considered rather insignificant *in vivo*^{8, 9}, lectins were redefined a little later by Barondes¹⁰ as carbohydrate-binding proteins to distinguish them from antibodies and enzymes.

1.2. Lectin-carbohydrate interactions

Cooperative hydrogen bonds form the basis for the interaction between sugars and lectins. Here, the sp³-hybridized oxygen atoms of the hydroxyl groups of the sugar are simultaneously acceptor of two and donor of one H-bridge each. The side chains of mostly acidic amino acids act as H-bridge acceptors, while the amino groups of the main chains of various amino acids and of the side chains of asparagine and, more rarely, glutamine act as donors. The oxygen atom of the sugar ring is also sp³ hybridized and can act as an acceptor in H-bridges with its two free electron pairs, but not in cooperative bonds. Furthermore, the positions of a sugar molecule forming H-bridges with the binding site of the lectin are responsible for the specific recognition process and for distinguishing the different sugars.

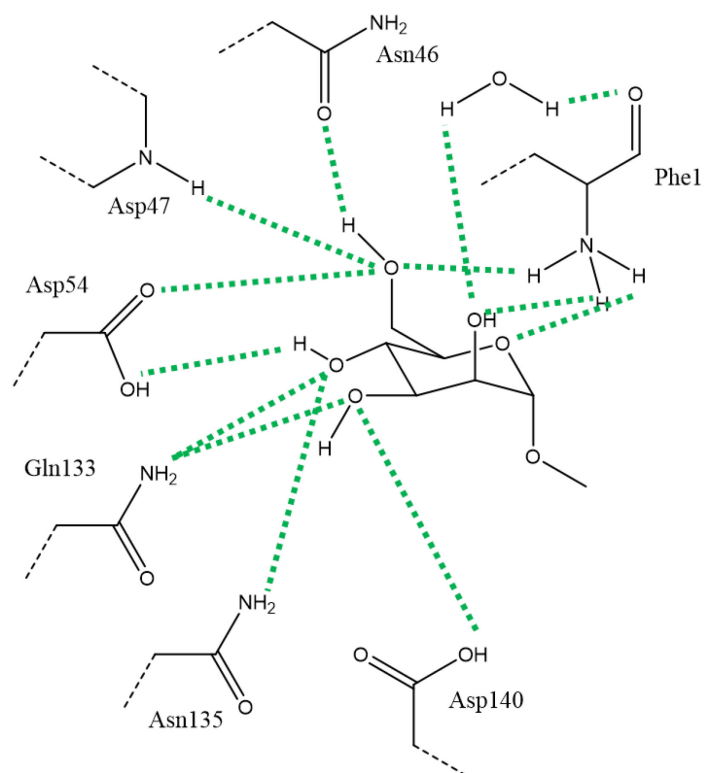


Figure 1: Schematic illustration of FimH and mannose as an example of lectin-carbohydrate binding event.

In contrast, the positions that are not involved in the recognition process are often in contact with the solvent. Concanavalin A, pea lectin, and a lectin from *Lathyrus ochrus* bind mannose and glucose by forming specific H-bridges with the 3-, 4-, and 6-hydroxyl groups of the sugars, while the 2-hydroxyl group that distinguishes the two monosaccharides from each other remains uninvolved¹¹⁻¹³. In contrast, the 2-hydroxyl group is part of the lectin-sugar interaction of snowdrop lectin (*Galanthus nivalis*), which binds mannose exclusively¹⁴. Some of the H-bridges in lectin-carbohydrate complexes are directly mediated by water molecules, while others play a supporting role in the recognition process. For example, three water molecules are involved in the binding of galactose by the enterotoxin of *Escherichia coli* and by *cholera toxin* (CT)^{15, 16}. Divalent cations are involved in many lectin-sugar interactions in direct and indirect forms. For example, the binding pockets of many legume lectins contain Ca^{2+} and Mn^{2+} ions that stabilize the binding pocket by coordinating certain amino acids (indirect form). Direct interactions between cations and the bound sugars are observed, for example, in animal C-type lectins. There, Ca^{2+} ions are involved in direct coordinative bonds between the lectin and the ligand¹⁷⁻¹⁹. Non-polar interactions are also found in lectin-carbohydrate complexes. Aliphatic protons and the carbon atoms of the epimeric centers of the sugars, together with the exocyclic carbon, form a non-polar surface that in many structures is directed against the residue of an

aromatic amino acid. Thus, in all known lectin-galactose complexes, the non-polar surface is directed against the side chain of a tryptophan or a phenylalanine²⁰. While monosaccharides are bound by lectins with relatively low dissociation constants between 0.1 and 1 mM compared to the Quioco's group I carbohydrate-binding proteins, a constant in the micro molar range is often reached when branched carbohydrates are bound. This increase in affinity is due to the presence of a secondary binding site, usually located in proximity to the primary binding site and then referred to as an extended site²¹. While the terminal sugar of a complex carbohydrate is bound by the primary binding site, the secondary binding site binds a branched sugar. Since in many cases the lectin has significant affinity only for the terminal sugar as a monosaccharide, this is referred to as the primary determinant²². This mechanism for increasing affinity is referred to as sub-site multivalence. A further increase of the dissociation constant up to the nano molar range is achieved by the so-called subunit multivalence, which results from the binding of branched sugars at a second binding site that is spatially and thermodynamically distinct from the primary one²³. In this context, the secondary binding site may be located on the same protomer or on a second subunit of an oligomer. The presence of multiple, independent binding sites can further increase affinity²⁴. Most times, an increase in affinity is achieved by the accumulation of multiple identical binding domains. For some lectins, such as CT or the mammalian mannose-binding protein, this mechanism is also used for binding to membrane receptors and flat surface recognition²⁰.

1.3. Plant lectins

Of the lectins known today, plant lectins are the best studied. In plants, lectins have been detected in various organs and tissues of a variety of species. The physiological functions of plant lectins are very diverse²⁵. The mostly secreted proteins are involved in germination, among other functions. Proteins with this function include the well-studied lectins ConA, soybean agglutinin, pea lectin (*Vicia faba*), and flavin. These are synthesized during seed development along with the abundant storage proteins. During germination, both lectins and storage proteins are degraded and thus serve to supply the embryo with the required amino acids²⁶. However, it is unclear whether the lectins serve merely as a source of amino acids or whether they are more involved in the spatial organization of the often glycosylated storage proteins. Plant lectins also appear to play a role in initiating and maintaining symbiosis between rhizobia and legumes by causing immobilization of bacteria through agglutination^{27, 28}. In addition, lectins in some plants serve as protection against pests²⁹. For example, the toxicity of

beans (*Phaseolus vulgaris*) eaten raw to mammals^{29,30} and birds³¹ has long been known. The heat-labile phytohemagglutinin (PHA) contained in the vacuoles of beans binds to receptors of the intestinal epithelium of rats and causes lesions and abnormal development of microvilli, significantly impairing nutrient absorption³². The seeds of many gramineae contain the so-called chitin-binding lectins, such as wheat germ agglutinin (WGA), which have specificity for *N*-acetylglucosamine³³. WGA inhibits, among other things, the development of the plant pathogenic larva of the weevil³⁴. The galactose-specific lectin of mistletoe *Viscum album* is used in adjuvant cancer therapy due to its immunoactive effect³⁵.

1.3.1. Concanavalin A

Concanavalin A is a widely used, well-studied model lectin extracted from the jack bean. Its properties include carbohydrate binding, specifically mannose. It consists of subunits with the molecular weight of 25 kDa which form dimers of tetramers depending on the pH value of the solution. Each subunit presents a carbohydrate binding pocket adding up to a maximum of four neighboring binding sites in a tetrameric conformation.³⁶ To enable binding, divalent cations need to be present. Therefore, all interaction assays involving ConA in the lab employ the specific lectin binding buffer (LBB) contains Ca^{2+} and Mn^{2+} . The cations stabilize the local conformation of the subunits and additionally coordinate bonds between the protein and hydroxyl groups of the sugar³⁷.

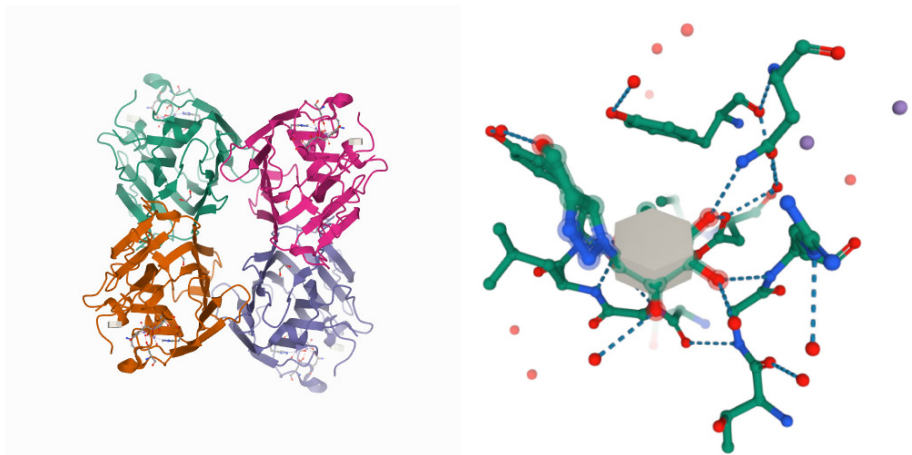


Figure 2: Structure of Concanavalin A tetramer (left) and an illustration of a carbohydrate recognizing domain binding 4-(hydroxymethyl)-1-(α -D-mannopyranosyl)-1H-1,2,3-triazole as an exemplary carbohydrate.

1.4. Lectins in microorganisms

Bacterial lectins are involved in the microbial infection process in a variety of ways. The bacterial AB toxins, such as the heat-labile enterotoxin of *E. coli*³⁸, CT³⁹, *diphtheria toxin*⁴⁰, or *botulinum neurotoxin*⁴¹ consist of two domains that are usually linked by disulfide bridges. The lectinoid B domain (binding domain) mediates the adhesion of the toxin to the host cell membrane, whereas the A domain (activity domain) is responsible for the cytotoxic effects after the holotoxin enters the cell^{42, 43}. Furthermore, lectins contribute to the pathogenicity of a bacterium already in the first phase of infection. Adhesion of pathogenic microorganisms to the host cell membrane is a crucial step in the development of infection. In addition to the enhanced uptake of nutrients, it confers on pathogens increased resistance to the host organism's self-cleaning mechanisms and to attack by the immune system^{44, 45}. In addition, bacterial adhesion enables tissue invasion and the introduction of bacterial toxins into host cells. For these reasons, the elucidation of adhesion mechanisms has been the subject of numerous scientific studies. Microbial adhesion is triggered in part by nonspecific factors, such as hydrophobic interactions and electrostatic forces.^{46, 47} Most important, however, are the lectin-carbohydrate interactions responsible for the recognition and binding of complementary receptors on the surface of host cells. For example, binding of *E. coli* to the uroepithelium is mediated by the mannose-specific lectin FimH, which is localized to the type 1 pili of the bacteria⁴⁸. Over ten different lectins are involved in the initiation and maintenance of gastrointestinal tract infections by *Helicobacter pylori*⁴⁹. Besides bacterial lectins, carbohydrate-binding proteins of host cell membranes also contribute to specific adhesion⁴⁵. Adhesins of the mucosa are partly responsible for colonization of the intestine by *Shigella flexneri*⁵⁰. Infections of the pharynx with group A streptococci are triggered by the binding of polysaccharides of the bacterial capsule to the hyaluronic acid-binding the host protein CD44⁵¹. This reciprocal interaction of lectins with complementary glycostructures localized both on the bacterial surface and at the periphery of host cells⁵² results in a dual recognition mechanism responsible for the organotropism of pathogenic and symbiotic microorganisms⁵³⁻⁵⁵. Infections by *Vibrio cholerae* occur primarily in the gastrointestinal tract, whereas *Streptococcus pneumoniae* affects the lungs and *Staphylococcus saprophyticus* affects the urinary tract^{46, 56}. Organotropism is also observed in viral infections⁵⁷. Infections caused by influenza viruses A, B, and C exclusively affect the respiratory tract⁵⁸. The so-called viral attachment proteins of the viral envelope are involved in the specific adhesion of these viruses.

1.4.1. Escherichia coli

Escherichia coli (*E. coli*) is a bacterium which is present in the human gut biome but is also responsible for the various gastrointestinal diseases such as travelers' diarrhea. The infection is initiated by adhering to glycosylated cell surfaces. For this purpose, the bacteria have evolved highly specialized hair-like structures, the pili. At the tip of each such pili a protein structure (FimH) able to recognize and to bind mannose moieties is located⁴⁶. As previously described, such a binding event is individually weak but is compensated by presentation in high numbers on the surface.

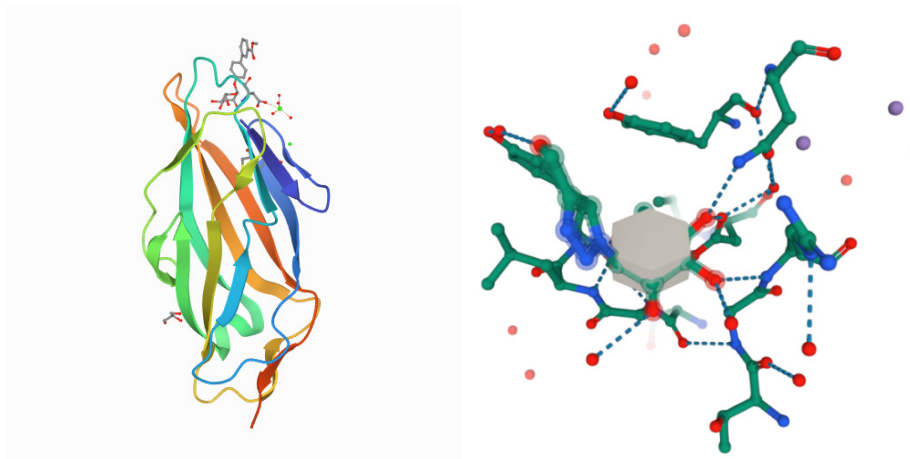


Figure 3: The structure of FimH (left) and an illustration of the carbohydrate recognizing domain in interaction with heptyl- α -D-mannopyrannoside as an exemplary carbohydrate.

1.5. Anti-adhesion therapy

The increasing emergence of pathogenic microorganisms that exhibit resistance mechanisms to a variety of conventional antibiotics has necessitated the development of novel drugs to combat viral and bacterial infections^{59,60}. Blockade of lectin-carbohydrate interactions by anti-adhesive agents is seen as a hopeful therapeutic approach for the treatment of previously poorly treatable infections⁶¹⁻⁶³. The development of resistance to such antiadhesive therapeutics, which prevent pathogenic microorganisms from binding to the host epithelium and thus prematurely stop an incipient infection, is unlikely⁶⁴. The use of these substances neither leads to the death of the germs nor do they have a direct influence on the growth behavior of the bacteria. Due to the specificity of the blockade, apathogenic organisms of the natural flora are spared. These can compete with resistant germs for the available nutrient supply⁶³. Selection of resistant organisms that have developed new means of adhesion to the host epithelium is thus prevented. Suitable anti-adhesion therapeutics include compounds that have an analogue to the receptor or

lectin, and anti-lectin antibodies that block the binding site of the lectin⁶². Several studies have shown that the use of simple sugars inhibits the adhesion of some species to the corresponding host tissue. Co-injection of uropathogenic *E. coli* cells with methyl- α -mannopyranoside into the bladder of mice could reduce the number of immobilized bacteria by two-thirds compared to corresponding controls⁶⁵. Infections of rhesus monkeys with *H. pylori* were successfully treated by issuing the animals with sialyl-3'-lactose, an oligosaccharide also found in human breast milk⁶⁶. In another study, the use of sugars was shown to inhibit the attachment of several bacterial species, including *Burkholderia cenocepacia*, *Pseudomonas aeruginosa*, *Legionella pneumophila*, and *Yersinia pestis*, to alveolar epithelial cells⁶⁰. The problem with inhibiting bacterial adhesion by simple sugars is that high concentrations must be used due to the low binding constant. This can be circumvented by using multivalent carbohydrate ligands⁶⁷ or glycomimetics⁶⁸. The use of substances that have an analogy to lectins can also prevent bacterial adhesion. A peptide consisting of 20 amino acids that mimics the structure of a surface adhesin of *Streptococcus mutans* has been reported to relax or prevent the binding of this bacterium to receptors present in saliva⁶⁹. In addition, anti-adhesion antibodies have been shown to inhibit pili/fimbriae-mediated binding of *P. aeruginosa* and *Candida albicans* to Asialo-GM1 receptors, as well as cell adhesion to receptors in the human buccal epithelium⁷⁰. In addition, drugs that block lectin-carbohydrate interactions could be used to prevent the binding of bacterial AB toxins to the host epithelium or to halt the progression as well as metastasis of cancer cells⁷¹.

1.6. Synthetic approaches toward mimicking multivalent cellular glycan structures and anti-adhesin drugs

The counterpart for the lectins, carbohydrates, are typically arranged densely and in a great variety on a cells surface^{72, 73}. An example of such a structure is the glycocalyx, consisting of oligo- and polysaccharides attached to the cell surface and responsible for cell-cell communication fertilization but also pathogen adherence⁷⁴⁻⁷⁶.

An approach to emulate biological structures to study complex interactions in a controlled and simplified environment or develop therapeutics based on biological interactions are biomimetic materials⁷⁷⁻⁷⁹. This can produce a variety of different resulting compounds with varying complexity and valency ranging from bioinspired single molecules to complex macromolecular scaffolds or surface coatings.

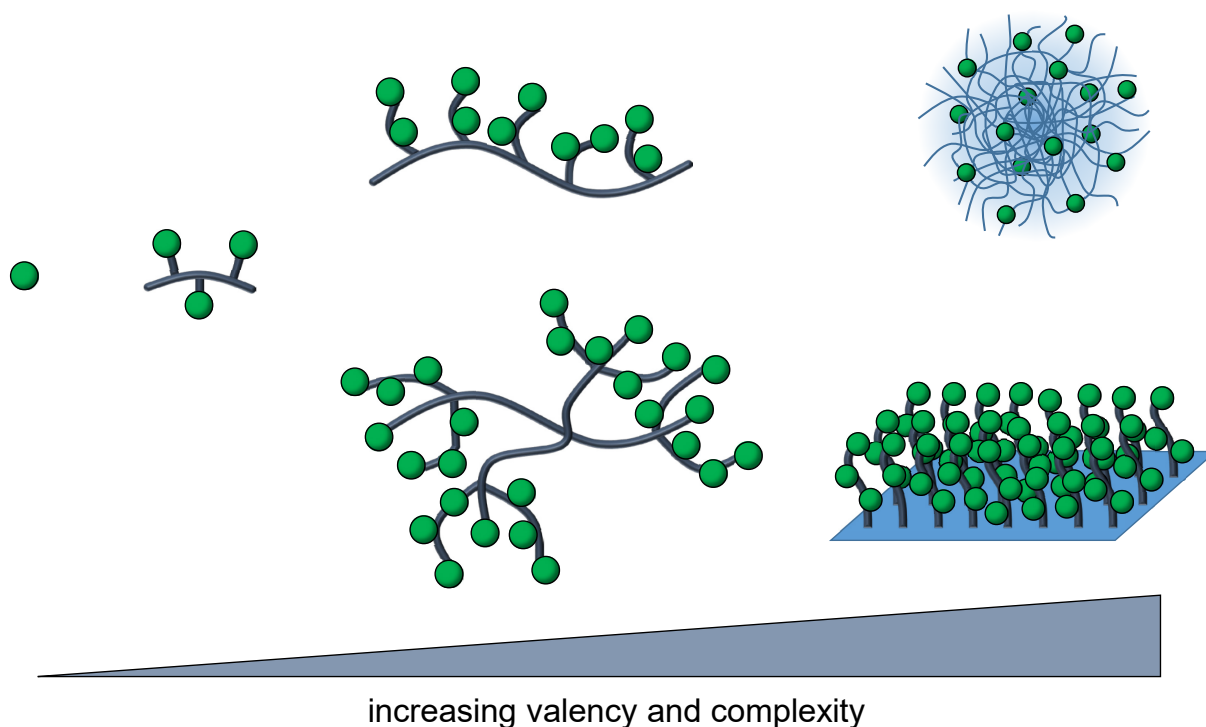


Figure 4: Inspired by biological motifs, single active molecules are synthesized for a variety of possible uses. Applying multivalency principles, the demand for more complex structures from brush polymers and dendrimeric structures to microgels or coated surfaces increases.

The more complex and multivalent structures take advantage of the important multivalency effect found in many biological interactions⁸⁰. Compared to a single carbohydrate-lectin bond, several combined increase adhesion manifold. This can be attributed to four mechanisms acting in ensemble namely clustering, chelating statistical rebinding and sterical shielding.

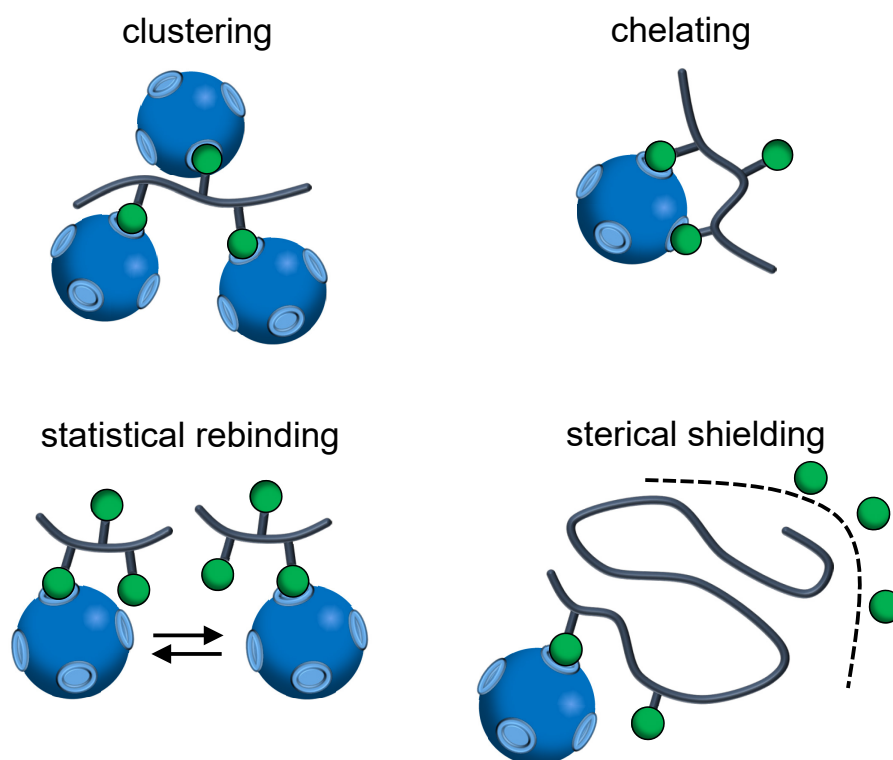


Figure 5: Schematic illustration of the binding mechanisms occurring during binding events of multivalent glycooligomers if several binding domains are present.

For the effects to be effective several binding domains must be presented. This can be either a multivalent lectin or several proteins immobilized in vicinity of each other. Clustering or the cluster glycoside effect takes effect if the carbohydrate ligands act as crosslinkers, increasing the overall avidity by additive effects⁸¹. Binding to a single lectin can be increased by the chelate effect. Known from many examples in chemistry, binding of a single multivalent ligand is entropically more favorable compared to several separate ligands^{82, 83}. This in turn is attributed to the entropic loss in conformational degrees of freedom on binding, which in case of a multivalent ligand is paid upon the first binding event excluding the subsequent events⁸⁴. Chelating can drastically enhance avidity but is strongly depended on sufficient ligand distancing and backbone flexibility⁸⁵. The statistical rebinding effect is reliant on the dynamic dissociation and re-association of carbohydrate-lectin bonds⁸⁶. As the single bond is weak it can quickly detach, but by increasing the ligand concentration in the immediate vicinity the association rate can be increased leading to overall high avidity⁸⁷. Sterical shielding is not affecting the binding event directly but is rather protecting it from competing ligands⁸⁸. The shielding can be done by a completely non-specific part of the scaffold such as PEG polymer chains or other sterically demanding ligands⁸⁹.

These effects occur in natural systems but can be emulated and optimized in designed compounds. As for studies of carbohydrate-ligand interactions and moreover cell or pathogen adhesion they cannot be discounted, therefore microgels are highly suitable scaffolds to create biomimetic structures as they can carry either carbohydrates or lectins in a sufficiently high number and steric availability⁹⁰⁻⁹².

1.7. Microgels

The general focus of this work is the study on interactions in biological systems on the microscale. An important tool to create biomimetic materials are hydrogel microparticles referred to as microgels⁹³. In the past decades microgels saw a constant rise in popularity in academics as they have possible applications as drug carriers, filters, sensors or antifouling agents further increasing versatility by being adsorbed to a surface or used in solution⁹⁴⁻⁹⁶. They can be synthesized to have a wide range of sizes, morphologies and additional properties such as responsiveness to temperature or pH change^{97, 98}. Arguably the most straightforward and mostly used way to exploit the reversible swelling is by using temperature responsive polymers such as PNIPAM and PEG.

These systems exhibit thermo-responsive behavior as the ratio of polymer-water to polymer-polymer interactions varies with temperature changes, allowing reversible swelling and deswelling of microgels^{99, 100}.

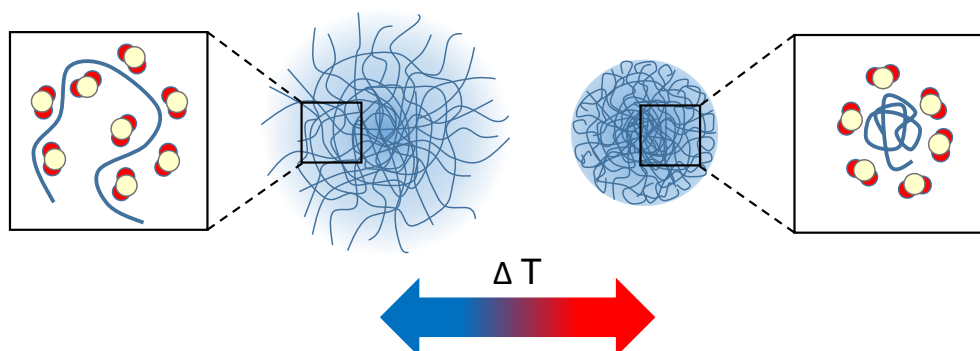


Figure 6: Below the LCST the polymer chains are elongated in water as the molecules form hydrogen bonds. For microgels this means phase separation occurs at temperatures above 32 °C as these hydrogen bonds are released, termed the volume phase transition temperature (VPTT).

Depending on the monomers, functional groups can be introduced to enable post-functionalization with small molecules, oligomeric structures, proteins or inorganic nanoparticles^{101, 102}.

1.7.1. Synthesis

Reactive microgels can be prepared by a variety of synthesis strategies. Precipitation polymerization is one of the most widely used methods for the preparation of thermoresponsive microgels¹⁰³. It is a versatile technique that offers various advantages for the production of aqueous microgels¹⁰⁴. For example, the polymerization process can be carried out as a batch, semi-batch or continuous process¹⁰⁵. Consequently, reaction conditions can be specifically

optimized and adjusted to synthesize microgels with tailored properties. Moreover, by using surfactants or co-monomers, the size of the microgels can be specifically controlled over a wide range (100 nm to 3 μm)¹⁰⁶. Further, microgels with low polydispersity can be prepared, which is of great interest for a variety of applications, especially optical applications^{96, 107}. The incorporation of different types of co-monomers into the microgel network during the polymerization process results in microgels that respond to different stimuli. Another advantage is that hybrid colloids can be prepared relatively easily by incorporating nanoparticles during microgel formation or by in situ synthesis of nanoparticles. However, this method is also associated with some disadvantages. For example, the synthesis of microgels with diameters smaller than 50 nm is extremely difficult without the addition of surfactants. Due to the higher polymerization temperature, only thermostable materials can be used, which makes the incorporation of biomacromolecules very problematic. The formation of a sol fraction during the polymerization process can also become a problem.

Surfactant-free precipitation polymerization of a temperature-sensitive NIPAM-based microgel was first carried out by Robert Pelton and Philip Chibante in 1986. Using TEM measurements, a particle diameter of 500 nm in the collapsed state was determined for the synthesized particles. Freitag et al. reported the surfactant-free synthesis of thermoresponsive poly-(*N,N'*-diethylacrylamide)(pNDEAm) microgels. In their study, they investigated the effect of stirring speed on the particle size of the microgel. It was found that the microgel particle size decreased with increasing stirring speed for the pNIPAM reference, while no significant effect of stirring speed was observed for pNDEAm microgels. Another way to influence the size and swelling properties under surfactant-free conditions can be achieved by using different types of crosslinkers. This was demonstrated using pNIPAM microgels prepared with different crosslinkers such as *N,N'*-methylenebisacrylamide (BIS), ethylene glycol dimethacrylate (EGDMA), and triethylene glycol dimethacrylate (TREGDMA) by Hellweg et al¹⁰⁸. The conventional crosslinker BIS was used as a reference. Hydrodynamic radii increased for the ethylene glycol crosslinkers with the highest radii obtained for TREGDMA. It was found that microgels synthesized with EGDMA and TREGDMA exhibited lower polydispersity and greater swelling capacity. The authors suggest, that the higher flexibility of ethylene glycol compared to the acrylamide-based crosslinkers results in difference in particle size and swelling capacity.

In precipitation polymerization, all components, including monomer, comonomer, crosslinker and initiator, are present dissolved in water. Microgel particles are formed via a homogeneous nucleation mechanism. At a polymerization temperature of 50-80 °C, thermal decomposition of the initiator molecules takes place and free water-soluble radicals are formed. Peroxide initiators such as potassium peroxydisulfate (KPS) or ammonium peroxydisulfate (APS) and azo initiators such as 2,2'-azobis(2-methylpropionamidine)dihydrochloride (V-50) are frequently used¹⁰⁹. The formed radicals grow into oligomer radicals by reaction with the water-soluble monomer present in the reaction solution. Above a critical chain length, the oligomeric radicals become water-insoluble, cluster and form precursor particles, also called precursor particles. The reason for this is the polymerization temperature, which is above the VPTT of the formed polymer. The unstable precursor particles can now grow by several mechanisms due to the strong polymer-polymer interactions above the VPTT¹¹⁰. First, they can aggregate into large, colloidally stable polymer particles. Second, they can deposit on the surface of already formed polymer particles. A third way to form precursor particles can be the addition of monomers or oligoradicals. Microgels that have reached a critical size are stabilized by an electrostatic stabilization mechanism. The charges result from initiator fragments incorporated into the polymer chains during the nucleation and growth process. At this stage, the microgels are in a collapsed state but still contain relatively large amounts of water. This is a significant difference between a precipitation polymerization and a classical emulsion polymerization of water-insoluble monomers such as styrene or butyl acrylate, where latex particles with a more compact structure are formed during the polymerization process. After the polymerization is complete and the reaction mixture cools to room temperature, the microgels begin to swell and form a "hairy" morphology on their surface when the temperature is below the VPTT of the polymer chains. At temperatures below the VPTT the microgels are stabilized by a steric mechanism due to the formation of hydrogen bonds between the polymer segments and the water molecules.

Since a variation of the particle sizes is not possible in a conventional, surfactant-free precipitation polymerization, one moves to a surfactant-assisted precipitation polymerization^{106, 111}. To produce very small particles, the growing precursor particles must be effectively stabilized at a very early stage of the polymerization process. However, stabilization by ionic initiator fragments incorporated into the polymer network is not sufficient to stabilize the relatively large surface area of the very small precursor particles. Therefore, a surfactant must be added to the reaction mixture to stabilize the precursor particles and minimize their growth

by aggregation. This leads to a reduction in the size of the microgel particles. The mechanism of surfactant-assisted precipitation polymerization is analogous to surfactant-free precipitation polymerization. One of the first publications on surfactant-assisted precipitation polymerization of pNIPAM latex particles in the presence of SDS was by Pelton in 1993, when it was shown that the radius of the produced pNIPAM microspheres decreased exponentially with increasing SDS concentration. PNIPAM microgels synthesized with high surfactant concentrations were found to have a more homogeneous structure than the microgels synthesized with lower surfactant concentrations¹¹².

1.7.2. Microgels from *N*-isopropylacrylamide

The polymer most widely used for fabrication of thermoresponsive material is poly-*N*-isopropylacrylamide (pNIPAM). It can be polymerized by free-radical precipitation polymerization in a straightforward and easily accessible way as water can be used as solvent. By adding comonomers the swelling behavior can be adjusted depending on the pNIPAM ratio and the possibly introduced functional groups. An example is the incorporation of carboxylic acid or amine groups to add a pH responsive trigger. Aside from linear chains microgels can be synthesized to create responsive particles. At room temperature pNIPAM is relatively hydrophilic which results in highly swollen particles. If the temperature is adjusted to be higher than the LCST of linear pNIPAM, at which the polymer becomes relatively hydrophobic and the particles collapse. For microgels consisting of pure pNIPAM this volume phase transition temperature is 32°C which can be considered relevant for biological applications as it is close to body temperature of mammals. Microorganisms can also typically survive temperature changes in this region.

1.7.3. Microgels from oligo(ethylene glycol methacrylate)

Similar to pNIPAM gels, ethylene glycol can be used to synthesize thermoresponsive gels. The polymers from oligoethylene glycol methacrylates are fabricated analogue to pNIPAM by free-radical precipitation polymerization and exhibit an LCST transition behavior at different temperatures depending on chain length. Where pNIPAM failed to translate into medical applications due to implications of carcinogenic or teratogenic effect of the monomer, the biocompatibility of PEG enables these materials to be applied in medical fields as implant base, regenerative medicine or as templates for cell engineering. As different chain lengths result in transition temperatures from 26 °C to 89 °C, copolymerization of different oligo ethylene glycols allows for precise adjustment of LCST in the final polymer. End group functionalities and the acidic H-atoms on the ethylene chains are sites for post functionalization, an example are core-shell particles.

1.8. Methods

1.8.1. Atomic Force Microscopy

Studies of interactions on a microscopic scale naturally require a microscope. Adhesion can be made visible a more intuitive way is haptic quantification. For this purpose, the atomic force microscopy (AFM) is an optimal fit. Developed by Binnig et al. in 1986 it can be used to record topological information of a surface or study elastic and adhesive forces. For both techniques a tip interacts with the sample surface, either scanning or indenting acquiring data with resolutions in the nanometer or pico-newton range.

1.8.2. Force-distance mode

In force measurement mode the cantilever is pressed against the sample and the concave bending is resulting in a change in laser deflection. The measured signal is translated to a value of applied force. If either the sample or the cantilever is functionalized to have adhesive properties convex bending occurs during pull-off so the adhesive force may be quantified. This allows for precise measurements of elastic properties¹¹³ or adhesion and rupture forces, gaining detailed insight into complex adhesion processes¹¹⁴. Modifying the original setup by functionalization of the cantilever or by fixing living cells or bacteria even allows for analysis of biomimetic and biological systems¹¹⁵. For successful measurements calibration is vital, it is done by determining the detector sensitivity and the cantilever spring constant.

1.8.3. Scanning mode

The setup consists of the tip typically made from silicon, a laser and a photodiode for deformation detection and a combination of motors and a piezo crystal for height control. Data detection is coupled to the height and bend of the tip, the extend is recorded as the laser is reflected on the reflective back side of the cantilever.

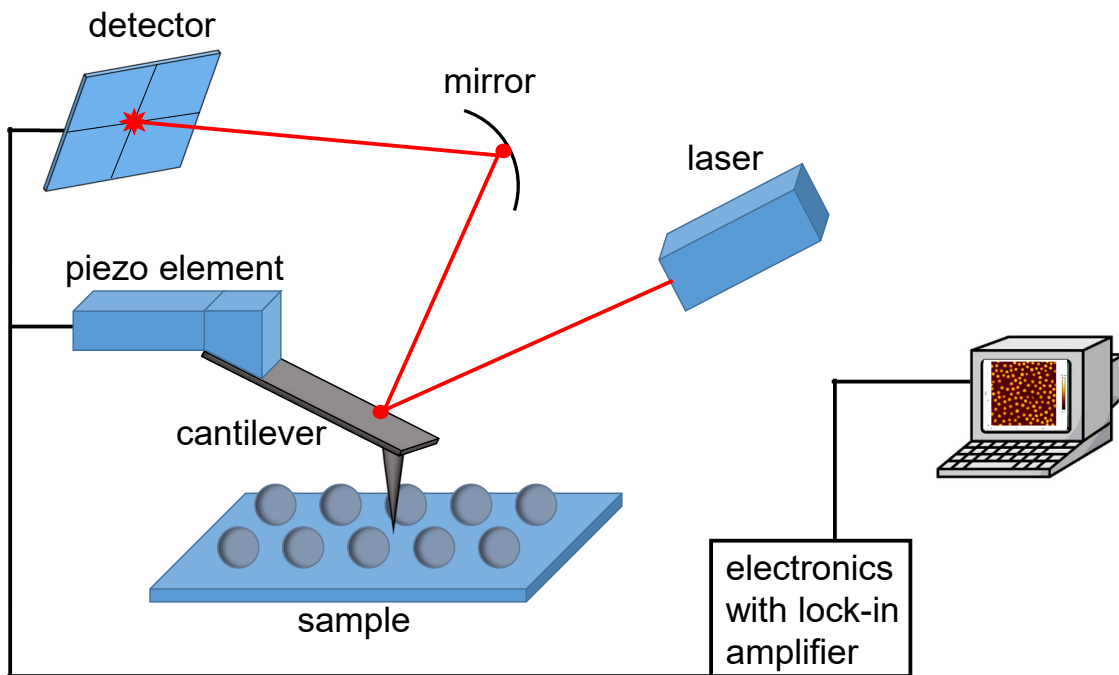


Figure 7: Schematic illustration of an AFM setup.

As the tip interacts with the sample the trajectory of the laser is changed. The recorded signal is used to gain information on sample topography or elastic properties and additionally to adjust the tip position accordingly. The cantilever is fixed to an extended glass rack allowing to work in air or liquid medium. This method allows for measurements at various interfaces and a large variety of samples e.g. organic, anorganic or biological. The typical cantilever is equipped with a sharp tip to allow for high resolution imaging, there are however cantilevers designed specifically for force microscopy without any modification allowing to adhere any possible probe depending on the experiment requirements.

1.8.4. Optical microscopy

The desire to inspect objects which have features too small to be recognized by the human eye seems to be ancient as first devices resembling lenses date back to several thousands of years¹¹⁶. Throughout human history several optical devices have been constructed to improve vision and many challenges of microscopy such as blurring, optical aberration and the resolution limits were overcome. Some early milestones were set by Lister and Amici introducing achromatic objectives or Ernst Abbe and Carl Zeiss producing apochromatic objectives. Illumination also saw improvement by August Köhler as he allowed for microscopes to improve even further. The development of fluorescence microscopy changes the approach from illuminating the sample externally to implementing molecules that emit light themselves for circumventing resolution limits. In recent times microscopy techniques moved far beyond even the Abbe limit

and can reliably determine the position of single fluorophores. In this work optical and fluorescence microscopy methods were implemented for sample characterization.

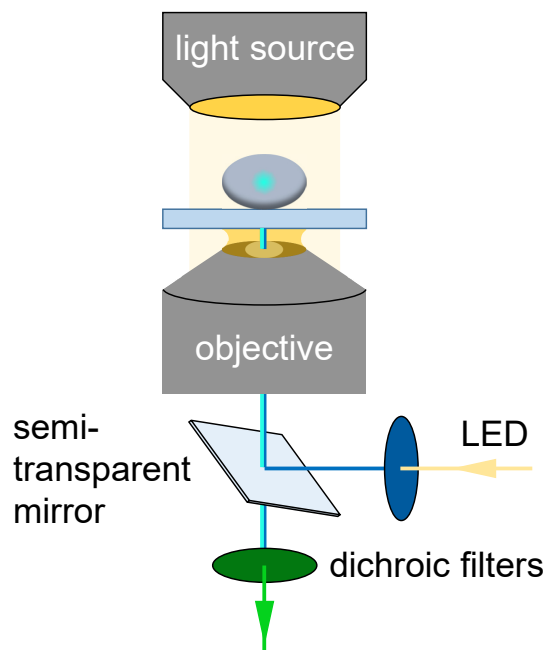


Figure 8: Schematic illustration of a basic microscopy setup for light and fluorescence microscopy.

For simple sample characterization imaging with an inverted light microscope in combination with an oil immersion objective is sufficient. Microgels with sizes of approximately 500 nm in diameter on average are visible especially if phase contrast is used.

1.8.5. Stochastic Optical Reconstruction Microscopy (dSTORM)

The Abbe limit was a hard barrier in microscopy, postulating that structures below 200 nm cannot be resolved properly. Several techniques have been developed since, which surpassed this limit one of which was awarded the Nobel prize in 2014. Stochastic Optical Reconstruction Microscopy is a fluorescence based method to create super-high resolution images far beyond the Abbe limit.

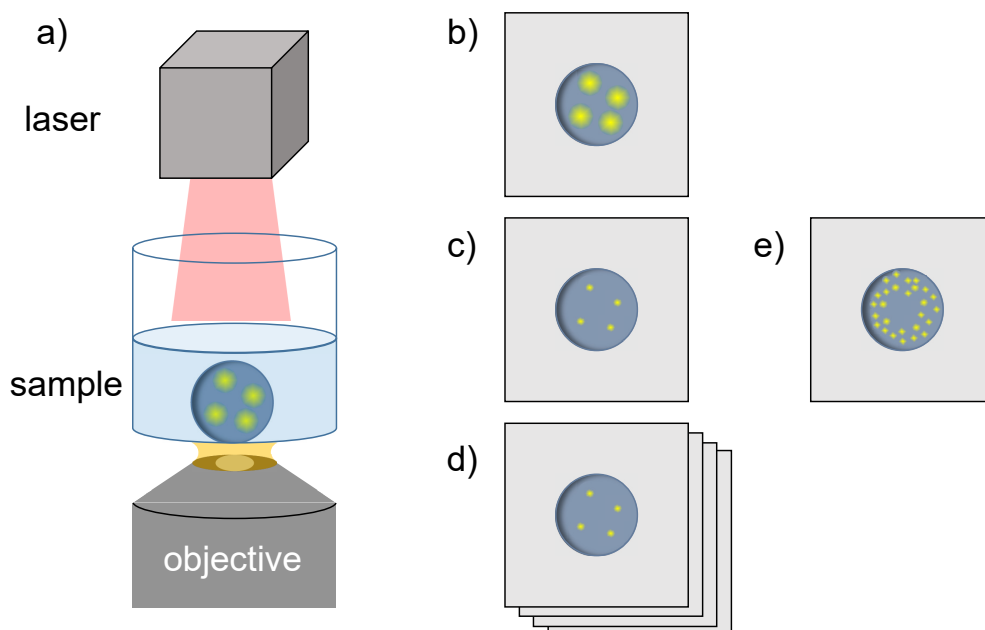


Figure 9: a) The sample is placed in a blinking buffer and illuminated with a laser to induce blinking of the individual fluorophores. b) Fluorescence images with blurry emitters are recorded. c) To reduce blur the images are post produced via the probability theory. d) Many images at different times are collected and optimized for further processing. e) A reconstruction image is created by merging all collected blinking images to visualize super-highly resolved structures.

The fluorophores are immersed in a blinking buffer resulting in a short emitting of a light pulse rather than continuous glowing. This ensures, that only a fraction of molecules is visible at a time ideally in a resolvable distance. Many images are then recorded over a span of time until a sufficient number is obtained. The single images show a collection of blurred single excitation events and need to be post processed using probability theory to determine the exact location of the light source. All the acquired images are then superimposed to create a single highly resolved image of the sample.

1.8.6. Dynamic Light Scattering (DLS)

Dynamic light scattering is a method for determination of particle size distributions based on the interaction of colloidal particles with light. The sample is suspended in a solvent, so the particles move freely due to Brownian motion.

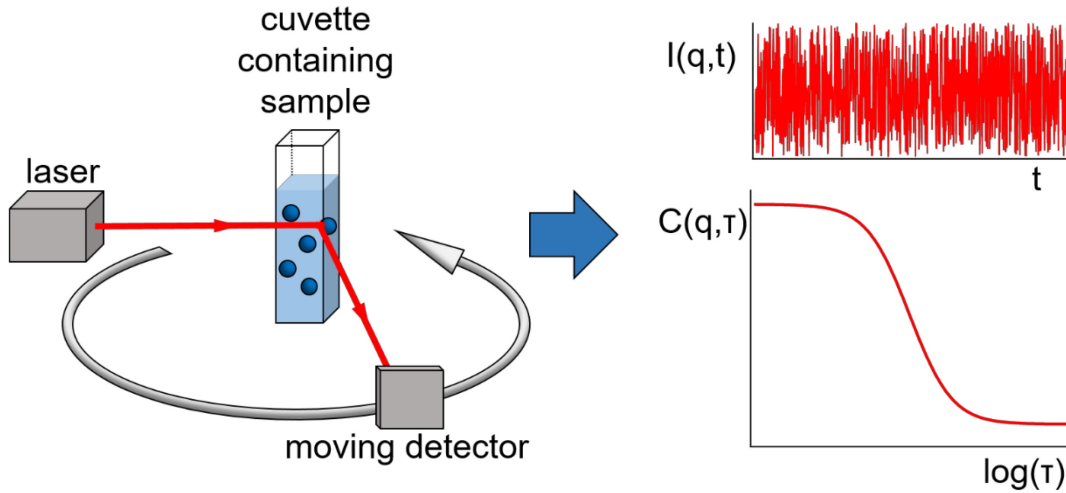


Figure 10: Schematic illustration of a DLS measurement setup and generated data.

If a light source, typically a laser, is directed at the sample scattering occurs. The scattering light intensity is measured over a range of angles and time steps, which fluctuates due to the random movement of the particles. This fluctuation can be characterized by an autocorrelation function providing values for size calculation. The method is based on the principle of large particles behaving differently in solution compared to small particles regarding movement speed. In turn this leads to a difference in intensity fluctuation and thus a characteristic difference in decay of the autocorrelation function. The hydrodynamic radius R_H can be calculated from the Stokes-Einstein relation:

$$R_H = \frac{k_B T}{6\pi\eta\langle\Gamma\rangle} q^2$$

with the Boltzmann constant k_B , temperature T , viscosity of the solvent η and the decay rate $\langle\Gamma\rangle$.¹¹⁷

2. Aims and Outline

Pathogens, bacterial or viral, rely on lectin-carbohydrate interactions to adhere to healthy tissue and cause infection. Typical treatments involve drugs which cause damage to the pathogen and possibly also to the native bio-flora of the patient. Additionally, continuous treatment with, for example, antibiotics causes a response in form of drug resistant germs. One opportunity to circumvent these problems is to make use of the natural and highly selective lectin-carbohydrate interactions and prevent the initial adhesion event of the pathogen. Targeting the highly conserved ability to undergo carbohydrate binding is highly unlikely to lead to antimicrobial resistance.

To be able to formulate such anti-adhesive compounds, we need to understand the relations between host and pathogen in great detail. For this, a stripped-down, cell-free model system can be of great interest. One such system are microgels, functionalized with biological motifs such as carbohydrates or proteins. This system is easily accessible by a one-pot synthesis and versatile deposition options on various surfaces.

In the first part of the project, single cell force spectroscopy (SCFS) is employed to quantify the adhesion between mannose binding *E. coli* bacteria and a mannose bearing microgel monolayer. Such an experiment provides detailed insight into the adhesion process as quantifiable values *e.g.* adhesion force and energy as well as elongation distance to full separation are obtained. In this setup a single *E. coli* bacterium is fixated on an AFM cantilever and used to probe how carbohydrate presenting responsive polymer particles interact with it and if this interaction can be influenced by a remote trigger. For this purpose, pNIPAM or pOEGMA microgels are functionalized with varying mannose amount and deposited on a hard substrate. The experiment is performed at room temperature and at 40 °C above the VPTT in a buffered solution so that the binding event can be studied with the microgels in the swollen and collapsed state. The binding affinity is expected to be significantly larger upon exceeding the VPTT and the particles are collapsed with the mannose density on the surface increased. Additionally, the surface of the otherwise fuzzy particles becomes smooth as the loose polymer chains collapse and sterical repulsion is reduced. Furthermore, methyl- α -mannopyranoside is added as a specific inhibitor to verify if the adhesion occurs due to specific binding between FimH and mannose and possibly determine the ratio between specific and non-specific binding. The AFM allows for full control of the loading rate when pressing the bacteria against the microgel surface. This enables additional examination of how the contact time and pull-off speed influences overall adhesion. In a solution, these correspond to naturally occurring forces

as bacteria are propelled by flagella and microgel particles move due to Brownian motion. Understanding of how these factors influence overall adhesion makes it possible to tune the microgels accordingly.

Results from the previous part indicate that the elastic modulus influences the adhesive properties of carbohydrate loaded microgels. To understand the structural differences between pNIPAM and pOEGMA based microgels depending on crosslinking density, high resolution AFM force maps are acquired. From the comparison between the density profiles of ultra-low crosslinked microgels, synthesized in the absence of bi-functional crosslinker and a conventional composition, information on the structure of the particles can be derived. The binding of mannose-functionalized ultra-low crosslinked microgels is compared to the binding of microgels synthesized in presence of the bifunctional crosslinker BIS. The absence and presence of a dedicated crosslinker leads to different microgels architectures, thus the effect on carbohydrate binding needs to be studied above and below the VPTT. As for biomedical applications, PEG-derived microgels are of great interest due to high biocompatibility and low toxicity. Thus, microgels containing OEGMA₄₇₅, MEO₂MA and EGDMA as crosslinker were also studied as an alternative to pNIPAM microgels. These microgels contain three different components with different reactivity, presumably resulting in a highly inhomogeneous polymer density distribution. Here high-resolution AFM force maps grant an extensive insight into the structure of individual microgels, which in turn greatly influences adhesive properties of the sample. To increase homogeneity, the most straightforward approach is to reduce the number of different monomers used for synthesis. This leads to homo-polymerized self-crosslinked microgels with crosslinking relying on statistical deprotonation. For OEGMA based microgels, the problem of adjusting the VPTT to 32 °C remains as OEGMA with different chain lengths needs to be co-polymerized to adjust the transition temperature in the physiological range.

In the final part, self-crosslinked carbohydrate bearing microgels are tested in solution on their ability to reliably capture and release *E. coli* bacteria. Microgels are synthesized in absence of a crosslinker as they have been found to be most promising in previous studies. This is due to their homogeneous polymer density distribution and high swelling degree and consequentially effective switching behavior. NIPAM-based and OEGMA-bases self-crosslinked microgels are dispersed in buffered solution and incubated with *E. coli* bacteria are heated to 37 °C and cooled to 20 °C to investigate the capture and release capabilities of the microgels. Comparison with microgels prepared with an additional crosslinker, ultra-resolution microscopy to determine ligand positioning will shed light on the molecular mechanisms involved on capture and release.

These insights, in combination with the straightforward synthesis of carbohydrate functionalized microgels enable applications in solvent purification and non-invasive cell isolation. Furthermore, targeting can be done by specific functionalization and the capture and release process is controlled via a remote switch making microgels a wide-ranging tool.

3. Conclusion and Perspectives

Quantification of adhesive forces between *E. coli* bacteria and a carbohydrate bearing microgel layer was achieved by the means of single cell force spectroscopy. Measurements were conducted at temperatures above and below the volume phase transition temperature to gain further insight into the difference in adhesion between the collapsed and swollen state of the microgels. For the experiments pNIPAM and pOEGMA microgels were prepared with mannose ligand incorporated at different concentrations. As anticipated, the adhesion forces increased at a temperature above the VPTT, likely due to an increase in mannose density per area and volume of an individual microgel particle. An increase in ligand density contributes to multivalent binding and an overall increase in avidity. Additionally, loose chain ends on the particle surface collapse resulting in a smooth surface decreasing steric repulsion. Moreover, methyl- α -mannopyranoside was added as an inhibitor to test the specificity of the interaction. The adhesion indeed was reduced by 75 % on average meaning non-specific binding contributes to one quarter of overall binding. Partly, this can be attributed to entanglements between the microgel network and the bacteria fimbriae. This is reflected in a significantly higher work of adhesion at low temperatures, due to the elastic stretching of polymer chains during pull-off. A noteworthy observation is the influence of elastic modulus on adhesion as the samples vary in composition. Gels with higher stiffness are known to have a decreased swelling degree, these also showed a decreased difference in adhesion below and above VPTT. This finding is explored further in the second article.

The structure of individual microgel particles was investigated by acquisition of high resolution force maps via AFM indentation measurements. Structural and compositional differences between several microgel samples have shown varying adhesion behavior. The greatest difference is expected between microgels synthesized in presence or absence of bi-functional crosslinker. For the experiments pNIPAM and pOEGMA microgels were prepared containing and excluding a crosslinker. Prior to force map acquisition the samples were deposited on glass and immersed in water. The obtained elastic modulus maps showed gradients from center to outer edges of the particles, which were synthesized from more than one component. Different monomers have also varying reactivity, which leads to an inhomogeneous polymer density distribution. This is most pronounced if a bi-functional crosslinker is incorporated as it has a significantly higher reactivity. Additionally, it is depleted faster than mono-functional monomers, which results in a less dense outer network with a lower stiffness. In turn the homopolymerized microgels show a homogeneous elastic modulus distribution and presumably also

a smoother surface. In addition to a high swelling degree this makes self-crosslinked microgels most suitable for capture and release applications.

For the controlled capture and release of pathogens in solution, carbohydrate bearing self-crosslinked pNIPAM and pOEGMA microgels were synthesized. The samples were incubated together with mannose binding *E. coli* bacteria at 37 °C to ensure bacteria viability, while still exceeding the VPTT of the microgels. After successfully capturing the bacteria, visible by formation of aggregates, the solution was cooled down to room temperature. To fully re-disperse the microgels and bacteria only very little external agitation was needed. This finding proves the viability of self-crosslinked carbohydrate bearing microgels for controlled specific target capture and gentle release. Possible applications can be as solution purification or cell isolation for example. The ability to capture the mannose binding bacteria is presumably due to a drastic increase in mannose on the particle surface after collapsing. The calculated values for carbohydrate density per volume increase several orders of magnitude, thus increasing affinity. The mannose distribution was investigated via high-resolution fluorescence microscopy and determined to be rather homogeneous throughout an individual particle. The measurements were conducted at room temperature and yielded similar results for pNIPAM and pOEGMA microgels. This means only a small fraction of mannose is accessible to the bacteria in the swollen state making the density and affinity difference compared to collapsed particles even more pronounced. The p(OEGMA₄₇₅-co-MEO₂MA)_{SCL}-Man microgels have an additional advantage over pNIPAM as the release of captured bacteria is supported by sterical repulsion of OEGMA₄₇₅ chains on the particle surface. This is due to slower incorporation rate of the OEGMA₄₇₅ monomer as is presumably has a lower diffusion speed and thus is incorporated less in the core region.

4. Publications

4.1. Switchable Adhesion of *E. coli* to Thermosensitive Carbohydrate-Presenting Microgel Layers: A Single-Cell Force Spectroscopy Study

Authors: **Dimitri Wilms**, Fabian Schröer, Tanja J. Paul and Stephan Schmidt

Journal: Langmuir

Issue: **2020**, 36, 12555-12562

DOI: 10.1021/acs.langmuir.0c02040

Impact Factor: 3.882 (2020)

Own contribution (first author):

Establishing and performing of single cell force spectroscopy with pNIPAM and pOEGMA microgels loaded with mannose. Establishing of *E. coli* fixation technique and performing force spectroscopy experiments on deposited microgel monolayers. Characterization and deposition of mannose loaded microgels on PMMA substrate. Evaluation of collected data, collaborative visualization of the results and writing of first manuscript draft followed by collaborative finalization of the manuscript.

Reproduced with permission from Dimitri Wilms, Fabian Schröer, Tanja J. Paul and Stephan Schmidt as well as the American Chemical Society, copyright © 2022. DOI: 10.1021/acs.langmuir.0c02040.

Switchable Adhesion of *E. coli* to Thermosensitive Carbohydrate-Presenting Microgel Layers: A Single-Cell Force Spectroscopy Study

Dimitri Wilms, Fabian Schröer, Tanja J. Paul, and Stephan Schmidt*

Cite This: *Langmuir* 2020, 36, 12555–12562

Read Online

ACCESS |



Metrics & More

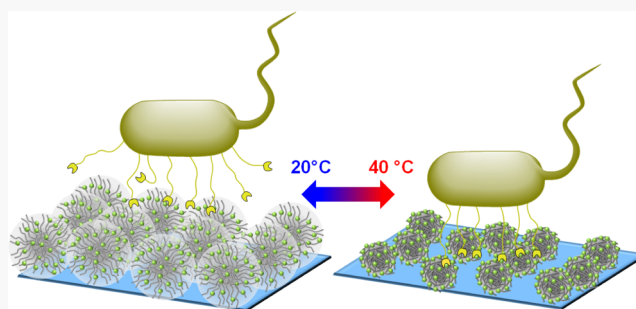


Article Recommendations



Supporting Information

ABSTRACT: Adhesion processes at the cellular scale are dominated by carbohydrate interactions, including the attachment and invasion of pathogens. Carbohydrate-presenting responsive polymers can bind pathogens and inhibit pathogen invasion by remote stimuli for the development of new antibiotic strategies. In this work, the adhesion forces of *E. coli* to monolayers composed of mannose-functionalized microgels with thermosensitive poly(*N*-isopropylacrylamide) (PNIPAM) and poly(oligo(ethylene glycol)) (PEG) networks are quantified using single-cell force spectroscopy (SCFS). When exceeding the microgels' lower critical solution temperature (LCST), the adhesion increases up to 2.5-fold depending on the polymer backbone and the mannose density. For similar mannose densities, the softer PNIPAM microgels show a significantly stronger adhesion increase when crossing the LCST as compared to the stiffer PEG microgels. This is explained by a stronger shift in swelling, mannose density, and surface roughness of the softer gels when crossing the LCST. When using nonbinding galactose instead of mannose, or when inhibiting bacterial receptors, a certain level of adhesion remains, indicating that also polymer–fimbria entanglements contribute to adhesion. The presented quantitative analysis provides insights into carbohydrate-mediated bacterial adhesion and the relation to material properties and shows the prospects and limitations of interactive polymer materials to control the attachment of bacteria.



INTRODUCTION

At the cellular level, carbohydrate–receptor interactions govern numerous processes, e.g., cell–cell communication, cell development, or the invasion of pathogens.¹ Thus, investigating carbohydrate interactions is important to further understand these processes and to develop new therapeutic strategies, e.g., to fight infections.^{2–4} One of the key pathogens well known to cause infections by adhering to glycosylated cell surfaces is *Escherichia coli*. For the initial attachment to cells, *E. coli* and other bacteria have evolved specialized hairlike fimbriae, which bind to specific carbohydrates.⁵ For example, *E. coli* bind to mannosides via the carbohydrate recognition domain FimH at the tip of the fimbriae. However, the specific carbohydrate-driven adhesion of pathogens is still not fully understood despite vigorous research activities in the past decades due to the complex interplay of many factors.^{6–10} For example, the strength of single carbohydrate–receptor complexes is low compared to potential bond-breaking forces that can act on adhered bacteria under physiological conditions,^{11,12} e.g., shear forces acting on *E. coli* in the urinary tract. This is compensated by the multivalent surface presentation of structurally complex cellular glycans and bacterial receptors.^{13–18} Furthermore, *E. coli* receptors binding to carbohydrates are known to strengthen under mechanical force^{19–21} and the ability of the binding motifs to probe for

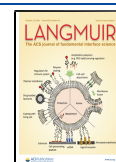
binding sites on a contacting surface depends on their flexibility and the stiffness of the involved materials.^{22–24}

Nevertheless, significant progress has been made to understand the effect of the glycan architecture on their binding to bacterial receptors. Various surface printing and lithography tools were employed to anchor glycans to analyze their interactions using labeled receptors or label-free detection.^{25–31} However, these methods only indicate the adhered amount of binding partner but not the nature of the underlying interaction, e.g., the extent of specific and nonspecific binding cannot be directly analyzed. Therefore, the exact multivalent carbohydrate-binding modes were difficult to interpret from these experiments. Force-based techniques, e.g., based on soft colloidal probes or atomic force microscopy (AFM),^{32–35} are suited to directly quantify the interactions of glycans with pathogens and their receptors. In particular, SCFS employing bacteria attached to an AFM cantilever gave a quantitative insight into the interactions

Received: July 10, 2020

Revised: September 25, 2020

Published: September 25, 2020



between bacteria and carbohydrate layers and other model surfaces.^{21,36–40} However, these model surfaces usually lack the cell-like material properties, in particular low stiffness and a glycocalyx-like carbohydrate presenting scaffold. A class of such carbohydrate-presenting biomimetic surfaces are soft microgel layers composed of polymer scaffolds with a lower critical solution temperature (LCST), which achieve a very low size dispersity.^{41–43} In addition, microgels composed of poly(*N*-isopropylacrylamide) (PNIPAM) or poly(oligo(ethylene glycols)) (PEG) have an LCST in the physiological temperature range and can readily be copolymerized with carbohydrate units targeting bacterial receptors.^{44,45} This may allow us to control the interaction to the bacteria when crossing the LCST to capture and release the bacteria upon temperature stimulus.⁴⁶ Heating such microgels above the LCST removes the hydration layer from the polymer backbone, which causes the microgel to collapse and form polymer–polymer contacts.⁴⁷ It is believed that above the LCST the hydrophilic carbohydrate units enrich on the surface of the microgels, which in combination with the polymer collapse leads to a drastically increased carbohydrate surface density and increased bacterial binding (Figure 1). However, the

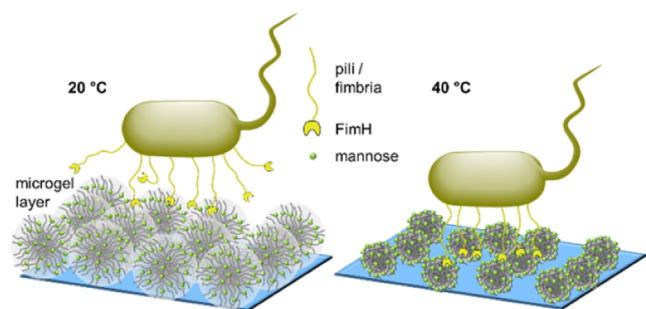


Figure 1. Illustration of the mannose-functionalized microgel layers and the proposed change of *E. coli* binding upon varying the temperature below (left) and above (right) the LCST. Above the LCST, polymer–polymer contacts are formed, water is expelled, and the microgel hydrodynamic radius decreases by a factor of 1.5–3. This leads to an overall increase of the mannose density, a smoother microgel surface, and possibly also surface enrichment of mannose units, increasing specific binding to FimH.

interaction of bacteria to such carbohydrate presenting networks and the effect of microgel composition as well as mechanical properties are not well understood. In addition, there is no quantitative analysis of how the polymer phase transition upon temperature change affects the carbohydrate-mediated interactions.

Along these lines, we use an AFM-based SCFS approach to quantify the temperature-dependent *E. coli* adhesion to

mannose-decorated microgel layers. Microgels based on PNIPAM and PEG are compared to test the effect of using different LCST polymers with an LCST of around 30–35 °C. Additionally, the effect of varying degrees of mannose functionalization is quantified and first insight into the role of the stiffness and swelling degree of the microgels is obtained. Using SCFS, specific and nonspecific adhesion owing to entanglements of the fimbriae with the polymer network can be discriminated to shed further light on the complex adhesion phenomena between bacteria and interactive polymer materials.

EXPERIMENTAL SECTION

Microgel Synthesis. PNIPAM–mannose microgels were prepared by surfactant-assisted precipitation polymerization.⁴⁶ Briefly, the monomers *N*-isopropylacrylamide and *N*-(2-(α -D-mannopyranosyloxy)ethyl) methacrylamide (ManEMAm), the cross-linker *N,N'*-methylenebisacrylamide (MBA), and the surfactant sodium dodecyl sulfate were dissolved in ultrapure water. Their exact amounts are shown in Table 1; see Supporting Information S1 for the synthesis of the carbohydrate monomers. Under stirring, the mixture was heated to 70 °C while purging with N₂, followed by adding ammonium persulfate (APS) to initiate polymerization. After 55 min of continuous stirring and purging, the reaction was stopped and the reaction mixture was purified by filtration and repeated centrifugation. The resulting microgels had a hydrodynamic radius of 350 nm and a functionalization degree of 39 $\mu\text{mol}\cdot\text{mg}^{-1}$.

PEG–mannose microgels were prepared by surfactant-assisted precipitation polymerization as described by Cai et al.⁴⁸ The monomers 2-(2-methoxyethoxy)ethyl methacrylate (MeO₂MA) and poly(ethylene glycol)methylether methacrylate (OEGMA, $M_n = 500 \text{ g}\cdot\text{mol}^{-1}$), the cross-linker ethylene glycol dimethacrylate (EGDMA), and sodium dodecyl sulfate were dissolved in ultrapure water and added to a three-necked flask. The mixture was purged with N₂ and heated to 70 °C while stirring. The initiator (APS) and the monomer *N*-ethylacrylamide- α -D-mannopyranoside (ManEAm) or, respectively, *N*-ethylacrylamide- α -D-galactopyranoside (GalEAMm) were added subsequently, and after 6 h reaction time, the mixture was cooled down followed by purification via repeated centrifugation. The resulting microgels had a hydrodynamic radius of around 120 nm and a functionalization degree between 20 and 135 $\mu\text{mol}\cdot\text{mg}^{-1}$.

Microgel Characterization. The hydrodynamic radii were determined by dynamic light scattering (DLS) in water at a concentration of 1 $\text{mg}\cdot\text{mL}^{-1}$. The measurements were conducted on a Zetasizer Nano Series Nano ZS (Malvern GmbH, Germany) at a wavelength of 633 nm and a backscattering angle of 173°. The mannose functionalization degree was determined via a colorimetric phenol sulfuric acid assay.⁴⁹

Monolayer Preparation. Solutions of the microgels at a concentration of 1 $\text{mg}\cdot\text{mL}^{-1}$ were cast on a polystyrene cell culture dish surface. After drying at room temperature, the spots were washed with ultrapure water several times to remove excess microgels. Mannan layers were prepared by dissolving the polysaccharide in the carbonate buffer solution (pH 9.6) at a concentration of 1.2 $\text{mg}\cdot\text{mL}^{-1}$.

Table 1. Amount of Chemicals Used for the Synthesis and the Degree of Carbohydrate Functionalization as Determined by the Phenol Sulfuric Acid Assay^a

microgel sample	monomer [mmol]	cross-linker [mmol]	mannose (in reaction) [mmol]	mannose (in microgel) [$\mu\text{mol g}^{-1}$]	mannose/monomer ratio [%]
PNIPAM–Man _{0.4}	6.19	0.324	0.309	37	0.4
PEG–Man _{0.4}	8.13/0.9 ^b	0.09	0.116	20	0.4
PEG–Man _{0.8}	8.13/0.9 ^b	0.09	0.718	40	0.8
PEG–Man _{2.7}	8.13/0.9 ^b	0.09	3.113	135	2.7
PEG–Gal _{0.5}	8.13/0.9 ^b	0.09	0.087	25	0.5

^aThe initiator (APS) concentration is 0.9 mmol for PNIPAM and 0.25 mmol for PEG microgels. ^bMeO₂MA/OEGMA.

A droplet of this solution was cast on a polystyrene cell culture dish and dried at room temperature.

Cantilever Preparation. For the SCFS measurements, we used colloidal probe cantilevers with bacteria bound at the probe's apex (Supporting Information S2). Compared to flat cantilevers or probes with sharp tips, the colloidal probe configuration ensures reproducible probe geometries and well-defined probe–sample contacts. There are various ways of immobilizing bacteria on AFM probes.³⁷ Here, noninvasive methods keeping the bacteria alive were preferred to ensure an intact bacterial surface.³⁶ Therefore, a thin layer of polydopamine was used as an adhesive since it binds to both the silica surface of the colloidal probe and the biomolecules on the bacterial surface, ensuring a noninvasive and stable attachment (Figure 2).⁵⁰

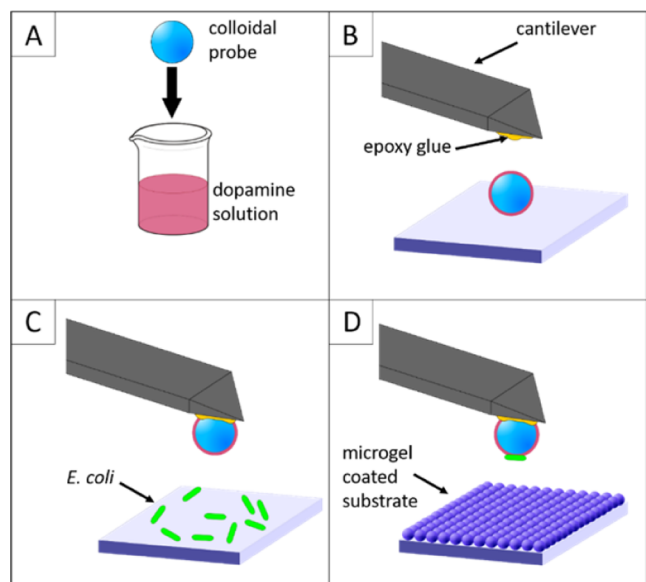


Figure 2. Preparation of the SCFS probes. (A) Silica beads were coated with polydopamine. (B) Coated beads were attached to the cantilevers with epoxy glue. (C) Single *E. coli* were attached in liquid using the AFM in combination with a fluorescence microscope. (D) AFM adhesion measurements were conducted against microgel or mannan layers in PBS buffer.

SCFS Measurements. The spring constant determination of the cantilever was carried out after attaching the bead but before picking up a bacterium via the thermal noise method. After the fixation of the bacterium on the cantilever, the Petri dish with the bacteria was exchanged for the one with the microgel coating, which already contains the buffer solution. Measurements were conducted in PBS buffer (pH 7.4). The cantilever was approached and retracted at a loading rate of $10 \text{ nN}\cdot\text{s}^{-1}$, and a constant force of 1 nN was applied for 5 s at contact. The same bacterium can be used for approximately 3 h ³⁷ and for several heating and cooling cycles between 25 and $40 \text{ }^\circ\text{C}$ without detaching. The pull-off force and work of adhesion values on the different microgel films were determined with at least three different bacteria at $20 \text{ }^\circ\text{C}$. Although using similar-sized bacteria, a

standard deviation of up to 30% in the adhesion parameters was obtained owing to the attachment of different bacteria (Supporting Information S3). Therefore, the data on the effect of temperature shown here were obtained with a single bacterium showing the expected adhesion values at $20 \text{ }^\circ\text{C}$. At least 500 force curves were taken on each film under each temperature condition.

RESULTS AND DISCUSSION

Microgel Surface Coatings. The microgel coatings were prepared on hydrophobic polystyrene culture dishes via drop-casting followed by drying and washing to remove excess microgel layers.⁵¹ After removing the excess microgels, quite regular microgel monolayers can be formed, which proved to be stable on the hydrophobic surfaces. The AFM images (Figure 3) confirm the sizes measured in solution via dynamic light scattering (Supporting Information S4). It should be noted that the AFM images were taken on dry microgel films; due to lateral swelling, the gaps between the microgels were closed in solution.

Typical Force–Distance Curves. A typical SCFS measurement with a bacteria-modified AFM probe on a microgel-coated surface is shown in Figure 4. The slope of the

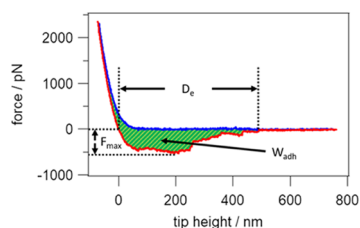


Figure 4. Exemplary force curve of a single *E. coli* against a microgel surface. Approach, blue; retract, red. The green area represents the work of adhesion (W_{adh}). F_{max} denotes the pull-off force, and D_e is the maximum elongation distance.

approach curve indicated the stiffness of the microgel layer, which increased when increasing the temperature above the LCST (Supporting Information S5).^{52–54} The retraction trace provided the pull-off force and the work of adhesion, i.e., the area between the baseline and the retraction trace. Multiple rupture events seen in the retraction trace were due to dangling chains of the polymer network and the bacteria's fimbriae when they were stretched until the rupture force was reached. The elongation distance describes the path length of the retraction trace between the intersection with the x -axis at low separations and the separation at the probe–sample detachment. This parameter shows how far the bacterial fimbriae and the polymer chains extend until all adhesive bonds rupture.

Confirming Specific Binding via FimH Inhibition. To determine the specificity of the interaction between *E. coli* at the cantilever and the mannose ligands in the microgel layer,

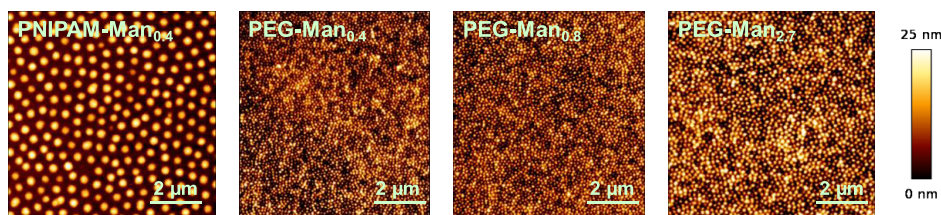


Figure 3. AFM images of the dry microgel surfaces. The dry microgels attain a flat “pancake” shape on the surface with gaps between the microgels. In the solution, the microgels swell, closing the gaps and attaining a spherical cap shape on the surface.⁵²

an adhesion inhibition experiment was conducted. Methyl mannose (MeMan) was used as an adhesion inhibitor for the FimH receptor at a concentration of 200 μM . After adding MeMan, the pull-off force decreased by 50%, showing that FimH was partially inhibited, thus confirming the specific adhesion between *E. coli* and the microgel layer (Figure 5).

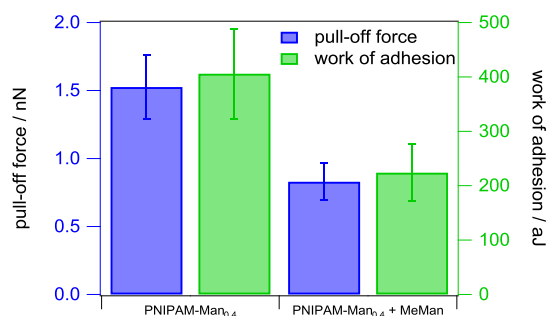


Figure 5. Adhesion before and after inhibiting FimH interactions with methyl mannose (MeMan).

The inhibition experiment also suggests that a significant part of adhesion was due to nonspecific binding between the bacterial membrane and the microgel. AFM adhesion measurements suggest that entanglements of polymer chains account for the adhesion between soft polymer gels.^{34,55} Therefore, we suspect that entanglements between the bacterial fimbriae and the brushlike microgel network might be responsible for the nonspecific adhesion observed here.

Temperature-Dependent Adhesion on Mannose-Presenting PNIPAM Microgels. Next, we studied the temperature-dependent adhesion of the bacteria on mannose-functionalized PNIPAM microgels. These microgels showed an LCST at 34 $^{\circ}\text{C}$ and a decrease in their hydrodynamic radius from 700 to 300 nm when increasing the temperature from 20 to 40 $^{\circ}\text{C}$, which equals a swelling degree of 2.3 (Supporting Information S4), suggesting a 12-fold increase of mannose density. The exemplary force–distance curves (Figure 6) on

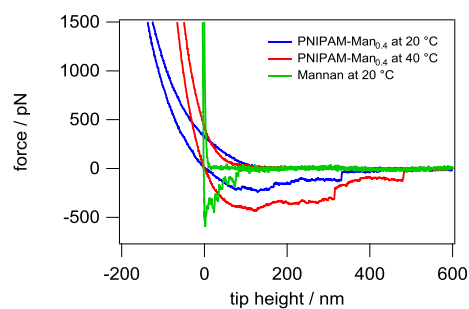


Figure 6. Force curves of PNIPAM–Man_{0.4} microgels at different temperatures (blue for 20 $^{\circ}\text{C}$, red for 40 $^{\circ}\text{C}$) and mannan as a reference (green, at 20 $^{\circ}\text{C}$).

the same microgels and the pull-off force histograms (Figure 7) suggest that the adhesion overall increases above the LCST of the microgels, in agreement with previous studies showing increased aggregation and binding of *E. coli* to mannose-functionalized microgels in solution.⁵⁶ A series of force curves (Supporting Information S6) shows that PNIPAM microgels below the LCST exhibit extended plateaus, i.e., near-constant force while retracting. This could be attributed to dangling chains on the fuzzy microgel surface where extending fimbriae

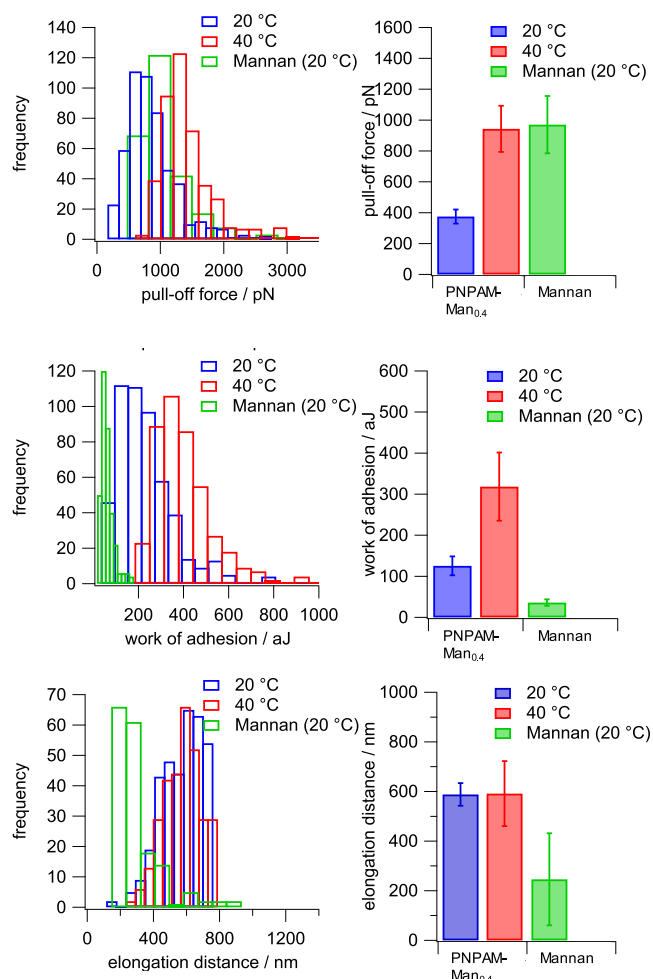


Figure 7. Adhesion of *E. coli* on PNIPAM_{0.4} and mannan coatings. Histograms (left) and average values (right) of the pull-off force (top), the work of adhesion (middle), and the elongation distance (bottom). The error bars denote the standard deviation.

and polymer chains slide along each other. We estimate that the mannose density in the microgels always exceeded the FimH concentration; therefore, the increased adhesion can be attributed to a 12-fold increase of the mannose density at 40 $^{\circ}\text{C}$, which improves the binding of the FimH groups due to a statistical effect.⁵⁷ In addition, the steric repulsion of the loosely cross-linked microgel surface was reduced upon collapse of the microgel network, which broadly increases adhesion when crossing the LCST.^{41–43} However, the collapse of the microgels and the contraction of the dangling chains did not lead to a reduction of the elongation length, i.e., the path length in the z -direction until detachment from the microgel surface above and below the LCST was the same. This was somewhat unexpected since the extended and softer microgels below the LCST should be able to stretch more under the tensile stress as compared to the collapsed state above the LCST. We assume that the overall increased adhesion above the LCST and larger pull-off forces enable the increased elongation of dangling chains, resulting in similar elongation lengths above and below the LCST.

To compare these results, we performed SCFS on a mannan-coated surface. Mannan is a small polysaccharide consisting of mannose units (666.6 g mol^{-1}). In contrast to the soft microgels, mannan coatings form a dense, thin layer on the

substrate. SCFS measurements on mannan coatings showed no indentation and high pull-off forces owing to the high density of mannose units. In addition, the long extended horizontal plateaus found in the force curves on microgels below the LCST were absent in the case of mannan coatings because the mannan chains are very short compared to the fuzzy microgel surface.⁵⁸ The pull-off forces on mannan surfaces were quite similar to the values obtained for the PNIPAM–Man_{0.4} microgels at 40 °C, although the microgels showed a mannose functionalization degree of only 0.4%. This suggests that nearly all *E. coli* binding sites were bound when brought into contact with the PNIPAM–Man_{0.4} microgels, indicating that the FimH density of the bacteria was low in comparison to the mannose density of the microgels. Therefore, when further increasing the mannose surface density, e.g., by the dense mannan coating, the specific binding of FimH does not benefit significantly due to the large size of the protein receptor carrying only a single binding site. On the other hand, the work of adhesion for mannan coatings and their elongation distance were comparatively small, which suggests that for soft microgel layers the elastic deformation and potential entanglements between bacterial fimbriae and the microgel network increase the work of adhesion.

Temperature-Dependent Adhesion on Mannose-Presenting PEG Microgels. The PEG microgels were prepared by radical copolymerization of the monomers OEGMA, MeO₂MA, and ManHEAA and the cross-linker EGDMA. Generally, these PEG-based microgels are interesting for physiological applications due to their low inflammatory response and reduced toxicity when compared to PNIPAM scaffolds.⁵⁹ A series of microgels with varying mannose functionalization degrees was prepared: PEG–Man_{0.4}, PEG–Man_{0.8}, and PEG–Man_{2.7}, where the numbers denote the ratio between the PEG monomer and the mannose monomer. The microgels showed an LCST at 32 °C and a decrease in their hydrodynamic radius by a factor of 1.8–1.5 when increasing the temperature from 20 to 40 °C (Supporting Information S4). In addition, surfaces with galactose-functionalized microgels (PEG–Gal_{0.5}) were prepared as a negative control since galactose does not bind to FimH. At comparable carbohydrate functionalization degrees, PEG–Man_{0.4} achieved a 2–5 times larger adhesion compared to PEG–Gal_{0.5} (Figure 8). The extend of nonspecific binding in terms of maximum pull-off forces was on the order of 70 pN, less than 25% even for the microgel with the lowest mannose functionalization degree.

The SCFS measurements showed that the pull-off force and the work of adhesion increased with a higher mannose loading (Figure 8). The PEG–Man_{2.7} sample only showed a moderate increase in pull-off force in relation to the more than threefold increase in mannose density compared to PEG–Man_{0.8}, which again suggests that the FimH receptor was already saturated at lower mannose densities. Notably, the PEG–Man_{2.7} sample at 20 °C showed an exceptionally strong increase of work of adhesion values, which might be attributed to rebinding events during pull-off, owing to the high density of mannose in the soft microgel network with large dangling chains. Along these lines, the retraction traces (Supporting Information S6) for PEG–Man_{2.7} at 20 °C had a large horizontal part, indicating prolonged adhesive contacts between bacteria and microgels upon retraction, whereas for lower Man densities and collapsed microgels, the traces were more curved. We suspect that these prolonged contacts could be due to rebinding of fimbriae at the mannose-rich PEG–Man_{2.7} microgels. In terms of temperature

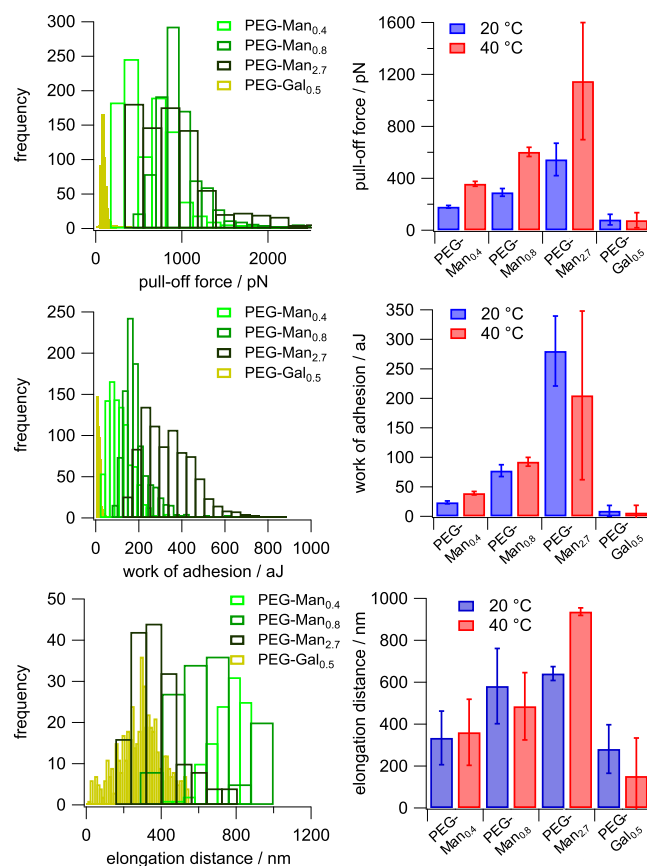


Figure 8. Adhesion of *E. coli* on PEG–Man microgel films with different mannose loadings and the PEG–Gal_{0.5} microgel film as a negative control. Pull-off force, work of adhesion, and elongation distance histograms (left) at 20 °C. The average values (right) show the change of adhesion parameters above and below the LCST.

response, the PEG–Man microgels show similar behavior to PNIPAM gels. Above the LCST, the adhesion increases due to a higher ligand density on the collapsed particle surface and the reduced steric repulsion. The PEG–Man_{2.7} sample shows a decreasing work of adhesion at 40 °C compared to that at 20 °C contrary to all other microgels. We suspect that the collapse of the PEG–Man_{2.7} microgels at 40 °C may result in a reduced stretching of the polymer chains during pull-off, which results in a reduction of rebinding events and a reduced work of adhesion. This observation is different from all other microgels with lower degrees of functionalization, including the PNIPAM microgels, which showed an increased work of adhesion in the collapsed state. To achieve a significant rebinding effect to increase the work required to detach the bacteria, it seems that the carbohydrate density should be large. It could be argued that for large carbohydrate densities where rebinding is strong, the affinity of collapsed polymers decreased above the LCST rather than increased as observed for the majority of samples here. Interestingly, such diverging results regarding the affinity of thermoresponsive glycopolymers were reported in the literature. On the one hand, affinities toward carbohydrate-binding proteins or bacteria decreased above the LCST,^{60–62} whereas other works showed increasing affinities.^{56,63–67} The varying accessibility of carbohydrate unity above and below the LCST⁶⁸ or rebinding events⁶⁹ may explain these diverging findings.

The difference in the microgel stiffness and the degree of swelling between PEG and PNIPAM microgels might show the dependence of *E. coli* adhesion on these material parameters. It should be noted that the measurements on PEG and PNIPAM microgels were performed with different *E. coli* samples, introducing an error of up to 30% in adhesion parameters (Supporting Information S3); therefore, a direct comparison might be limited by these errors. Nevertheless, when comparing PEG and PNIPAM microgels, the absolute values for pull-off force and work of adhesion for PEG gels were smaller (cf. PNIPAM–Man_{0.4} and PEG–Man_{0.4}). This could be explained by an increased Young's modulus of the PEG–Man_{0.4} microgels compared to that of the PNIPAM–Man_{0.4} microgels (1.2 MPa for PEG₀₄ vs 0.2 MPa for PNIPAM–Man_{0.4}, Supporting Information S5). These results hint at an adverse effect of microgel stiffness on adhesion, in line with studies by Miura and co-workers on the interaction of a lectin receptor with mannose-presenting microgels under cross-linker variation.⁷⁰ Alternatively, the radial distribution of mannose units might be different for PNIPAM and PEG microgels owing to the different polymerization kinetics of their monomers. For example, in case the mannose monomer is introduced at a slower rate into the microgel compared to the other monomers, a high-affinity core–shell structure could be expected. Further high-resolution microscopy studies might reveal the presence of such core–shell architectures. The difference in adhesion at above and below the phase transition temperature was higher for the PNIPAM microgels compared to that for the PEG microgels. This is most likely due to the higher degree of swelling of the PNIPAM microgel, the larger increment of the mannose density, and a larger reduction of surface roughness as the gel collapses.

CONCLUSIONS

Using single-cell force spectroscopy, the adhesion of *E. coli* on layers of mannose-decorated, thermoresponsive microgels was investigated. An increase of the adhesion above the microgels' LCST was observed, which was likely caused by an increase of mannose density as the microgel network collapsed. Moreover, the microgel surfaces attain a smooth structure above the LCST, which might help in reducing the steric repulsion between the bacteria and the microgel film to further increase the adhesion. The reduced work of adhesion measured upon increasing the temperature for the PEG microgel layer with the highest degree of mannose functionalization represents an exception to the general LCST effect on adhesion. For the high-mannose-density microgels, the reduced rebinding during retracting the bacteria from the collapsed microgel layer owing to the smoother microgel surface and less accessible mannose units due to network collapse, may explain this finding. A more in-depth study of such potential rebinding events may prove valuable to further understand the effect of network density and carbohydrate functionalization degree on the specific bacterial adhesion. Although the inhibition test showed that specific adhesion between the bacteria and microgel surface was present, up to 25% of the bacterial adhesion was due to nonspecific interactions, e.g., entanglements between the microgels and the bacterial fimbriae. We also found some indication that the degree of swelling and the elastic modulus (both are related to the effective mesh width of the network) affect the overall adhesion and the difference in adhesion above and below the LCST, where softer, less cross-linked gels show a larger difference. Therefore, significantly softer gels, e.g., via

cross-linker-free microgels, could enable a large enough adhesion difference to switch between attachment and detachment of bacteria. Overall, this study showed that thermosensitive carbohydrate-functionalized PNIPAM microgels as well as biocompatible PEG-based microgels can be remotely switched to control the specific interactions to carbohydrate-binding bacteria, which may give the blueprint for the design of highly functional interactive biomaterials.

ASSOCIATED CONTENT

Supporting Information

The Supporting Information is available free of charge at <https://pubs.acs.org/doi/10.1021/acs.langmuir.0c02040>.

Details on the carbohydrate monomer synthesis, cantilever modification, adhesion variation by attaching different bacteria, microgel swelling, force–indentation curves, exemplary force curves, and the contact time dependence of adhesion (PDF)

AUTHOR INFORMATION

Corresponding Author

Stephan Schmidt – Institute for Organic and Macromolecular Chemistry, Heinrich-Heine-University, 40225 Düsseldorf, Germany; orcid.org/0000-0002-4357-304X; Email: stephan.schmidt@hhu.de

Authors

Dimitri Wilms – Institute for Organic and Macromolecular Chemistry, Heinrich-Heine-University, 40225 Düsseldorf, Germany

Fabian Schröer – Institute for Organic and Macromolecular Chemistry, Heinrich-Heine-University, 40225 Düsseldorf, Germany

Tanja J. Paul – Institute for Organic and Macromolecular Chemistry, Heinrich-Heine-University, 40225 Düsseldorf, Germany

Complete contact information is available at: <https://pubs.acs.org/10.1021/acs.langmuir.0c02040>

Author Contributions

D.W. and F.S. contributed equally to this paper.

Notes

The authors declare no competing financial interest.

ACKNOWLEDGMENTS

The authors acknowledge funding by the German Research Foundation through the project SCHM 2748/S-1.

REFERENCES

- (1) Hudak, J. E.; Bertozzi, C. R. Glycotherapy: new advances inspire a reemergence of glycans in medicine. *Chem. Biol.* **2014**, *21*, 16–37.
- (2) Ofek, I.; Hasty, D. L.; Sharon, N. Anti-adhesion therapy of bacterial diseases: prospects and problems. *FEMS Immunol. Med. Microbiol.* **2003**, *38*, 181–91.
- (3) Papp, I.; Sieben, C.; Ludwig, K.; Roskamp, M.; Bottcher, C.; Schlecht, S.; Herrmann, A.; Haag, R. Inhibition of influenza virus infection by multivalent sialic-acid-functionalized gold nanoparticles. *Small* **2010**, *6*, 2900–6.
- (4) Soria-Martinez, L.; Bauer, S.; Giesler, M.; Schelhaas, S.; Materlik, J.; Janus, K.; Pierzyna, P.; Becker, M.; Snyder, N. L.; Hartmann, L.; Schelhaas, M. Prophylactic Antiviral Activity of Sulfated Glycomimetic Oligomers and Polymers. *J. Am. Chem. Soc.* **2020**, *142*, S252–S265.

- (5) Klemm, P.; Christiansen, G. Three fim genes required for the regulation of length and mediation of adhesion of *Escherichia coli* type 1 fimbriae. *Mol. Gen. Genet.* **1987**, *208*, 439–445.
- (6) Bernardi, A.; Jimenez-Barbero, J.; Casnati, A.; De Castro, C.; Darbre, T.; Fieschi, F.; Finne, J.; Funken, H.; Jaeger, K. E.; Lahmann, M.; Lindhorst, T. K.; Marradi, M.; Messner, P.; Molinaro, A.; Murphy, P. V.; Nativi, C.; Oscarson, S.; Penades, S.; Peri, F.; Pieters, R. J.; Renaudet, O.; Reymond, J. L.; Richichi, B.; Rojo, J.; Sansone, F.; Schaffer, C.; Turnbull, W. B.; Velasco-Torrijos, T.; Vidal, S.; Vincent, S.; Wennekes, T.; Zuilhof, H.; Imberty, A. Multivalent glycoconjugates as anti-pathogenic agents. *Chem. Soc. Rev.* **2013**, *42*, 4709–4727.
- (7) Poole, J.; Day, C. J.; von Itzstein, M.; Paton, J. C.; Jennings, M. P. Glycointeractions in bacterial pathogenesis. *Nat. Rev. Microbiol.* **2018**, *16*, 440–452.
- (8) Peterson, R.; Cheah, W. Y.; Grinyer, J.; Packer, N. Glycoconjugates in human milk: Protecting infants from disease. *Glycobiology* **2013**, *23*, 1425–1438.
- (9) Severi, E.; Hood, D. W.; Thomas, G. H. Sialic acid utilization by bacterial pathogens. *Microbiology* **2007**, *153*, 2817–2822.
- (10) Imberty, A.; Wimmerova, M.; Mitchell, E. P.; Gilboa-Garber, N. Structures of the lectins from *Pseudomonas aeruginosa*: insights into the molecular basis for host glycan recognition. *Microb. Infect.* **2004**, *6*, 221–228.
- (11) Helm, C. A.; Knoll, W.; Israelachvili, J. N. Measurement of ligand-receptor interactions. *Proc. Natl. Acad. Sci. U.S.A.* **1991**, *88*, 8169.
- (12) Moy, V. T.; Florin, E. L.; Gaub, H. E. Intermolecular forces and energies between ligands and receptors. *Science* **1994**, *266*, 257.
- (13) Lee, R. T.; Lee, Y. C. Affinity enhancement by multivalent lectin-carbohydrate interaction. *Glycoconjugate J.* **2000**, *17*, 543–551.
- (14) Mammen, M.; Choi, S. K.; Whitesides, G. M. Polyvalent Interactions in Biological Systems: Implications for Design and Use of Multivalent Ligands and Inhibitors. *Angew. Chem., Int. Ed.* **1998**, *37*, 2754–2794.
- (15) Lundquist, J. J.; Toone, E. J. The Cluster Glycoside Effect. *Chem. Rev.* **2002**, *102*, 555–578.
- (16) Kiessling, L. L.; Pohl, N. L. Strength in numbers: non-natural polyvalent carbohydrate derivatives. *Chem. Biol.* **1996**, *3*, 71–77.
- (17) Gestwicki, J. E.; Cairo, C. W.; Strong, L. E.; Oetjen, K. A.; Kiessling, L. L. Influencing Receptor-Ligand Binding Mechanisms with Multivalent Ligand Architecture. *J. Am. Chem. Soc.* **2002**, *124*, 14922–14933.
- (18) Sauer, M. M.; Jakob, R. P.; Luber, T.; Canonica, F.; Navarra, G.; Ernst, B.; Unverzagt, C.; Maier, T.; Glockshuber, R. Binding of the Bacterial Adhesin FimH to Its Natural, Multivalent High-Mannose Type Glycan Targets. *J. Am. Chem. Soc.* **2019**, *141*, 936–944.
- (19) Thomas, W. E.; Trintchina, E.; Forero, M.; Vogel, V.; Sokurenko, E. V. Bacterial adhesion to target cells enhanced by shear force. *Cell* **2002**, *109*, 913–923.
- (20) Yakovenko, O.; Sharma, S.; Forero, M.; Tchesnokova, V.; Aprikian, P.; Kidd, B.; Mach, A.; Vogel, V.; Sokurenko, E.; Thomas, W. E. FimH forms catch bonds that are enhanced by mechanical force due to allosteric regulation. *J. Biol. Chem.* **2008**, *283*, 11596–11605.
- (21) Viljoen, A.; Mignolet, J.; Viela, F.; Mathelié-Guinlet, M.; Dufrene, Y. F. How Microbes Use Force To Control Adhesion. *J. Bacteriol.* **2020**, *202*, e00125–20.
- (22) Wang, H. Q.; Jacobi, F.; Waschke, J.; Hartmann, L.; Lowen, H.; Schmidt, S. Elastic Modulus Dependence on the Specific Adhesion of Hydrogels. *Adv. Funct. Mater.* **2017**, *27*, 1702040.
- (23) Jacobi, F.; Camaleno de la Calle, A.; Boden, S.; Grafmuller, A.; Hartmann, L.; Schmidt, S. Multivalent Binding of Precision Glycoooligomers on Soft Glycocalyx Mimicking Hydrogels. *Biomacromolecules* **2018**, *19*, 3479–3488.
- (24) Missirlis, D.; Spatz, J. P. Combined Effects of PEG Hydrogel Elasticity and Cell-Adhesive Coating on Fibroblast Adhesion and Persistent Migration. *Biomacromolecules* **2014**, *15*, 195–205.
- (25) Liang, P.-H.; Wang, S.-K.; Wong, C.-H. Quantitative Analysis of Carbohydrate-Protein Interactions Using Glycan Microarrays: Determination of Surface and Solution Dissociation Constants. *J. Am. Chem. Soc.* **2007**, *129*, 11177–11184.
- (26) Oyelaran, O.; Li, Q.; Farnsworth, D.; Gildersleeve, J. C. Microarrays with Varying Carbohydrate Density Reveal Distinct Subpopulations of Serum Antibodies. *J. Proteome Res.* **2009**, *8*, 3529–3538.
- (27) Godula, K.; Bertozzi, C. R. Density Variant Glycan Microarray for Evaluating Cross-Linking of Mucin-like Glycoconjugates by Lectins. *J. Am. Chem. Soc.* **2012**, *134*, 15732–15742.
- (28) Valles, D. J.; Naeem, Y.; Rozenfeld, A. Y.; Aldasooky, R. W.; Wong, A. M.; Carbonell, C.; Mootoo, D. R.; Braunschweig, A. B. Multivalent binding of concanavalin A on variable-density mannoside microarrays. *Faraday Discuss.* **2019**, *219*, 77–89.
- (29) Gómez-García, M.; Benito, J. M.; Gutierrez-Gallego, R.; Maestre, A.; Mellet, C. O.; Fernandez, J. M. G.; Blanco, J. L. J. Comparative studies on lectin-carbohydrate interactions in low and high density homo- and heteroglycoclusters. *Org. Biomol. Chem.* **2010**, *8*, 1849–1860.
- (30) Guégan, C.; Garderes, J.; Le Pennec, G.; Gaillard, F.; Fay, F.; Linossier, L.; Herry, J. M.; Fontaine, M. N. B.; Réhel, K. V. Alteration of bacterial adhesion induced by the substrate stiffness. *Colloids Surf., B* **2014**, *114*, 193–200.
- (31) Igde, S.; Röblitz, S.; Müller, A.; Kolbe, K.; Boden, S.; Fessele, C.; Lindhorst, T. K.; Weber, M.; Hartmann, L. Linear Precision Glycomacromolecules with Varying Interligand Spacing and Linker Functionalities Binding to Concanavalin A and the Bacterial Lectin FimH. *Macromol. Biosci.* **2017**, *17*, No. 1700198.
- (32) Camaleño de la Calle, A.; Gerke, C.; Chang, X. J.; Grafmuller, A.; Hartmann, L.; Schmidt, S. Multivalent Interactions of Polyamide Based Sequence-Controlled Glycomacromolecules with Concanavalin A. *Macromol. Biosci.* **2019**, *19*, No. e1900033.
- (33) Pussak, D.; Ponader, D.; Mosca, S.; Ruiz, S. V.; Hartmann, L.; Schmidt, S. Mechanical Carbohydrate Sensors Based on Soft Hydrogel Particles. *Angew. Chem., Int. Ed.* **2013**, *52*, 6084–6087.
- (34) Pussak, D.; Ponader, D.; Mosca, S.; Pompe, T.; Hartmann, L.; Schmidt, S. Specific adhesion of carbohydrate hydrogel particles in competition with multivalent inhibitors evaluated by AFM. *Langmuir* **2014**, *30*, 6142–50.
- (35) Schmidt, S.; Wang, H.; Pussak, D.; Mosca, S.; Hartmann, L. Probing multivalency in ligand-receptor-mediated adhesion of soft, biomimetic interfaces. *Beilstein J. Org. Chem.* **2015**, *11*, 720–729.
- (36) Kang, S.; Elimelech, M. Bioinspired Single Bacterial Cell Force Spectroscopy. *Langmuir* **2009**, *25*, 9656–9659.
- (37) Beaussart, A.; El-Kirat-Chatel, S.; Sullan, R. M. A.; Alsteens, D.; Herman, P.; Derclaye, S.; Dufrene, Y. F. Quantifying the forces guiding microbial cell adhesion using single-cell force spectroscopy. *Nat. Protoc.* **2014**, *9*, 1049–1055.
- (38) Thewes, N.; Loskill, P.; Jung, P.; Peisker, H.; Bischoff, M.; Herrmann, M.; Jacobs, K. Hydrophobic interaction governs nonspecific adhesion of staphylococci: a single cell force spectroscopy study. *Beilstein J. Org. Chem.* **2014**, *5*, 1501–1512.
- (39) Rodriguez-Emmenegger, C.; Janel, S.; de los Santos Pereira, A.; Bruns, M.; Lafont, F. Quantifying bacterial adhesion on antifouling polymer brushes via single-cell force spectroscopy. *Polym. Chem.* **2015**, *6*, 5740–5751.
- (40) Sullan, R. M. A.; Beaussart, A.; Tripathi, P.; Derclaye, S.; El-Kirat-Chatel, S.; Li, J. K.; Schneider, Y.-J.; Vanderleyden, J.; Lebeer, S.; Dufrene, Y. F. Single-cell force spectroscopy of pili-mediated adhesion. *Nanoscale* **2014**, *6*, 1134–1143.
- (41) Jacobi, F.; Wilms, D.; Seiler, T.; Queckboerner, T.; Tabatabai, M.; Hartmann, L.; Schmidt, S. The effect of PEGylation on receptor anchoring and steric shielding at interfaces: an adhesion and surface plasmon resonance study with precision polymers. *Biomacromolecules* **2020**, DOI: 10.1021/acs.biomac.0c01060.
- (42) Uhlig, K.; Wegener, T.; Hertle, Y.; Bookhold, J.; Jaeger, M.; Hellweg, T.; Fery, A.; Duschl, C. Thermoresponsive Microgel Coatings as Versatile Functional Compounds for Novel Cell Manipulation Tools. *Polymers* **2018**, *10*, 12.

- (43) Uhlig, K.; Wegener, T.; He, J.; Zeiser, M.; Bookhold, J.; Dewald, I.; Godino, N.; Jaeger, M.; Hellweg, T.; Fery, A.; Duschl, C. Patterned Thermoresponsive Microgel Coatings for Noninvasive Processing of Adherent Cells. *Biomacromolecules* **2016**, *17*, 1110–6.
- (44) Tang, J. S. J.; Rosencrantz, S.; Tepper, L.; Chea, S.; Klöpzig, S.; Krüger-Genge, A.; Storsberg, J.; Rosencrantz, R. R. Functional Glyco-Nanogels for Multivalent Interaction with Lectins. *Molecules* **2019**, *24*, 1865.
- (45) Siirilä, J.; Hietala, S.; Ekholm, F. S.; Tenhu, H. Glucose and Maltose Surface-Functionalized Thermoresponsive Poly(N-Vinyl-caprolactam) Nanogels. *Biomacromolecules* **2020**, *21*, 955–965.
- (46) Paul, T. J.; Rübél, S.; Hildebrandt, M.; Strzelczyk, A. K.; Spormann, C.; Lindhorst, T. K.; Schmidt, S. Thermosensitive Display of Carbohydrate Ligands on Microgels for Switchable Binding of Proteins and Bacteria. *ACS Appl. Mater. Interfaces* **2019**, *11*, 26674–26683.
- (47) Heskins, M.; Guillet, J. E. Solution Properties of Poly(N-isopropylacrylamide). *J. Macromol. Sci., Part A: Chem.* **1968**, *2*, 1441–1455.
- (48) Cai, T.; Marquez, M.; Hu, Z. Monodisperse Thermoresponsive Microgels of Poly(ethylene glycol) Analogue-Based Biopolymers. *Langmuir* **2007**, *23*, 8663–8666.
- (49) Dubois, M.; Gilles, K.; Hamilton, J. K.; Rebers, P. A.; Smith, F. A Colorimetric Method for the Determination of Sugars. *Nature* **1951**, *168*, 167.
- (50) Lee, H.; Dellatore, S. M.; Miller, W. M.; Messersmith, P. B. Mussel-Inspired Surface Chemistry for Multifunctional Coatings. *Science* **2007**, *318*, 426.
- (51) Schmidt, S.; Hellweg, T.; Klitzing, R. Packing Density Control in P(NIPAM-co-AAc) Microgel Monolayers: Effect of Surface Charge, pH, and Preparation Technique. *Langmuir* **2008**, *24*, 12595–12602.
- (52) Schmidt, S.; Zeiser, M.; Hellweg, T.; Duschl, C.; Fery, A.; Mohwald, H. Adhesion and Mechanical Properties of PNIPAM Microgel Films and Their Potential Use as Switchable Cell Culture Substrates. *Adv. Funct. Mater.* **2010**, *20*, 3235–3243.
- (53) Fernandes, P. A. L.; Schmidt, S.; Zeiser, M.; Fery, A.; Hellweg, T. Swelling and mechanical properties of polymer gels with cross-linking gradient. *Soft Matter* **2010**, *6*, 3455–3458.
- (54) Burmistrova, A.; Richter, M.; Uzum, C.; von Klitzing, R. Effect of cross-linker density of P(NIPAM-co-AAc) microgels at solid surfaces on the swelling/shrinking behaviour and the Young's modulus. *Colloid Polym. Sci.* **2011**, *289*, 613–624.
- (55) Oréface, R. L.; Clark, A. E.; Brennan, A. B. AFM Study on the Interactions Across Interfaces Containing Attached Polymer Chains. *Macromol. Mater. Eng.* **2006**, *291*, 377–386.
- (56) Paul, T. J.; Rübél, S.; Hildebrandt, M.; Strzelczyk, A. K.; Spormann, C.; Lindhorst, T. K.; Schmidt, S. Thermosensitive Display of Carbohydrate Ligands on Microgels for Switchable Binding of Proteins and Bacteria. *ACS Appl. Mater. Interfaces* **2019**, *11*, 26674–26683.
- (57) Schmidt, S.; Paul, T. J.; Strzelczyk, A. K. Interactive Polymer Gels as Biomimetic Sensors for Carbohydrate Interactions and Capture-Release Devices for Pathogens. *Macromol. Chem. Phys.* **2019**, *220*, No. 1900323.
- (58) Witte, J.; Kyrey, T.; Lutzki, J.; Dahl, A. M.; Houston, J.; Radulescu, A.; Pipich, V.; Stingaciu, L.; Kühnhammer, M.; Witt, M. U.; von Klitzing, R.; Holderer, O.; Wellert, S. A comparison of the network structure and inner dynamics of homogeneously and heterogeneously crosslinked PNIPAM microgels with high crosslinker content. *Soft Matter* **2019**, *15*, 1053–1064.
- (59) Cooperstein, M. A.; Canavan, H. E. Assessment of cytotoxicity of (N-isopropyl acrylamide) and poly(N-isopropyl acrylamide)-coated surfaces. *Biointerphases* **2013**, *8*, 19.
- (60) Pasparakis, G.; Cockayne, A.; Alexander, C. Control of bacterial aggregation by thermoresponsive glycopolymers. *J. Am. Chem. Soc.* **2007**, *129*, 11014–5.
- (61) Mahon, C. S.; Wildsmith, G. C.; Haksar, D.; de Poel, E.; Beekman, J. M.; Pieters, R. J.; Webb, M. E.; Turnbull, W. B. A 'catch-and-release' receptor for the cholera toxin. *Faraday Discuss.* **2019**, *219*, 112–127.
- (62) Dalier, F.; Eghiaian, F.; Scheuring, S.; Marie, E.; Tribet, C. Temperature-Switchable Control of Ligand Display on Adlayers of Mixed Poly(lysine)-g-(PEO) and Poly(lysine)-g-(ligand-modified poly-N-isopropylacrylamide). *Biomacromolecules* **2016**, *17*, 1727–36.
- (63) Vasani, R. B.; Janardanan, N.; Prieto-Simon, B.; Cifuentes-Rius, A.; Bradley, S. J.; Moore, E.; Kraus, T.; Voelcker, N. H. Microwave Heating of Poly(N-isopropylacrylamide)-Conjugated Gold Nanoparticles for Temperature-Controlled Display of Concanavalin A. *ACS Appl. Mater. Interfaces* **2015**, *7*, 27755–64.
- (64) Wang, Y.; Kotsuchibashi, Y.; Liu, Y.; Narain, R. Study of Bacterial Adhesion on Biomimetic Temperature Responsive Glycopolymer Surfaces. *ACS Appl. Mater. Interfaces* **2015**, *7*, 1652–1661.
- (65) Won, S.; Hindmarsh, S.; Gibson, M. I. Triggerable Multivalent Glyconanoparticles for Probing Carbohydrate-Carbohydrate Interactions. *ACS Macro Lett.* **2018**, *7*, 178–183.
- (66) Won, S.; Richards, S. J.; Walker, M.; Gibson, M. I. Externally controllable glycan presentation on nanoparticle surfaces to modulate lectin recognition. *Nanoscale Horiz.* **2017**, *2*, 106–109.
- (67) Anaya, L. M. B.; Petitdemange, R.; Rosselin, M.; Ibarboue, E.; Garbay, B.; Garanger, E.; Deming, T. J.; Lecommandoux, S. Design of Thermoresponsive Elastin-Like Glycopolypeptides for Selective Lectin Binding and Sorting. *Biomacromolecules* **2020**, DOI: 10.1021/acs.biomac.0c00374.
- (68) Paul, T. J.; Strzelczyk, A. K.; Feldhof, M. I.; Schmidt, S. Temperature-Switchable Glycopolymers and Their Conformation-Dependent Binding to Receptor Targets. *Biomacromolecules* **2020**, *21*, 2913–2921.
- (69) Dam, T. K.; Brewer, C. F. Effects of Clustered Epitopes in Multivalent Ligand-Receptor Interactions. *Biochemistry* **2008**, *47*, 8470–8476.
- (70) Nakamoto, M.; Hoshino, Y.; Miura, Y. Effect of physical properties of nanogel particles on the kinetic constants of multipoint protein recognition process. *Biomacromolecules* **2014**, *15*, 541–7.

Switchable adhesion of *E. coli* to thermosensitive carbohydrate presenting microgel layers: a single cell force spectroscopy study

Dimitri Wilms^{1#}, Fabian Schröer^{1#}, Tanja J. Paul¹ and Stephan Schmidt^{1*}

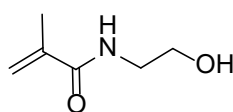
¹Institute for Organic and Macromolecular Chemistry, Heinrich-Heine-University, Universitätsstr. 1 40225 Düsseldorf Germany

Contents

S1 Glycomonomer synthesis.....	1
N-(2-hydroxyethyl)-2-methacrylamide (HEMAm)	1
2'-acrylamidoethyl-2,3,4,6-tetra-O-acetyl- α -D-mannopyranoside (AcManEMAm).....	2
N-ethylacrylamide- α -D-mannopyranoside (ManEAm)	5
N-ethylacrylamide- β -D-galactopyranoside (GalEAm)	7
S2 Bacteria attachment.....	10
S3 Variation of adhesion by attaching different bacteria	10
S4 Temperature-dependent microgel swelling.....	12
S5 Indentation experiments	12
S6 Exemplary force curves of measured samples and controls	14
S7 Contact time dependence of adhesion.....	16

S1 Glycomonomer synthesis

N-(2-hydroxyethyl)-2-methacrylamide (HEMAm)



Scheme S1a (HEMAm)

N-(2-hydroxyethyl)-2-methacrylamide was synthesized according to a protocol published by Parry et al.¹ Briefly, ethanolamine (8 mL, 132 mmol) was dissolved in anhydrous dry chloroform (100 mL) and cooled with an ice bath to 0 °C. Then a solution of methacryloyl chloride (6.4 mL, 67 mmol) and chloroform (75 mL) were slowly added, followed by stirring for 2 h at 0 °C. The formed solid was filtered off and the remaining chloroform was removed in vacuo. Next, the crude product was again dissolved in 250 mL chloroform and stirred over basic alumina for 15 h. On the next day the basic alumina was filtered off and the remaining solvent was removed under reduced pressure to give a pale-yellow oil. The product was purified by column chromatography (ethyl acetate/n-hexane 1:1). The overall yield of the synthesis was 80% (6.92 g).

$^1\text{H-NMR}$ (600 MHz, CDCl_3): δ 6.41 (s, 1H, -NH), 5.73 (t, $^3J_{\text{HH}} = 1.0$ Hz, 1H, -C=CH₂ E to -CH₃), 5.37 – 5.33 (m, 1H, -C=CH₂ Z to -CH₃), 3.75 (dd, $^3J_{\text{HH}} = 5.5, 4.5$ Hz, 2H, -NHCH₂CH₂), 3.50 – 3.46 (m, 2H, -NH-CH₂-CH₂), 2.57 (s, 1H, -OH), 1.97 – 1.95 (m, 3H, -CH₃).

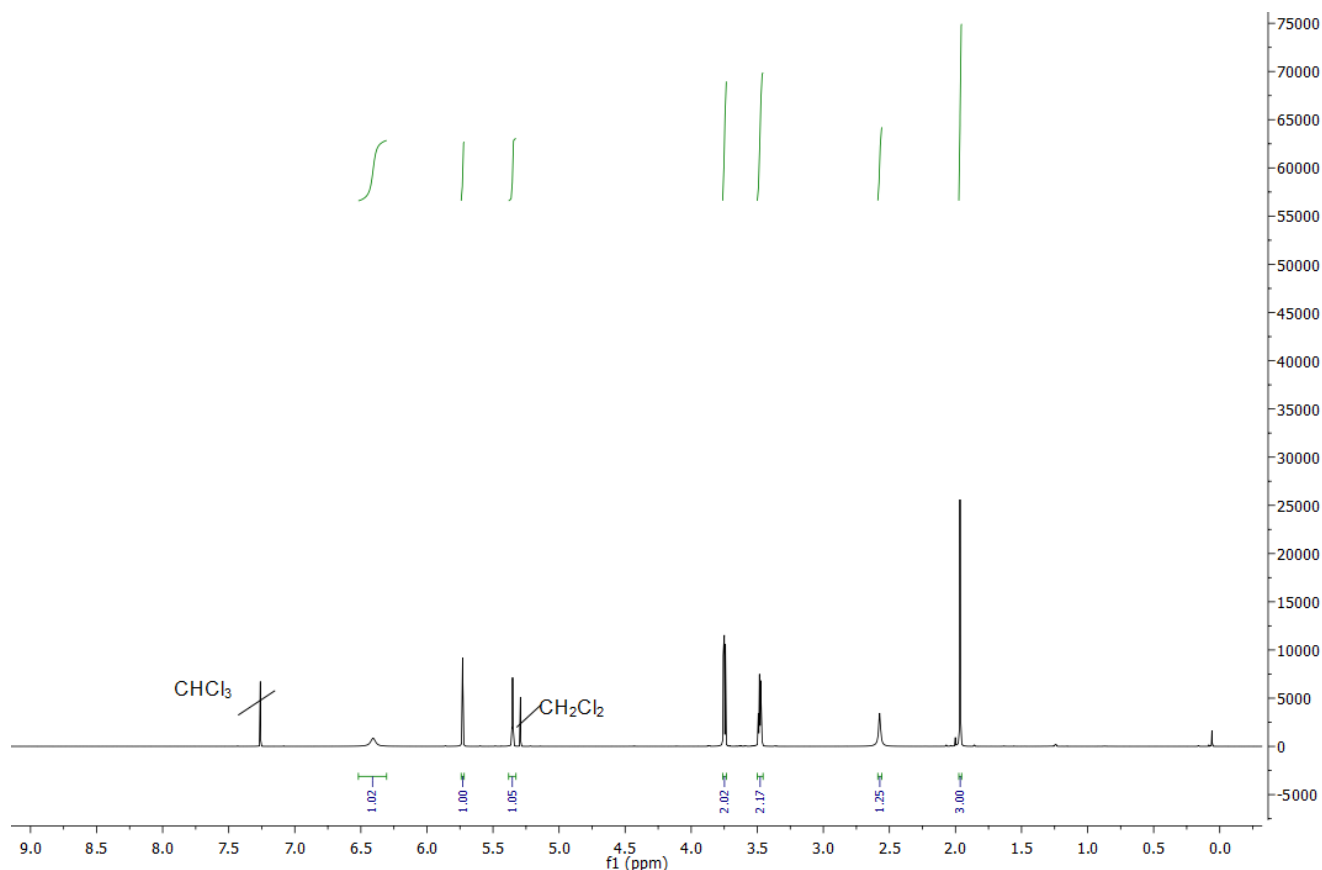
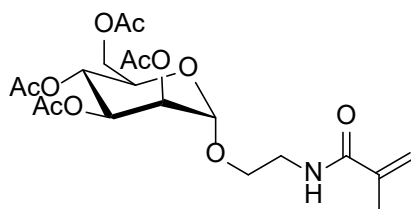


Figure S1a. $^1\text{H-NMR}$ (600 MHz, CDCl_3) HEMAm.

2'-acrylamidoethyl-2,3,4,6-tetra-O-acetyl- α -D-mannopyranoside (AcManEMAm)



Scheme S1b AcManEMAm

The synthesis was adapted from Gibson et al.² In a 1000 mL round bottom flask 1,2,3,4,6-Penta-O-acetyl- α -D-mannopyranoside (20.6 g, 52.8 mmol) and *N*-(2-hydroxyethyl)-2-methacrylamide (6.2 g, 48.2 mmol) were dissolved in dichloromethane (500 mL). Followed the solution was cooled to 0 °C and additionally purged with nitrogen for at least 15 min. After that slowly boron trifluoride diethyl etherate (35 mL, 276.2 mmol) was added to the solution.

After the addition of boron trifluoride diethyl etherate was completed the reaction solution was allowed to reach room temperature. After 48 h stirring at ambient temperature organic layer was washed with ice water, two times with saturated sodium hydrogen carbonate solution, distilled water and brine. The solution was dried with MgSO_4 , filtered and the remaining dichloromethane was removed under reduced pressure. The crude colorless gum was additionally purified by column chromatography (ethyl acetate/n-hexane 1:1). The overall yield of the colorless gum was 21% (4.65 g).

^1H NMR (600 MHz, CDCl_3) δ 6.29 (s, 1H, NH), 5.69 – 5.67 (m, 1H, $-\text{C}=\text{CH}_2$) 5.38 – 5.35 (m, 1H, $-\text{C}=\text{CH}_2$), 5.34 – 5.31 (m, 1H, H2), 5.29 (dd, $^3J_{\text{HH}} = 10.1, 3.4$ Hz, 1H, H3), 5.25 – 5.20 (m, 2H, H4), 4.80 (d, $^3J_{\text{HH}} = 1.8$ Hz, 1H, H1), 4.21 (dd, $^3J_{\text{HH}} = 12.2, 5.7$ Hz, 1H, H6), 4.08 – 4.05 (m, 2H, 1H, H6'), 3.95 – 3.90 (m, 1H, H5), 3.82 – 3.77 (m, 1H, $-\text{OCH}_2\text{CH}_2$), 3.63 – 3.52 (m, 2H, $-\text{OCH}_2\text{CH}_2$, $-\text{OCH}_2\text{CH}_2\text{NH}$), 3.51 – 3.44 (m, 1H, $-\text{OCH}_2\text{CH}_2\text{NH}$), 2.12 (s, 3H, $-\text{COCH}_3$), 2.06 (s, 3H, $-\text{COCH}_3$), 2.01 (s, 3H, $-\text{COCH}_3$), 1.96 (s, 3H, $-\text{COCH}_3$), 1.94 (s, 3H, $-\text{CH}_3$).

^{13}C NMR (600 MHz, CDCl_3) δ 170.66 (1C, $-\text{COCH}_3$), 170.11 (1C, $-\text{COCH}_3$), 170.05 (1C, $-\text{COCH}_3$), 169.70 (1C, $-\text{COCH}_3$), 168.51 (1C, $-\text{CONH}$), 139.84 (1C, $\text{COC}(\text{CH}_3)\text{CH}_2$), 119.93 (1C, $\text{COC}(\text{CH}_3)\text{CH}_2$), 97.69 (1C, C1), 69.42 (1C, C2), 69.06 (1C, C3), 68.87 (1C, C4), 67.32 (1C, C5), 66.15 (1C, $-\text{OCH}_2\text{CH}_2$), 62.52 (1C, C6), 39.29 (1C, NHCH_2CH_2), 21.10 (1C, $-\text{COCH}_3$), 20.92 (1C, $-\text{COCH}_3$), 20.76 (1C, $-\text{COCH}_3$), 18.68 (1C, $-\text{COCH}_3$), 14.25 (1C, $-\text{CH}_3$).

MS for $\text{C}_{20}\text{H}_{29}\text{NO}_{11}$ (ESI) m/z $[\text{M} + \text{H}^+]^+$ calc. 460.17; found 460.22, $[\text{M} + \text{Na}^+]^+$ calc.: 482.16; found 482.22.

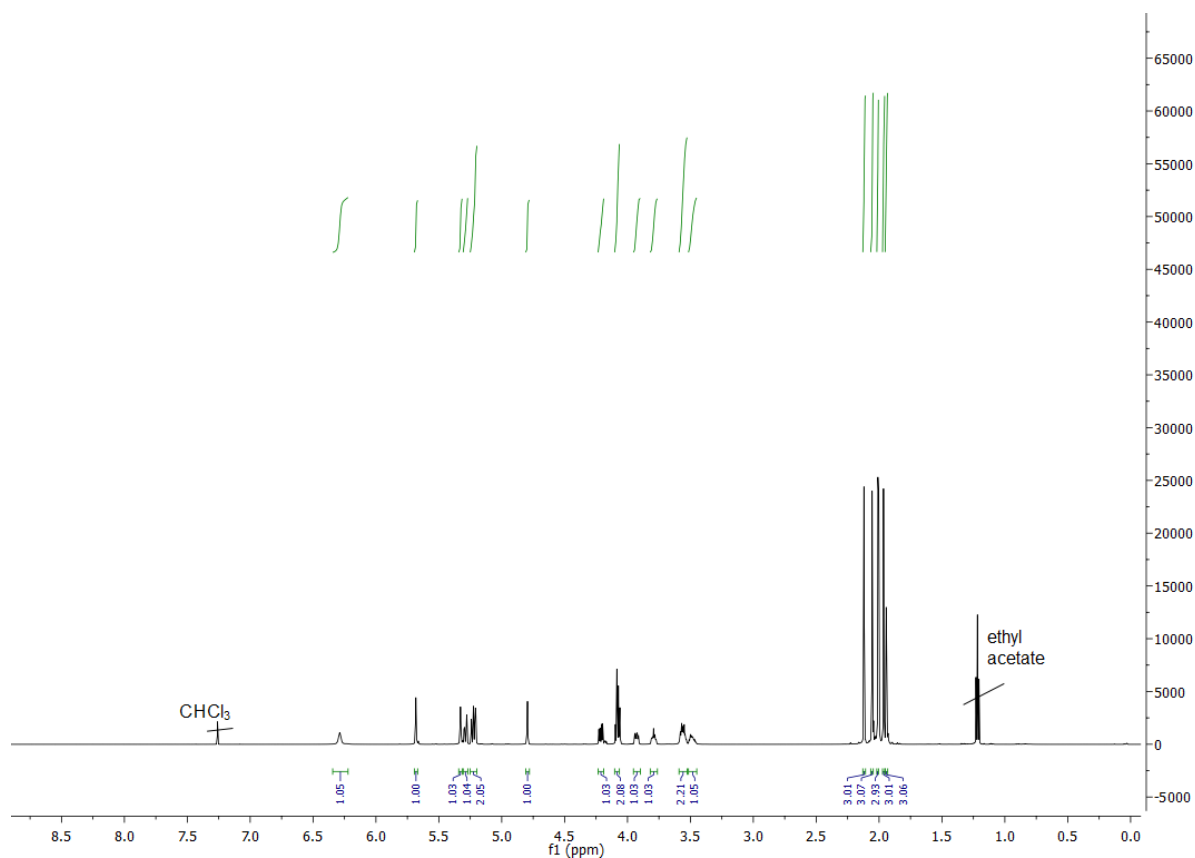


Figure S1b. ^1H -NMR (600 MHz, CDCl_3) AcManEMAm.

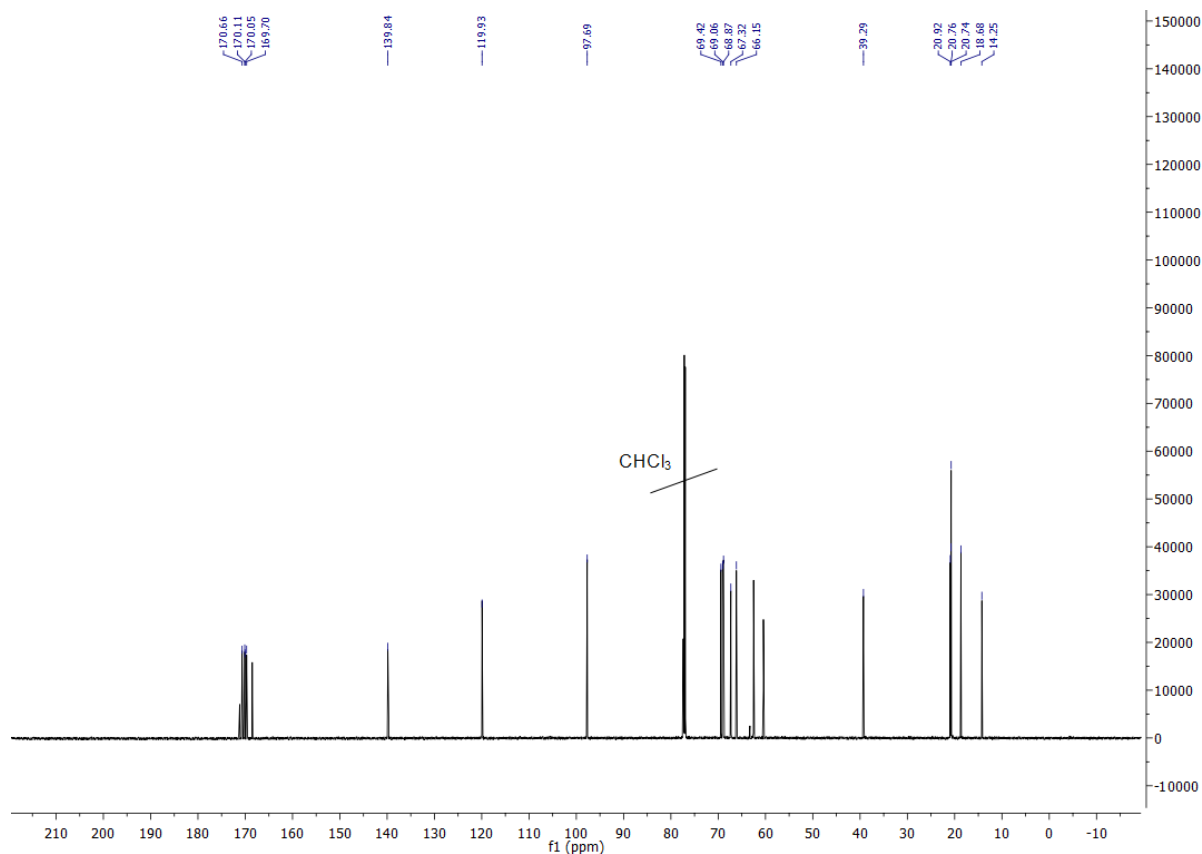


Figure S1c. ^{13}C -NMR (600 MHz, CDCl_3) AcManEMAm.

For polymerizations in water the glycomonomer had to be deprotected. Therefore, 0.5 g of the glycomonomer was given into 6.5 mL of a 0.3 M sodium methanolate solution in methanol and shaken for at least 2 h. The monomer formed a precipitate and was separated. The solid was washed with methanol 3 times. Afterwards, the remaining solid was dried *in vacuo*. The overall yield of the deprotection and the resulting white solid was 90 % (0.27 g).

^1H NMR (600 MHz, D_2O): δ 5.73 – 5.66 (m, 1H, $-\text{C}=\text{CH}_2$), 5.47 – 5.45 (m, 1H, $-\text{C}=\text{CH}_2$), 4.87 (d, $^3J_{\text{HH}} = 1.7$ Hz, 1H, H1), 3.93 (dd, $^3J_{\text{HH}} = 3.5, 1.7$ Hz, 1H, H2), 3.85 (dd, $^3J_{\text{HH}} = 12.2, 2.2$ Hz, 1H, H6), 3.83 – 3.80 (m, 1H, H3), 3.78 (dd, $^3J_{\text{HH}} = 9.5, 3.4$ Hz, 1H, H4), 3.74 (dd, $^3J_{\text{HH}} = 12.2, 5.9$ Hz, 1H, H6'), 3.71 – 3.62 (m, 2H, $-\text{OCH}_2\text{CH}_2\text{NH}$), 3.61 – 3.57 (m, 1H, H5), 3.56 – 3.51 (m, 1H, $-\text{OCH}_2\text{CH}_2\text{NH}$), 3.49 – 3.44 (m, 1H, $-\text{OCH}_2\text{CH}_2\text{NH}$), 1.93 (s, 3H, $-\text{CH}_3$).

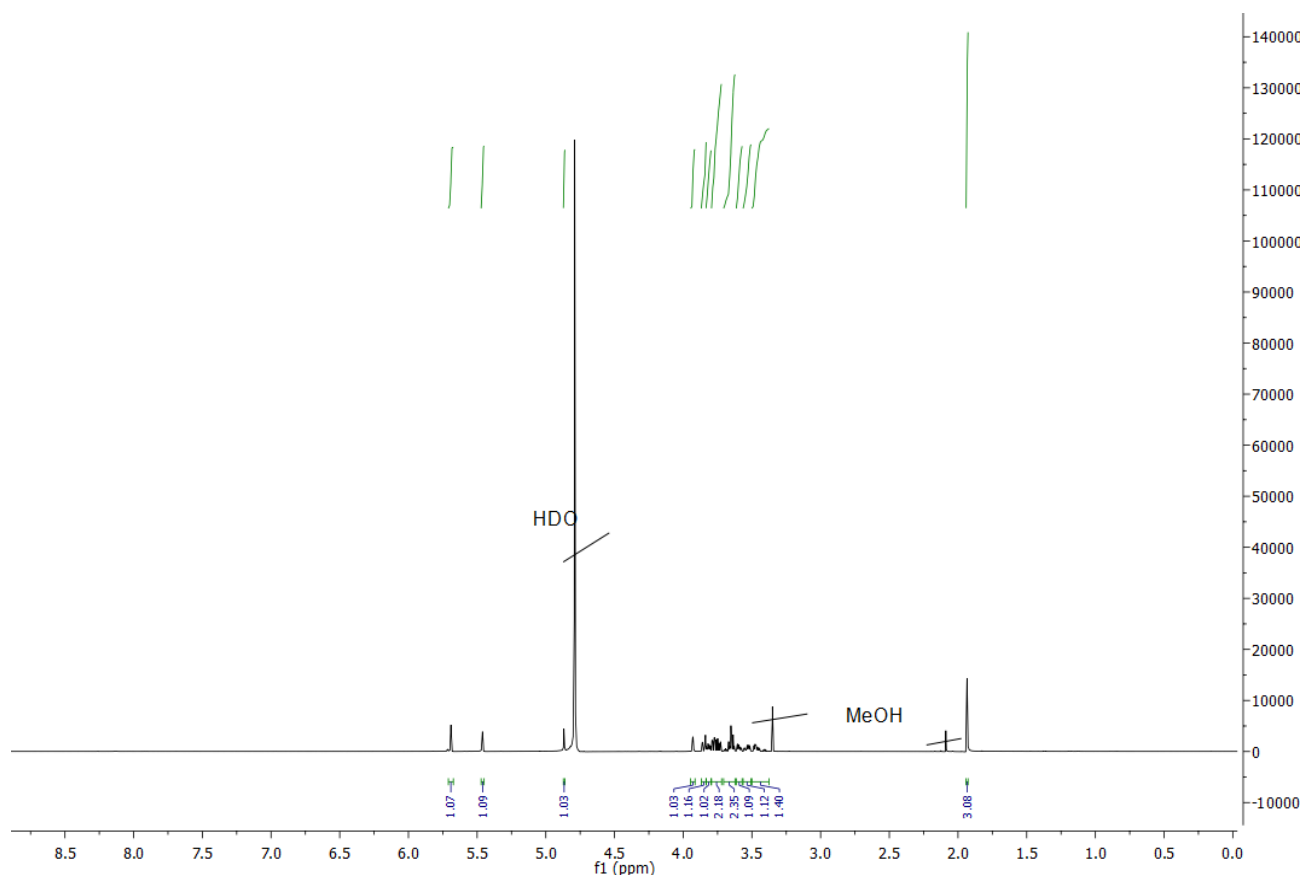
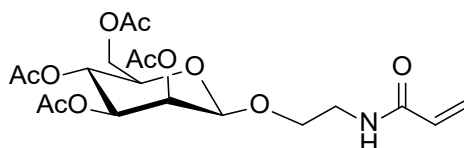


Figure S1d. $^1\text{H-NMR}$ (600 MHz, D_2O) ManEMAm.

***N*-ethylacrylamide- α -D-mannopyranoside (ManEMAm)**



Scheme S1c AcManEMAm

The synthesis of 2'-acrylamidoethyl-2,3,4,6-tetra-O-acetyl- α -D-mannopyranoside (AcManEMAm) is very similar to the synthesis of AcManEMAM. 10,0 g (78,2 mmol) *N*-(2-Hydroxyethyl)-acrylamid and 33,4 g (85,5 mmol) 1,2,3,4,6-Penta-O-acetyl- α -D-mannopyranoside are dissolved in 700 ml of dichloromethane, cooled down to 0 °C and flushed with nitrogen for 15 min inside a 1000 ml three-neck-flask. After the slow addition of 42 ml (331,4 mmol) boron trifluoride ethyl etherate, the reaction solution is stirred at room temperature for 48 h. The organic layer is washed with with icewater, 3 times with saturated sodium hydrogen carbonate solution and with ultrapure water. After drying the orangic layer over magnesium sulfate, dichloromethane is removed by distillation under vacuum and reduced pressure. The synthesized AcManEMAM is purified by column chromatography (Gradient: ethyl acetate/*n*-hexane 1:1 to pure *n*-hexane). The yield of the remaining product is 52 % (18,0 g, 40 mmol).

^1H NMR (600 MHz, DMSO- d_6) δ 8.31 (t, J = 5.7 Hz, 1H, NH), 6.25 (dd, J = 17.1, 10.2 Hz, 1H, -CH=CH $_2$), 6.09 (dd, J = 17.1, 2.2 Hz, 1H, -CH=CH $_2$), 5.60 (dd, J = 10.2, 2.2 Hz, 1H, -CH=CH $_2$), 5.20 – 5.15 (m, 1H, H2), 5.14 (dd, J = 3.6, 1.6 Hz, 1H, H3), 5.11 – 5.04 (m, 1H, H4), 4.89 (d, J = 1.7 Hz, 1H, H1), 4.12 (dd, J = 12.2, 5.3 Hz, 1H, H6), 4.04 – 4.01 (m, 1H, H6'), 4.01 – 3.97 (m, 1H, H5), 3.71 – 3.64 (m, 1H, -OCH $_2$ CH $_2$ NH), 3.57 – 3.51 (m, 1H, -OCH $_2$ CH $_2$ NH), 3.41 – 3.34 (m, 2H, -OCH $_2$ CH $_2$ NH), 2.11 (s, 3H, -COCH $_3$), 2.03 (s, 3H, -COCH $_3$), 2.02 (s, 3H, -COCH $_3$), 1.94 (s, 3H, -COCH $_3$).

^{13}C NMR (600 MHz, CDCl $_3$) δ 170.67 (1C, -COCH $_3$), 170.12 (1C, -COCH $_3$), 170.12 (1C, -COCH $_3$), 169.70 (1C, -COCH $_3$), 165.62 (1C, -CONH), 130.54 (1C, COCHCH $_2$), 126.98 (1C, COCHCH $_2$), 97.77 (1C, C1), 69.37 (1C, C2), 68.99 (1C, C3), 68.79 (1C, C4), 67.59 (1C, C5), 66.16 (1C, -OCH $_2$ CH $_2$), 62.52 (1C, C6), 39.14 (1C, NHCH $_2$ CH $_2$), 20.88 (1C, -COCH $_3$), 20.73 (1C, -COCH $_3$), 20.71 (1C, -COCH $_3$), 20.71 (1C, -COCH $_3$).

MS for C $_{19}$ H $_{27}$ NO $_{11}$ (ESI) m/z [M+H] $^+$ calc. 446.2; found 446.1, [M+Na] $^+$ calc.: 468.1; found 468.2.

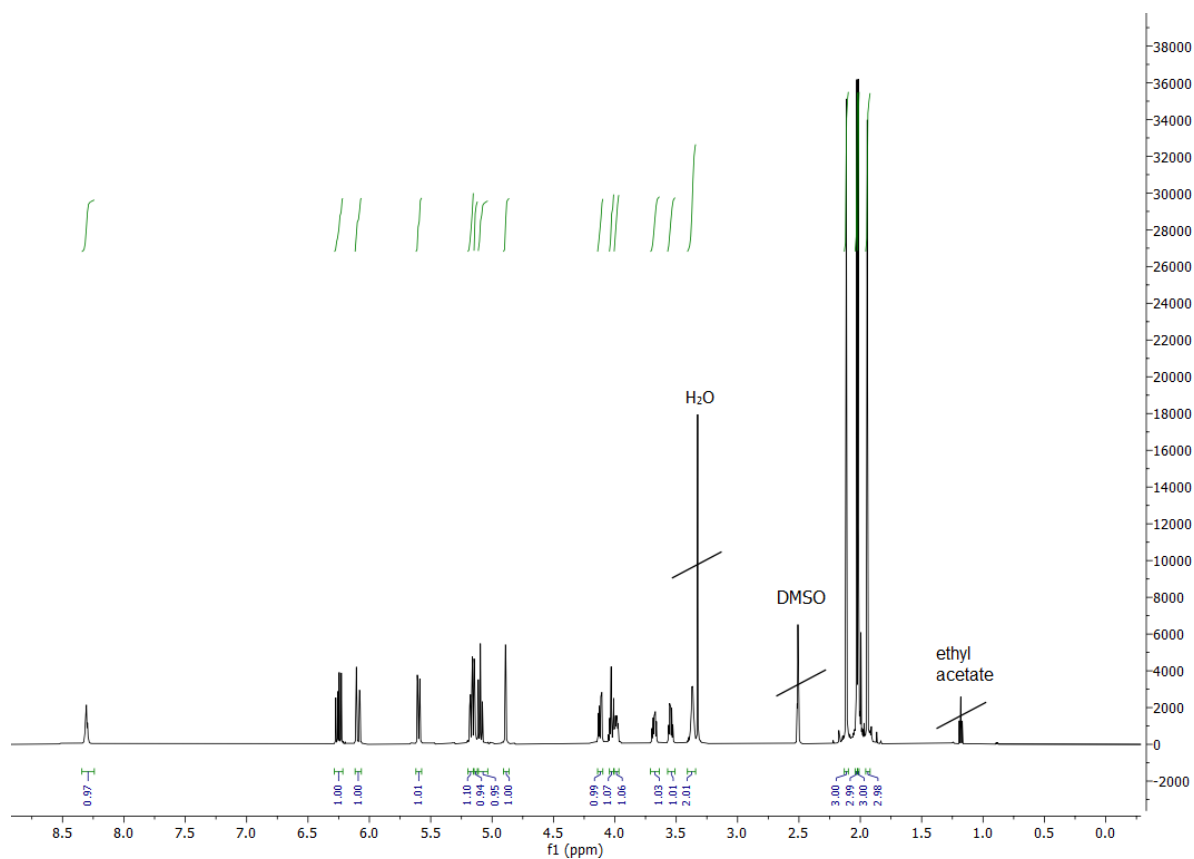


Figure S1e. ^1H -NMR (600 MHz, DMSO- d_6) AcManEAm.

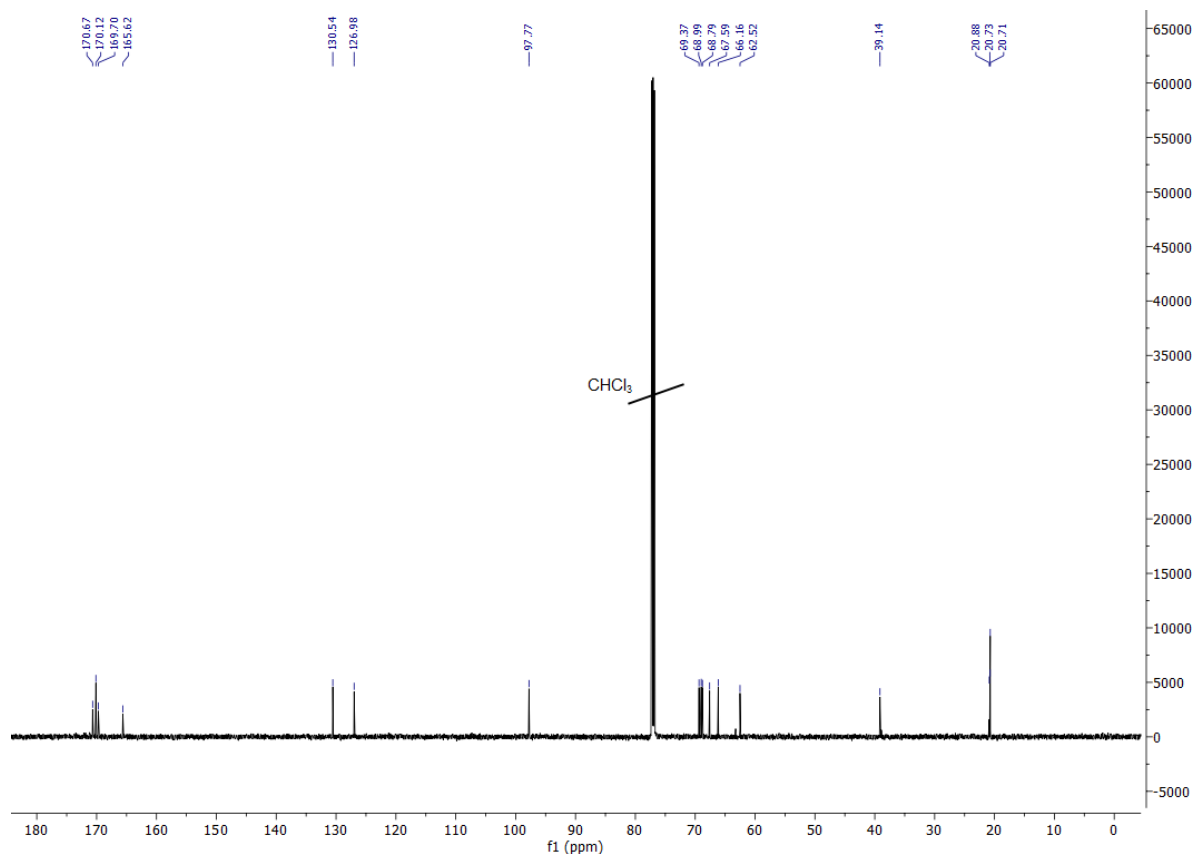
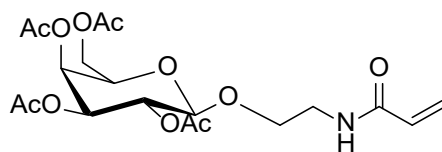


Figure S1f. ^{13}C -NMR (600 MHz, CDCl_3) AcManEAm.

The deprotection process of AcManEAm is the same process described for the deprotection of AcManEMAm.

N-ethylacrylamide- β -D-galactopyranoside (GalEAm)



Scheme S1d AcGalEAm

For the synthesis of 2'-acrylamidoethyl-2,3,4,6-tetra-O-acetyl- β -D-galactopyranose (AcGalEAm), 6,2 g (52,2 mmol) *N*-(2-Hydroxyethyl)-acrylamid and 20,6 g (51,7 mmol) 1,2,3,4,6-Penta-O-acetyl- β -D-Galactose are dissolved in 600 ml dichloromethane in a 1000 ml three-neck-flask. The reaction solution is cooled down to 0 °C and purged with nitrogen for 15 min. After a slow addition of 35 ml (278,7 mmol) boron trifluoride ethyl etherate, the solution is stirred for 48 h at room temperature. The organic layer is separated and washed with ice water, two times with saturated sodium hydrogen carbonate solution, brine and with ultrapure water. The washed organic layer is dried over magnesium sulfate. Dichloromethane is removed by distillation under vacuum and reduced pressure. The synthesized AcGalEAm is

purified by flash chromatography (Gradient: ethyl acetate/n-hexane 1:1 to pure n-hexane within 20 min). The yield of the remaining product is 14 % (3.63 g, 8.2 mmol).

^1H NMR (600 MHz, CDCl_3) δ 6.32 – 6.21 (m, 1H, $-\text{C}=\text{CH}_2$), 6.07 – 6.00 (m, 1H, $-\text{C}=\text{CH}_2$), 5.66 – 5.56 (m, 1H), 5.39 – 5.32 (m, 1H, $-\text{C}=\text{CH}_2$), 5.32 – 5.20 (m, 1H, H4), 5.14 – 5.06 (m, 1H, H2), 4.98 – 4.90 (m, 1H, H3), 4.47 (dd, $J=70.5, 7.9$ Hz, 1H, H1), 4.12 – 4.04 (m, 2H, H6), 4.04 – 4.00 (m, 1H, H5), 3.87 – 3.83 (m, 1H, $-\text{OCH}_2\text{CH}_2\text{NH}$), 3.74 – 3.63 (m, 1H, $-\text{OCH}_2\text{CH}_2\text{NH}$), 3.58 – 3.52 (m, 1H, $-\text{OCH}_2\text{CH}_2\text{NH}$), 3.43 (m, 1H, $-\text{OCH}_2\text{CH}_2\text{NH}$), 2.11 – 2.08 (m, 3H, $-\text{COCH}_3$), 2.00 – 1.98 (m, $-\text{COCH}_3$), 1.98 – 1.97 (m, 3H, $-\text{COCH}_3$), 1.94 – 1.92 (m, 3H, $-\text{COCH}_3$).

^{13}C NMR (600 MHz, CDCl_3) δ 170.41 (1C, $-\text{COCH}_3$), 170.18 (1C, $-\text{COCH}_3$), 170.08 (1C, $-\text{COCH}_3$), 169.81 (1C, $-\text{COCH}_3$), 165.47 (1C, $-\text{CONH}$), 130.69 (1C, COCHCH_2), 126.72 (1C, COCHCH_2), 101.49 (1C, C1), 70.89 (1C, C2), 70.69 (1C, C3), 69.15 (1C, C4), 68.97 (1C, C5), 66.98 (1C, $-\text{OCH}_2\text{CH}_2$), 61.40 (1C, C6), 39.18 (1C, NHCH_2CH_2), 20.86 (1C, $-\text{COCH}_3$), 20.69 (1C, $-\text{COCH}_3$), 20.67 (1C, $-\text{COCH}_3$), 20.58 (1C, $-\text{COCH}_3$).

MS for $\text{C}_{19}\text{H}_{27}\text{NO}_{11}$ (ESI) m/z $[\text{M} + \text{H}]^+$ calc. 446.2; found 446.2, $[\text{M} + \text{Na}]^+$ calc.: 468.1; found 468.2.

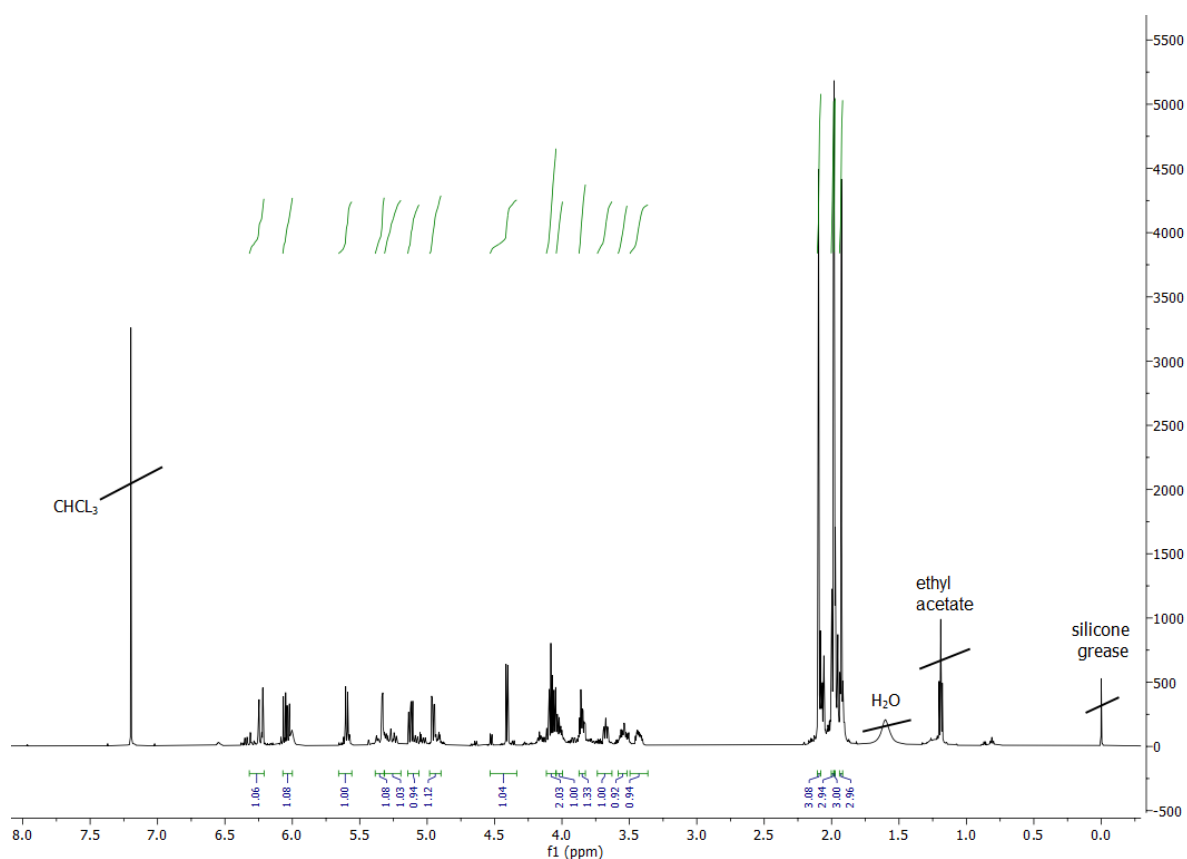


Figure S1g. ^1H -NMR (600 MHz, CDCl_3) AcGalEAm.

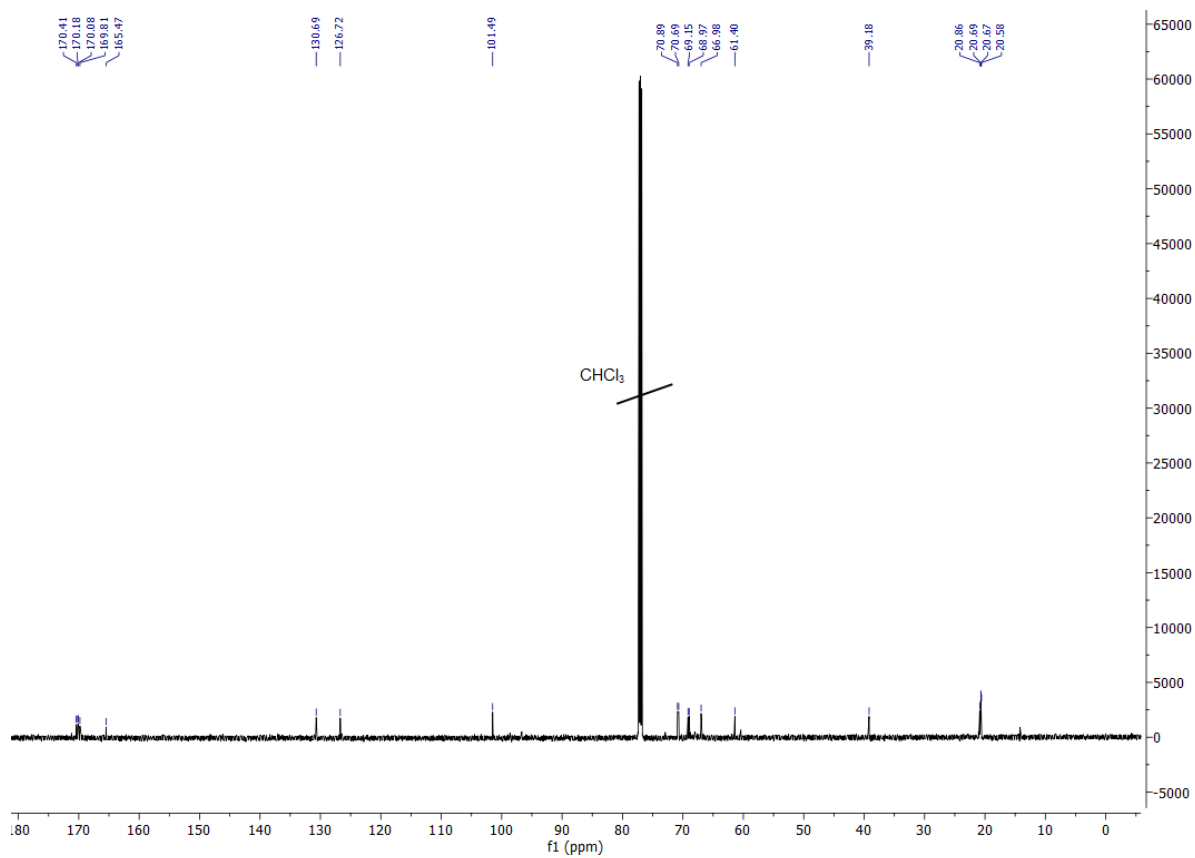


Figure S1h. ^{13}C -NMR (600 MHz, CDCl_3) AcGalEAm.

The deprotection process of AcGalEAm is the same process described for the deprotection of AcManEMAm.

S2 Bacteria attachment

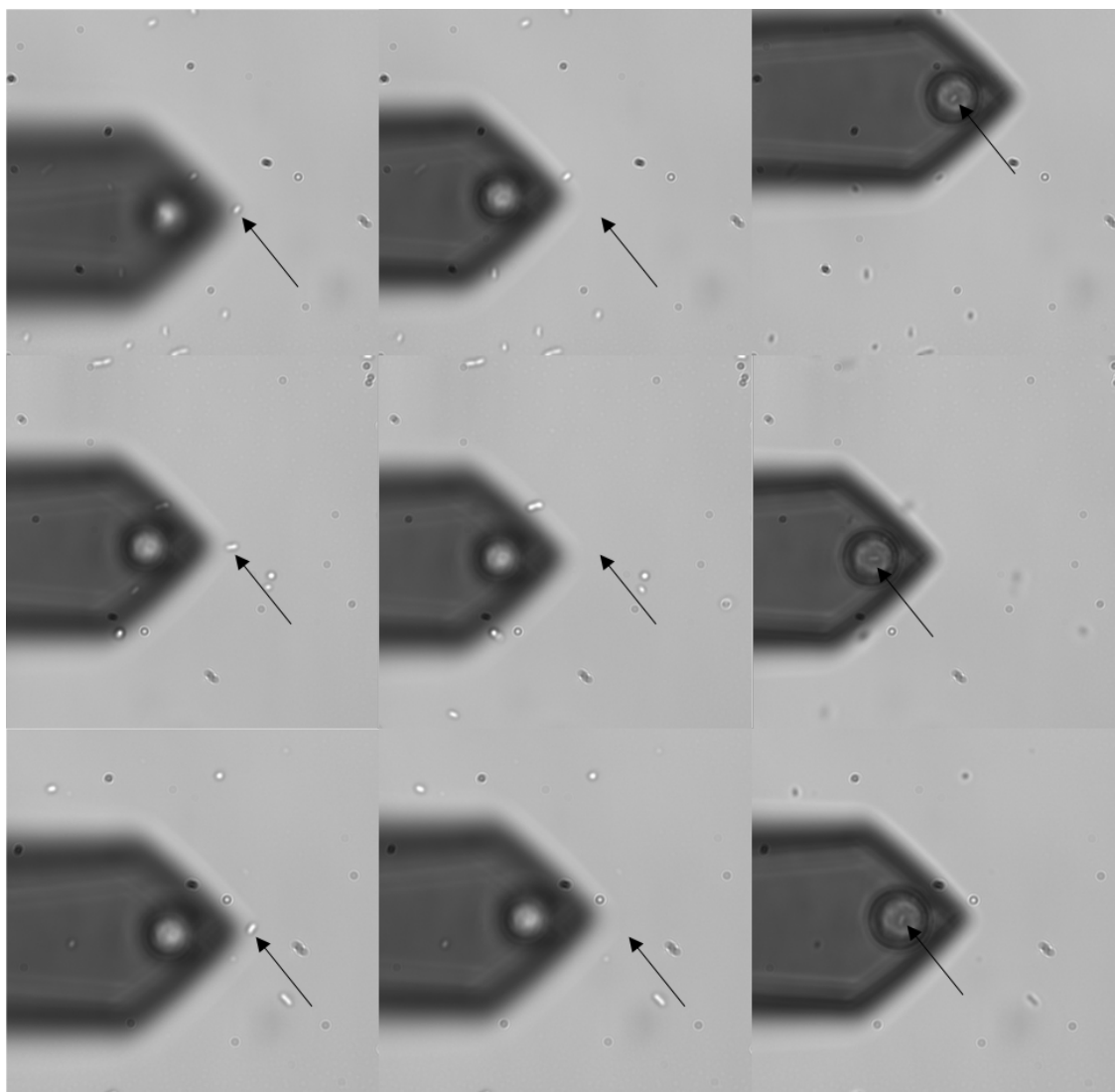


Figure S2: Bacteria attachment to the poly(L-dopa) coated colloidal probe (three examples). The left column shows the bacterium before attachment. The center column shows that the bacterium was “picked up” from the surface. The right column shows the bacterium at the colloidal probe.

S3 Variation of adhesion by attaching different bacteria

To determine the possible error between measurements with different bacteria, the results for pull-off force, work of adhesion and elongation distance were compared. The benchmark measurements were conducted at 20 °C against PNIPAM_{0.4} substrate.

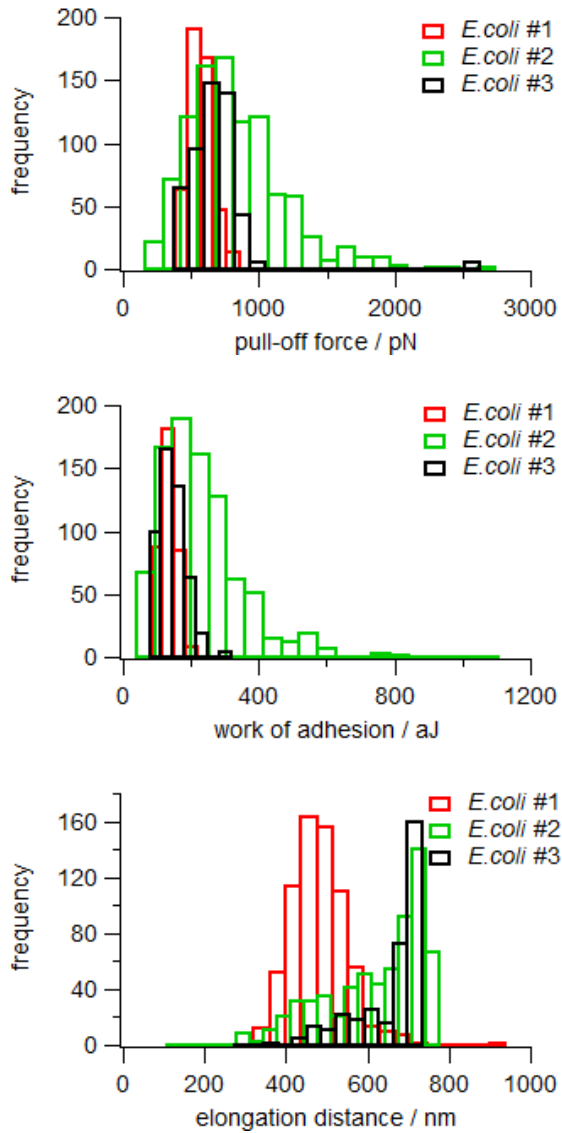


Figure S3: Histograms of measurements with 3 different *E.coli* bacteria on PNIPAM_{0.4} substrate.

Table S1. The average values and errors are summed up in the following table.

	<i>E. coli</i> #1	<i>E. coli</i> #2	<i>E. coli</i> #3	average	standard deviation [%]
pull-off force / pN	504	762	615	627	17
work of adhesion / 10^{-18} J	110	201	121	144	28
elongation distance / nm	460	588	620	556	12

S4 Temperature-dependent microgel swelling

The temperature dependent hydrodynamic radii were measured by dynamic light scattering (DLS)(Figure S4).

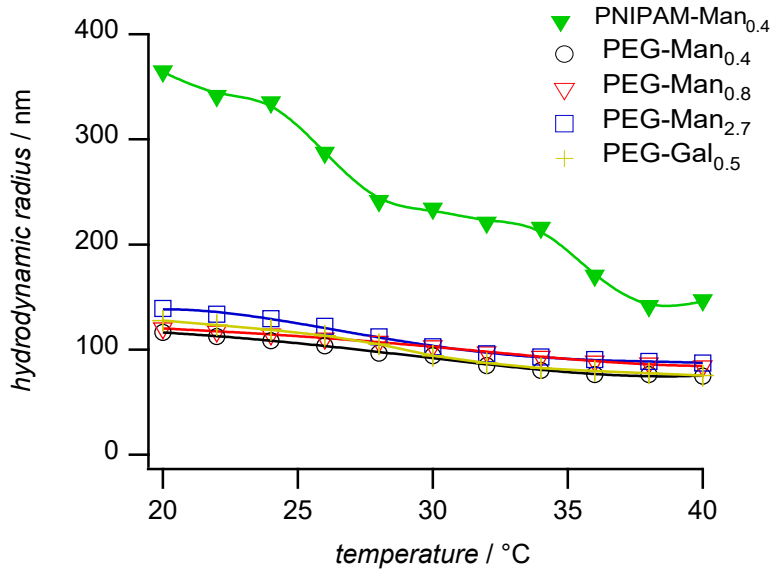


Figure S4: Swelling curves for all microgels used in this work.

Table S2: Hydrodynamic radii, PDI and the swelling ratio as measured by DLS

microgel sample	Rh at 20 °C [nm]	PDI (DLS)	swelling ratio (Rh _{20°C} /Rh _{40°C})
PNIPAM-Man _{0.4}	364	0.16	2.5
PEG-Man _{0.4}	113	0.069	1.8
PEG-Man _{0.8}	120	0.09	1.6
PEG-Man _{2.7}	139	0.115	1.5
PEG-Gal _{0.5}	128	0.072	1.7

S5 Indentation experiments

For the determination of the Young's modulus a force-volume map was taken using the JPK instrument software. From these maps force-deformation measurements at the center of the microgels can be selected (Figure S1). These traces were then fitted by the Hertz model:

$$F = \frac{4}{3} \frac{r_{tip}^{1/2}}{(1 - \nu^2)} E d^{3/2}$$

where r_{tip} is the radius of the AFM tip, ν the Poisson ratio, and E the Young's modulus of the microgel, F the force imposed by the AFM cantilever and d the sample deformation. The Hertz model proved to be valid for small tip-sample deformations (see fits in Figure S1). For larger deformations deviations from the Hertz model were present due to the crosslinking gradient of the microgels, which resulted in hard, highly crosslinked cores and soft, loosely crosslinked shells. The determined elastic moduli likely represent the moduli "felt" by the bacteria during adhesion measurements since the bacteria comes into contact mainly with the shell of the

microgels and the forces applied in the adhesion measurements were quite comparable to the force applied in the force-deformation measurements.

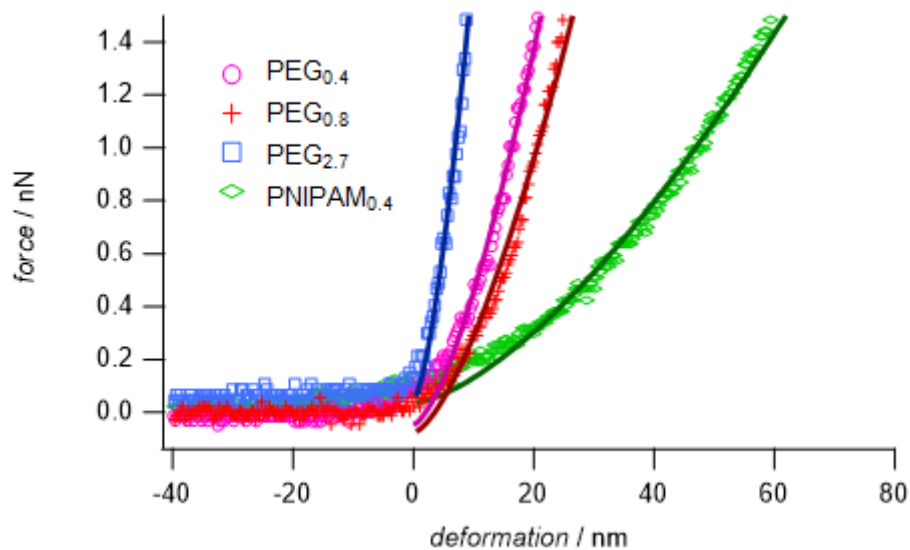


Figure S5: Exemplary force-deformation curves and Hertz fits

Table S3: Microgel elastic moduli

Sample	Young's modulus [MPa]
PEG _{0.4}	1.2 ± 0.4
PEG _{0.8}	1.0 ± 0.3
PEG _{2.7}	3.0 ± 0.8
PNIPAM _{0.4}	0.20 ± 0.06

S6 Exemplary force curves of measured samples and controls

Control measurements without bacteria (p(L-dopa) coated beads) on PNIPAM_{0.4} and with bacteria on non-binding PEG_{Gal} microgels.

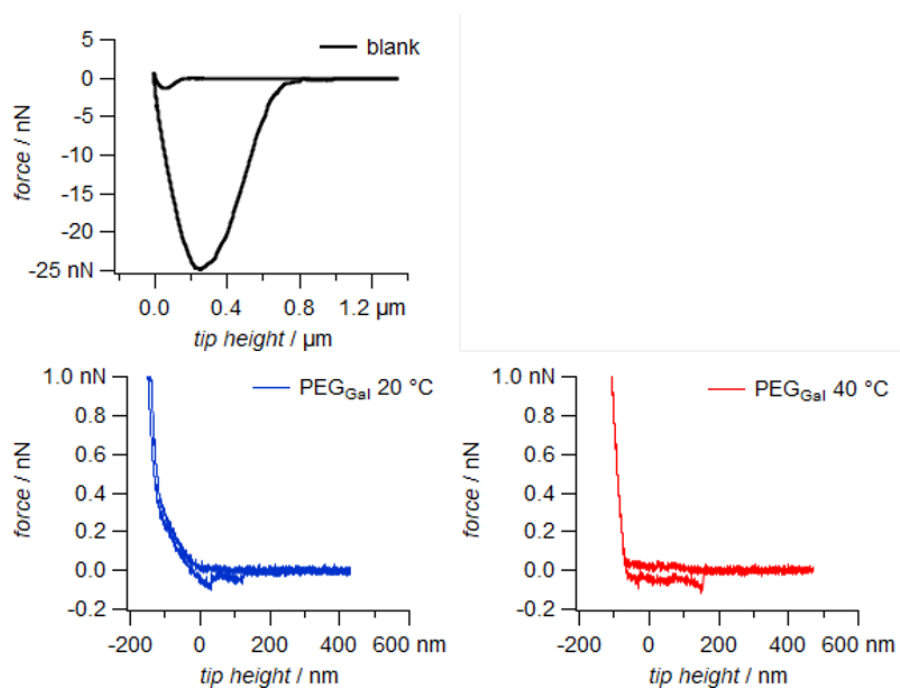


Figure S6a: Force curves of control measurements. Without bacteria, only a p(L-dopa) coated bead on PNIPAM_{0.4} substrate (black). With *E.coli* on PEG_{Gal} at different temperatures (blue: 20°C, red: 40°C).

Additional exemplary curves from measurements with *E.coli* on the different substrates.

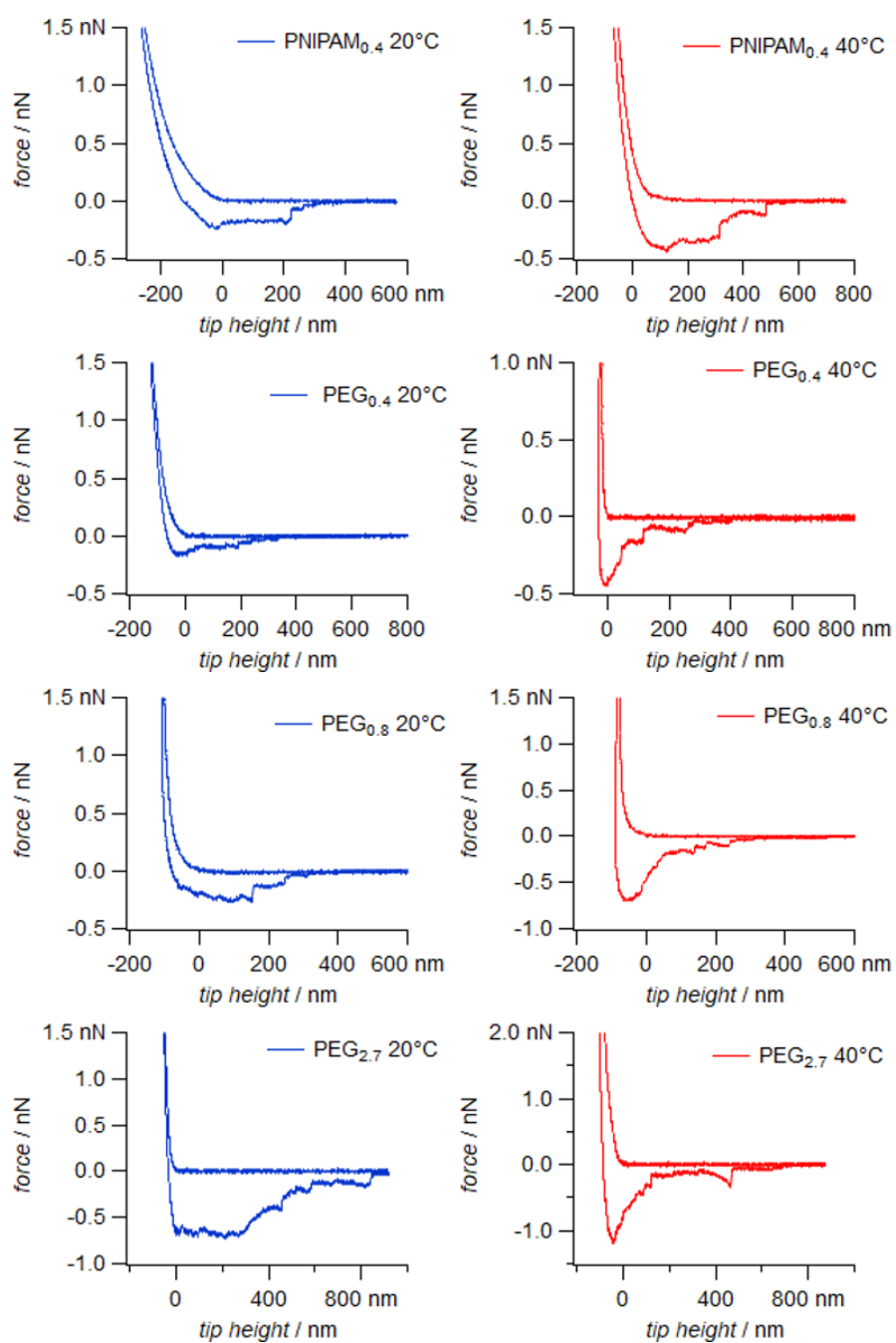


Figure S6b: Representative force curves taken from the measurements against the microgels used in this work at different temperatures (blue: 20°C, red: 40°C).

S7 Contact time dependence of adhesion

The adhesion depends on the contact time of the bacteria and the microgel as longer contact times increases the possibility of FimH receptors binding mannose ligands. In addition, larger contact times increase potential entanglement events. We have varied the contact time in a range between 1 to 5 seconds to test the resulting adhesion. This series of experiments was carried out with the same bacterium. The following figures show the rate of increase in adhesive force in relation to contact time. With increasing contact time an increase in maximum pull-off force and work of adhesion is observed as expected. Binding of FimH to mannose moieties becomes statistically more probable as time in proximity of the microgel surface increases. Also entanglement events increase as the bacterium is pressed for a longer period against the polymer network. The elongation does not change significantly between 1 and 5 seconds dwell time. As a very low amount of bonds between pili and loose ends on the microgel surface can be formed the combined binding strength is too low to extend the polymer chains and the pili to the full extent.

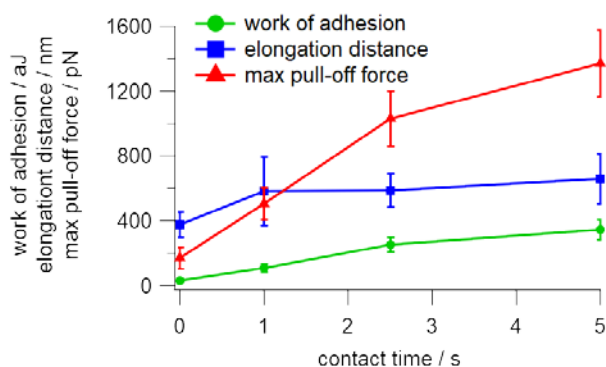


Figure S7: Maximum pull-off force and work of adhesion are affected by contact time, the detachment distance seems to be not.

4.2. Elastic modulus distribution in poly(N-isopropylacrylamide) and oligo(ethylene glycol methacrylate)-based microgels studied by AFM

Authors: **Dimitri Wilms**, Yanik Adler, Fabian Schröer, Lennart Bunnemann and Stephan Schmidt

Journal: Soft Matter

Issue: **2021**, 17, 5711

DOI: 10.1039/D1SM00291K

Impact Factor: 3.679 (2021-2022)

Own contribution (first author):

Collaborative establishing of synthesis route for self-crosslinked microgels from NIPAM and OEGMA. Synthesis, purification and characterization of microgels used in the experiments. Performing AFM high-resolution force mapping of microgel samples immobilized on solid substrate immersed in ddH₂O. Evaluation of acquired data consisting of Young's modulus calculation and special distribution calculation. Writing of first draft, collaborative visualization of the results and writing of first manuscript draft followed by collaborative finalization of the manuscript.

Reproduced with permission from Dimitri Wilms, Yanik Adler, Fabian Schröer, Lennart Bunnemann and Stephan Schmidt as well as the Royal Society of Chemistry, copyright © 2022.

DOI: 10.1039/D1SM00291K.



Cite this: *Soft Matter*, 2021, 17, 5711

Elastic modulus distribution in poly(*N*-isopropylacrylamide) and oligo(ethylene glycol methacrylate)-based microgels studied by AFM†

Dimitri Wilms, * Yanik Adler,  Fabian Schröer, Lennart Bunnemann and Stephan Schmidt

The spatial elastic modulus distribution of microgel networks in presence and absence of bifunctional crosslinkers is studied by AFM. Thermoresponsive poly(*N*-isopropylacrylamide) (PNIPAM) and poly(2-(2-methoxyethoxy)ethyl methacrylate-*co*-oligo(ethylene glycol)methacrylate) (P(MEO₂MA-*co*-OEGMA)) microgels are synthesized *via* precipitation polymerization above their lower critical solution temperature (LCST). High-resolution elastic modulus profiles are acquired using AFM force-indentation mapping of surface-deposited microgels at 25 °C. For both microgel systems, the use of a bifunctional crosslinker leads to a strong elastic modulus gradient with stiff microgel cores and soft networks toward the edge. In absence of a dedicated crosslinker (self-crosslinking), PNIPAM microgels show a homogeneous elastic modulus distribution, whereas self-crosslinked P(MEO₂MA-*co*-OEGMA) microgels still show decreasing elastic moduli from the centre to the edge of the microgels. However, POEGMA microgels without comonomer showed no elastic modulus gradient suggesting that different incorporation rates of MEO₂MA and OEGMA result in a radial variation of the polymer segment density. In addition, when varying the molecular weight of OEGMA the overall elastic modulus was affected, possibly due to molecular weight-dependent phase behavior and different reactivity. This shows that quite different microgel architectures can be obtained by the simple “one-pot” precipitation reaction of microgels which may open to new avenues toward advanced applications.

Received 25th February 2021,
Accepted 13th May 2021

DOI: 10.1039/d1sm00291k

rsc.li/soft-matter-journal

Introduction

Micro and nanoparticles composed of stimuli responsive polymers paved the way toward several promising applications, such as triggered drug delivery systems,^{1–5} materials with advanced optical properties,^{6,7} or bioactive coatings that are capable of responding to environmental parameters.^{8–13} A very prominent type of responsive microparticles are thermosensitive microgels composed of polymers with a lower critical solution temperature (LCST).¹⁴ When increasing the temperature above the LCST, the swollen microgels collapse due to the formation of polymer–polymer contacts and the partial removal of the hydration layer surrounding the polymer chains. In comparison to macroscopic polymer gels, microgels show a range of interesting properties, such as rapid and strong volume changes upon temperature variation, narrow size distribution, and straightforward processing toward coatings.^{15–18}

In addition, their synthesis *via* free radical polymerization is comparatively simple. Such microgels are often composed of polymers with an LCST in the physiological temperature range, *e.g.* poly(*N*-isopropylacrylamide) (PNIPAM) or 2-(2-methoxyethoxy)ethyl methacrylate and oligo(ethylene glycol) methacrylate (P(MEO₂MA-*co*-OEGMA)).^{14,19} In a single precipitation polymerization step in water above the polymer’s LCST, the monomers are reacted in presence of a crosslinker to form monodisperse microgels with diameters of a few hundred nanometers. For crosslinking, bifunctional acrylamides or acrylates are typically used. Since the crosslinkers are bivalent they tend to be incorporated at higher rates into the growing microgels during precipitation polymerization, leading to higher crosslinking in the microgel centre.^{20,21} The resulting microgels show a crosslinking density gradient, *i.e.* a stiff, highly crosslinked core with a soft and very fuzzy outer perimeter due to low crosslinking.^{22–24} For some applications, *e.g.* in drug release or tissue engineering, different network structures and higher overall deformability are required. To address these needs, hollow microgels and ultra-soft microgels have been developed.^{25,26} It has been shown that such microgel structures can be obtained by omitting bifunctional crosslinkers but instead using chain transfer

Institute for Organic Chemistry and Macromolecular Chemistry,
Heinrich-Heine-University, Universitätsstr. 1, 40225 Düsseldorf, Germany.
E-mail: dimitri.wilms@hhu.de

† Electronic supplementary information (ESI) available. See DOI: 10.1039/d1sm00291k

reactions to introduce crosslinks in the microgel network during the precipitation reaction procedure.²⁷ Such microgels can be considered “self-crosslinked” due to the absence of dedicated crosslinker molecules.

As of yet, such self-crosslinked, ultra-soft microgels were largely based on PNIPAM.^{26–30} For biomedical applications where the toxicity of the microgels’ degradation products is a concern,³¹ microgels with a polyethylene glycol (PEG)-based backbone are favoured instead.^{32,33} A pioneering study has confirmed the feasibility of self-crosslinked OEGMA-based microgels.²⁴ Therefore, in this study the network structure of self-crosslinked P(MEO₂MA-co-OEGMA) microgels of varying composition is investigated and compared to self-crosslinked PNIPAM microgels. In addition, a systematic comparison between self-crosslinked microgels and microgels crosslinked by bivalent crosslinkers is presented. As a tool to determine the network structure we use AFM force-indentation measurements, which give the elastic modulus of the microgel network and the crosslinking density at a resolution in the nanometer range.

Experimental section

Microgel synthesis

PNIPAM microgels with crosslinker were synthesized *via* surfactant-free non-stirred precipitation polymerization as described by Richtering and coworkers³⁴ (Table 1). *N*-Isopropylacrylamide (Sigma-Aldrich, >95%), *N,N'*-methylenebisacrylamide (Sigma-Aldrich, 99.5%) and ammonium peroxodisulfate (APS, Sigma-Aldrich, >99%) were used without further purification. For self-crosslinked PNIPAM microgels, NIPAM was dissolved in 20 mL ultra-pure water (1.4 mmol, 0.07 mol L⁻¹) and heated to 70 °C while purging with N₂ followed by adding APS dissolved in 1 mL ultra-pure water (0.06 mmol, 0.003 mol L⁻¹) after 30 min. The reaction was terminated by cooling in an ice bath after reacting at 70 °C under N₂ atmosphere for 16 h. To remove any unreacted or loose polymer the particles were washed by repeated centrifugation at 10 000g for 1 hour. In a final step the particles were freeze dried. Four different P(MEO₂MA-co-OEGMA) microgel samples were prepared by surfactant free emulsion polymerization. The presence of crosslinker (ethylene glycol

dimethacrylate, EGDMA), comonomer (MEO₂MA), and the molecular weight of OEGMA (300 g mol⁻¹, OEGMA₃₀₀ and 500 g mol⁻¹, OEGMA₅₀₀) was varied. OEGMA and EGMA (TCI Germany GmbH) the initiator potassium peroxodisulfate (KPS) and EGDMA (>95%, Sigma-Aldrich, Germany) were used without further purification. The monomers were dissolved in 84 mL of ultra-pure water and purged with N₂ for 30 min while stirring and heating to 80 °C followed by adding KPS dissolved in 1 mL ultra-pure water (0.255 mmol, 0.003 mol L⁻¹). The reaction was stopped after 6 hours by cooling down in an ice bath. The microgels were purified by repeated centrifugation at 10 000g for 2–3 hours.

Microgel surface deposition

Glass slides were cleaned by Hellmanex III solution and subsequently treated in a solution of water, hydrogen peroxide (30%) and ammonia (25%) at a 5:1:1 ratio at 70 °C for 30 min. After rinsing, the surfaces were used immediately for microgel deposition (0.1 wt%) *via* spin coating at 2000 rpm for 60 s.

Atomic force microscopy (AFM)

AFM measurements were performed on a JPK NanoWizard IV in quantitative imaging (QI™) mode with a setpoint force of 5 nN, a loading rate of about 175 μN s⁻¹ curve, and a sampling rate of 40 kHz. Cantilevers (HQ:XSC11/No Al, μMasch, Bulgaria) with a nominal spring constant of 7 N m⁻¹ were used. The AFM tip radius was obtained by imaging a porous alumina surface (PA01, μMasch, Bulgaria) and evaluation with Gwyddion.³⁵ Measurements were conducted in ultra-pure water at 20 °C. The obtained force–deformation maps were processed with the software provided by the AFM manufacturer to calculate the elastic modulus by fitting the approach cycle with the Hertzian model. To account for the limited thickness of the microgel layer selected force curves were fitted with the Dimitriadis model using the microgel thickness at the respective radial position to calculate corrected elastic moduli.³⁶ The fit range was limited by choosing a maximum indentation depth, which was up to 10–50% of the microgel thickness depending on how well the fits represented the data. Radial profiles of the elastic moduli maps from at least six similar-sized microgels were using the radial profile plugin for ImageJ.³⁷ Single pixels with elastic moduli greater than 100 MPa (outliers) were excluded from the analysis.

Results and discussion

High-resolution elastic modulus mapping

To determine the crosslinking gradient and the overall network structure we perform AFM nanoindentation measurements, which allow to map the elastic modulus on a nanometer scale. The elastic modulus can be directly related to the density of polymer crosslinks in a gel: The density of crosslinks in a polymer network with an average mesh width ξ is proportional to ξ^{-3} . According to de Gennes,^{38,39} for polymer networks in

Table 1 Composition of the microgel reaction mixture, the hydrodynamic radius (R_h) and the ratio of R_h above and below the LCST (swelling ratio) as measured by dynamic light scattering (DLS) (see ESI, S1). Microgels prepared without crosslinker (self-crosslinked) are termed “SCL”. Microgels prepared with crosslinker are termed according to the crosslinker (“BIS” or “EGDMA”)

Microgel sample	Monomer [mmol]	Crosslinker [mmol]	R_h [nm]	Swelling ratio
PNIPAM _{BIS}	6.19	0.32 (5 mol%)	350	2.5
PNIPAM _{SCL}	70	—	429	3.7
P(MEO ₂ MA-co-OEGMA ₃₀₀) _{SCL}	8.13/0.9 ^a	—	197	2.3
P(OEGMA ₃₀₀) _{SCL}	80.7	—	575	2.1
P(MEO ₂ MA-co-OEGMA ₅₀₀) _{EGDMA}	8.13/0.9 ^a	0.09 (1 mol%)	125	1.5
P(MEO ₂ MA-co-OEGMA ₅₀₀) _{SCL}	8.13/0.9 ^a	—	195	2.1

^a Ratio of OEGMA/MEO₂MA.

good solvents the concentration of polymer segments between crosslinks C scales with ξ as

$$\xi \sim C^{-3/4} \quad (1)$$

and the elastic modulus E is proportional to the density of crosslinks

$$E \sim \xi^{-3} \sim C^{9/4}. \quad (2)$$

Therefore, the polymer gel's elastic modulus as determined by AFM is a measure of the polymer segment concentration and crosslinking density of the gel. Previous work showed that AFM nanoindentation measurements on adsorbed BIS-crosslinked PNIPAM microgels reveal radial elastic modulus gradients, where higher elastic moduli were found in the centre of the microgels.^{9,22,40} Following these studies, the AFM investigations were also conducted with adsorbed microgels on glass slides in water. High-resolution AFM force–deformation mapping was performed followed by fitting the force-indentation traces with the Hertzian model of elastic contacts to obtain the elastic modulus E :

$$F = \frac{4r_{\text{tip}}^{1/2}d^{3/2}}{3(1-\nu^2)}, \quad (3)$$

where r_{tip} is the radius of the cantilever tip, ν the Poisson ratio, d the sample deformation, and F the applied force. This analysis yields high-resolution maps of the elastic modulus, e.g. for a P(MEO₂MA-co-OEGMA₅₀₀)_{SCL} microgel as shown in Fig. 1a. For further analysis, radial averages of the elastic moduli were calculated and plotted against the radial position where the origin is the centre of the microgels (Fig. 1b). To account for the finite thickness h of the microgel on the solid support, the force curves were additionally fitted using Dimitriadis' model (with ν set to 0.5) to obtain the corrected elastic modulus $E_{\text{corrected}}$:

$$F = f_{\text{correction}} \cdot \frac{16r_{\text{tip}}^{1/2}d^{3/2}}{9} E_{\text{corrected}}, \quad (4)$$

where $f_{\text{correction}}$ is defined as

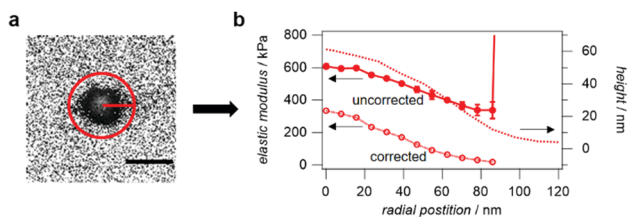


Fig. 1 High resolution elastic modulus maps and calculation of radial profiles. (a) An elastic modulus map of a single P(MEO₂MA-co-OEGMA₅₀₀)_{SCL} microgel particle (scale bar is 200 nm). The red circle indicates the range over which the elastic modulus distribution is averaged at certain radial positions to create a radial profile. (b) The resulting elastic modulus profile, ranging from the centre to the edge of the microgels (full circles, left axis). Additionally, the elastic modulus values were corrected according to the Dimitriadis model (hollow circles, left axis). The height profile was reconstructed from the high-resolution force maps (dashed line, right axis).

$$f_{\text{correction}} = 1 + 0.884\chi + 0.781\chi^2 + 0.386\chi^3 + 0.0048\chi^4, \quad (5)$$

with χ defined as

$$\chi = \frac{\sqrt{r_{\text{tip}}d}}{h}. \quad (6)$$

Selected force curves taken at certain radial positions giving similar (uncorrected) elastic moduli as compared to the radial averages were fitted again with the Dimitriadis model to obtain the corrected elastic modulus profiles (Fig. 1b).

Elastic modulus gradients of PNIPAM microgels

The well-studied BIS-crosslinked PNIPAM_{BIS} microgels were compared against self-crosslinked PNIPAM_{SCL} microgels prepared in absence of BIS where crosslinking takes place by chain transfer reactions. For an initial overview, three force–deformation curves taken at the centre, the very edge, and between the edge and centre are shown (Fig. 2a). The elastic moduli obtained at the centre of PNIPAM_{SCL} microgels were an order of magnitude smaller compared to PNIPAM_{BIS}, suggesting a reduced network density for PNIPAM_{SCL} due to the absence of a dedicated crosslinker (Table 2). An additional indication of the strongly reduced network density of PNIPAM_{SCL} is very their flat, pancake-like shape in the adhered state on the glass slide. Due to their higher crosslinking density adhered PNIPAM_{BIS} microgels attain truncated sphere shapes, with a peak height of 120 nm. As expected, the swelling behaviour of the microgels is affected by the overall

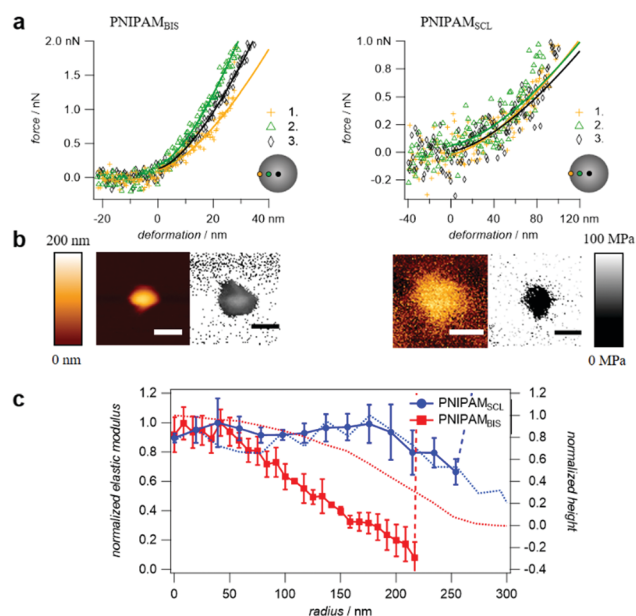


Fig. 2 The elastic moduli of deposited PNIPAM microgels as a function of the radial position. (a) Typical AFM force–distance measurements at the microgel centre (black), between centre and edge (blue) and the edge (red) for PNIPAM_{BIS} (left) and PNIPAM_{SCL} (right). (b) Typical topography and elastic modulus images of a single PNIPAM microgel. Scale bars: 200 nm. (c) Plot of the elastic modulus vs. the radial position calculated from at least five microgels using high-resolution elastic modulus mapping and height trace (dashed lines) reconstructed from vertical tip position during force map acquisition.

Table 2 Elastic moduli comparison from AFM indentation measurements taken at the microgels' apex

Microgel sample	Elastic modulus at centre [kPa]
PNIPAM _{BIS}	340 ± 10
PNIPAM _{SCL}	13 ± 3
P(MEO ₂ MA-co-OEGMA ₅₀₀) _{EGDMA}	63000 ± 500
P(MEO ₂ MA-co-OEGMA ₅₀₀) _{SCL}	850 ± 6
P(MEO ₂ MA-co-OEGMA ₃₀₀) _{SCL}	292 ± 2
P(OEGMA ₃₀₀) _{SCL}	123 ± 6

crosslinking density, where PNIPAM_{SCL} showed a significantly stronger collapse when increasing the temperature above the LCST (ESI,† S1). The detailed distribution of the elastic moduli and particle height on the solid surface was read from high-resolution AFM force maps. In agreement with recent work by Richtering and coworkers,²⁸ the PNIPAM_{SCL} microgels showed only small changes of the elastic modulus across the microgel, whereas the elastic modulus decreased toward the edge of PNIPAM_{BIS} microgels as found in earlier studies.^{9,22} From the apex to radii of about 50 nm, the elastic modulus of PNIPAM_{BIS} was constant indicating a homogeneous crosslinking density in the core region, which was also observed in scattering experiments and in super-resolution microscopy.^{41,42} However, here the core region appeared smaller owing to scanning only the microgel surface by AFM indentation. In absolute numbers, the elastic moduli of PNIPAM_{BIS} of 350 kPa in the microgel centre were a factor of 3 larger compared to previous work.^{9,28} The higher values could be attributed to several factors. For example, to achieve reasonable acquisition times of the high-resolution force maps, the force curves were recorded at high speed using loading rates on the order of 500 μN s⁻¹. Due to viscoelastic and hydrodynamic effects, the stiffness of hydrogels increases at high loading rates.^{43,44} In addition, the microgels were dried to immobilize them on the solid support. This may lead to an increase in network density even after rehydration since the network could stay partially adhered to the support. This results in overall increased elastic moduli compared to immobilization techniques that work without drying. Compared to previous work on self-crosslinked microgels,⁴⁵ here the molar ratio of NIPAM and peroxydisulfate initiator was 3-times larger leading to increased crosslinking and to a stiffness of the PNIPAM_{SCL} microgels. Overall, the results confirmed that PNIPAM_{BIS} radial density gradients owing to the increased incorporation rate of BIS compared to NIPAM. Microgels synthesized under self-crosslinking show a homogeneous segment concentration across the microgel.

Elastic modulus gradients of oligo(ethylene glycol)-based microgels

Different classes of oligo(ethylene glycol)-based microgels were prepared: (1) with comonomer and crosslinker (P(MEO₂MA-co-OEGMA)_{EGDMA}), (2) with comonomer and without crosslinker (P(MEO₂MA-co-OEGMA)_{SCL}), (3) without comonomer or crosslinker (POEGMA_{SCL}). In addition, the OEGMA molecular weight was varied (OEGMA₃₀₀, OEGMA₅₀₀). First the microgels synthesized with crosslinker and comonomer are discussed. Most frequently studied are P(MEO₂MA-co-OEGMA)_{EGDMA} microgels

with 1–5 mol% EGDMA crosslinker and a MEO₂MA/OEGMA ratio of about 9 : 1 because these microgels show an LCST in the physiological range and swelling properties that are comparable to PNIPAM_{BIS} microgels.¹⁹ Under the drying deposition method used here, the P(MEO₂MA-co-OEGMA₅₀₀)_{EGDMA} microgels showed large elastic moduli in the centre, on the order of 60 MPa, that were strongly decreasing toward the edge of the microgel (Fig. 3, left). Starting at a radial position of 50 nm, the elastic modulus trace showed an extended plateau where the elastic modulus was constant, about 20% compared to the maximum in the centre. This plateau coincides with a flat hairy-like structure seen in AFM images (ESI,† S4). The very high elastic modulus in the centre as well as the radial gradient in elastic modulus could be explained with the different reactivity of the three methacrylate reactants MEO₂MA, OEGMA₅₀₀ and EGDMA. MEO₂MA-rich domains with increased crosslinking density and stiffness are expected to form in the centre of the microgels owing to the increased reactivity of the crosslinker EGDMA, the fast diffusion rate and increased reactivity of the short monomer MEO₂MA, as well as the phase behaviour of MEO₂MA oligomers. EGDMA is known to exhibit an increased reactivity compared to BIS,⁴⁶ leading to small high-density cores and absence of an extended constant crosslinking region in the microgels centre. Regarding the phase behaviour, MEO₂MA oligomers have a lower LCST compared to OEGMA oligomers.⁴⁷ Therefore it is likely that stiff MEO₂MA-rich domains form in the beginning of the reaction that constitute the centre of the

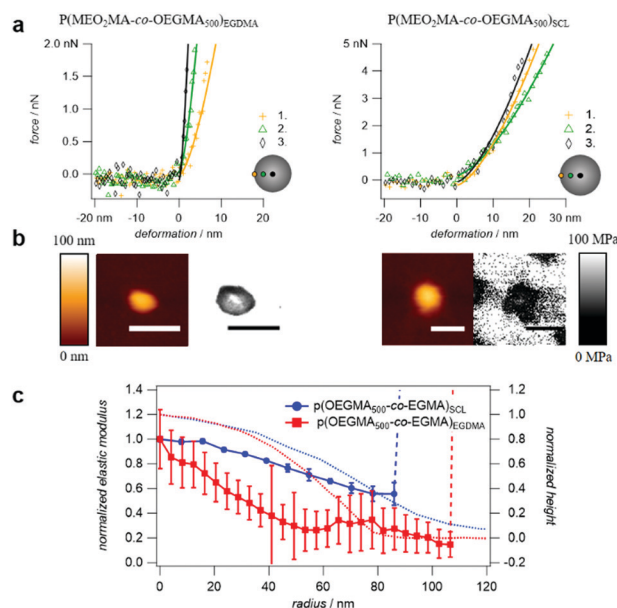


Fig. 3 The elastic moduli of P(MEO₂MA-co-OEGMA₅₀₀)_{EGDMA} and P(MEO₂MA-co-OEGMA₅₀₀)_{SCL} microgels as a function of the radial position. (a) Typical AFM force–distance measurements at the microgel centre (black), between centre and edge (blue) and the edge (red) for P(MEO₂MA-co-OEGMA)_{EGDMA} (right) and P(MEO₂MA-co-OEGMA₅₀₀)_{SCL} (left). (b) Typical topography and elastic modulus images of a single microgel. Scale bars: 200 nm. (c) Plot of the elastic modulus vs. the radial position calculated from at least six microgels using high-resolution elastic modulus mapping and height traces (dashed lines) reconstructed from vertical tip position during force map acquisition.

microgels. Indeed, using neutron scattering, Wellert and co-workers found high density inhomogeneities in EGDMA-crosslinked P(MEO₂MA-co-OEGMA) microgels which they interpreted as MEO₂MA rich-domains forming during the reaction.²¹ Overall, these results suggest that the observed radial elastic modulus gradients for P(MEO₂MA-co-OEGMA₅₀₀)_{EGDMA} microgels are not only due to the increased reactivity of the bivalent crosslinker but also due to different monomer diffusion rates and phase behaviour of the oligomeric methacrylates forming during the reaction.

To confirm this observation, we analysed the P(MEO₂MA-co-OEGMA₅₀₀)_{SCL} microgels prepared in absence of crosslinker while maintaining the 9 : 1 ratio between MEO₂MA and OEGMA monomers (Fig. 3, right). The absence of a bifunctional crosslinker resulted in overall softer microgels and also the very stiff core regions found in P(MEO₂MA-co-OEGMA₅₀₀)_{EGDMA} microgels were not present. Interestingly, the force curves and high-resolution maps showed a radial elastic modulus gradient although a crosslinker was absent (Fig. 3, right). The elastic modulus decreased to 60% from centre to edge, a lower gradient compared to microgels prepared with crosslinker. Both MEO₂MA and OEGMA₅₀₀ are monofunctional and have the same reactive groups. Therefore, the elastic modulus gradient is perhaps due to an increased diffusion rate of MEO₂MA compared to OEGMA₅₀₀ in addition to differences in phase behaviour of the various oligomers formed during the reaction (Fig. 5). Owing to the smaller LCST of MEO₂MA-rich oligomers compared to OEGMA-rich oligomers, MEO₂MA is incorporated faster in the seed particles formed at the early stages of the reaction. On the other hand, since OEGMA is incorporated at slower rates OEGMA-rich domains are formed at the outer radii of the microgels. Given the longer side chain and the increased sterical repulsion of OEGMA compared MEO₂MA a decreasing density of polymer segments and a lower elastic modulus toward the edge of the microgels is observed.

From the analysis of the self-crosslinked samples P(MEO₂MA-co-OEGMA₅₀₀)_{SCL} and PNIPAM_{SCL} one could expect that a homogeneous elastic modulus distribution can only be achieved by using a single type of monomer for microgel synthesis. To test this, we compared microgels prepared by homopolymerization, P(OEGMA₃₀₀)_{SCL}, with microgels prepared by copolymerization, P(MEO₂MA-co-OEGMA₃₀₀)_{SCL} (Fig. 4). OEGMA₃₀₀ readily forms monodisperse microgels by homopolymerization using the standard precipitation polymerization method.²⁴ This allows for the synthesis of poly(oligo ethylene) microgels consisting of only one, self-crosslinked monomer, which could not be achieved with OEGMA₅₀₀. Typical force curves at different positions on individual particles and high resolution force maps showed that P(OEGMA₃₀₀)_{SCL} had no elastic modulus gradient while the copolymerized microgel P(MEO₂MA-co-OEGMA₃₀₀)_{SCL} showed decreasing elastic moduli toward the edge of the microgels, quite similar to the P(MEO₂MA-co-OEGMA₅₀₀)_{SCL} microgels. The elastic modulus at the microgels' apex was larger for P(MEO₂MA-co-OEGMA₅₀₀)_{SCL} compared to P(MEO₂MA-co-OEGMA₃₀₀)_{SCL} (Table 2).

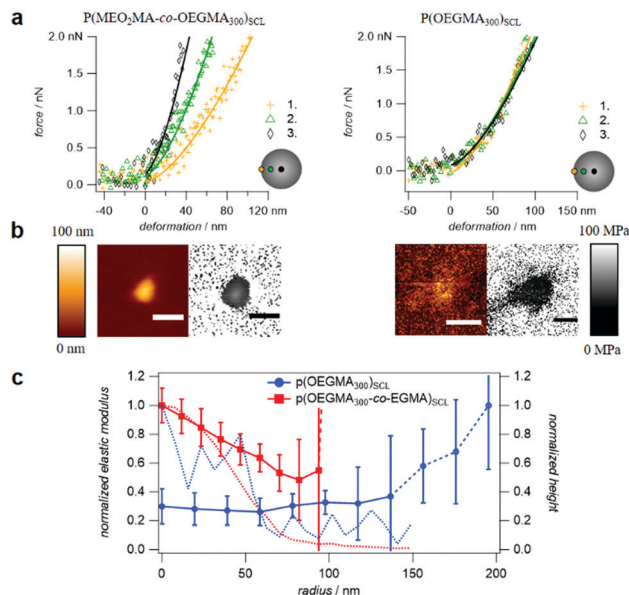
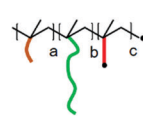
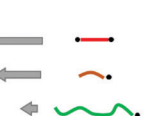
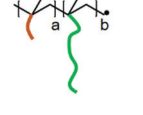
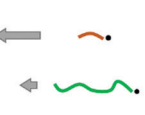
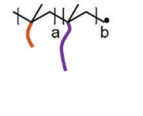
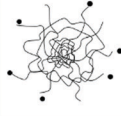
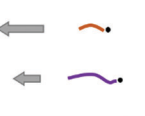
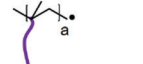


Fig. 4 The elastic moduli of P(MEO₂MA-co-OEGMA₅₀₀)_{SCL} and P(OEGMA₃₀₀)_{SCL} microgels as a function of the radial position. (a) AFM force-indentation measurements at the microgel centre (black) and edge (blue) and the edge (red) for P(MEO₂MA-co-OEGMA₃₀₀)_{SCL} (right) and P(OEGMA₃₀₀)_{SCL} (left). (b) Typical topography and elastic modulus images of a single microgel. Scalebars: 200 nm. (c) Plot of the elastic modulus vs. the radial position (left) calculated from at least five microgels using high-resolution elastic modulus mapping (right).

The increased elastic modulus of P(MEO₂MA-co-OEGMA₅₀₀)_{SCL} compared to P(MEO₂MA-co-OEGMA₃₀₀)_{SCL} could be explained by a reduced incorporation of OEGMA₅₀₀ in relation to OEGMA₃₀₀ since larger contents of OEGMA should lead to increased excluded volume and softer networks. A less effective incorporation of the larger OEGMA₅₀₀ monomer could be caused by a lower diffusion rate and lower reactivity owing to the increased molecular weight and sterical shielding. In addition, the different LCSTs of OEGMA₅₀₀-rich and OEGMA₃₀₀-rich oligomers⁴⁷ that may form to a certain extent at the beginning of the reaction may affect the overall incorporation of OEGMA. While OEGMA₅₀₀-rich oligomers have an LCST above the reaction temperature (80 °C) reducing their incorporation in the growing microgel networks, the OEGMA₃₀₀-rich oligomers have an LCST below the reaction temperature and undergo a phase transition enabling increased incorporation in the microgel network (Fig. 5). This leads to a higher OEGMA content and lower elastic moduli for P(MEO₂MA-co-OEGMA₃₀₀)_{SCL} microgels compared to P(MEO₂MA-co-OEGMA₅₀₀)_{SCL}.

Overall, quite different elastic moduli distributions prepared by radical precipitation polymerization of microgels can be achieved by varying the type and composition of monomers. Homogeneous crosslinking could only be achieved *via* self-crosslinking and homopolymerization. It was also notable that the elastic modulus of P(OEGMA₃₀₀)_{SCL} was lower compared to PNIPAM_{SCL} (Table 2). This is likely due to an increased amount of persulfate initiator for the synthesis of PNIPAM_{SCL} (1 mol%) compared to P(OEGMA₃₀₀)_{SCL} (0.5 mol%). The amount of initiator was chosen to obtain microgels of similar size, where

sample	monomers	various oligoradicals	growing microgel	monomer incorporation rate
$P(\text{MEO}_2\text{MA-co-OEGMA}_{500})_{\text{EGDMA}}$	EGDMA  MEO ₂ MA  OEGMA ₅₀₀  APS, T = 80 °C	 a >> b, T > LCST → a ~ b, T > LCST → a << b, T < LCST ✗ not precipitating		
$P(\text{MEO}_2\text{MA-co-OEGMA}_{500})_{\text{SCL}}$	MEO ₂ MA  OEGMA ₅₀₀  APS, T = 80 °C	 a >> b, T > LCST → a ~ b, T > LCST → a << b, T < LCST ✗ not precipitating		
$P(\text{MEO}_2\text{MA-co-OEGMA}_{300})_{\text{SCL}}$	MEO ₂ MA  OEGMA ₃₀₀  APS, T = 80 °C	 a >> b, T > LCST → a ~ b, T > LCST → a << b, T < LCST →		
$P(\text{OEGMA}_{300})_{\text{SCL}}$	OEGMA ₃₀₀  APS, T = 80 °C	 T > LCST →		

overall elastic modulus

Fig. 5 Overview of the proposed mechanisms for the elastic modulus gradient and the different overall elastic moduli of oligo(ethylene glycol)-based microgels. The reactivity and diffusion rate of MEO₂MA is larger when compared to OEGMA. In addition, MEO₂MA-rich oligomers have a low LCST, which leads to dense domains in presence of a bifunctional crosslinker and elastic modulus gradients when copolymerized with OEGMA even in absence of a crosslinker. Consequently, the homopolymerization of OEGMA₃₀₀ results in microgels without elastic modulus gradient. For $P(\text{MEO}_2\text{MA-co-OEGMA}_{300})_{\text{SCL}}$ all possible oligomers that can form have an LCST below 80 °C whereas OEGMA₅₀₀-rich oligomers have an LCST above 80 °C and do not precipitate during the reaction. Considering the larger reactivity of OEGMA₃₀₀ when compared to OEGMA₅₀₀ this leads to an increased OEGMA₃₀₀ incorporation and lower overall elastic moduli for $P(\text{MEO}_2\text{MA-co-OEGMA}_{300})_{\text{SCL}}$ when compared to $P(\text{MEO}_2\text{MA-co-OEGMA}_{500})_{\text{SCL}}$.

adding more initiator typically leads to a size increase.³⁴ Nevertheless the increased elastic modulus for $\text{PNIPAM}_{\text{SCL}}$ may be due to intrinsic effects, *e.g.* the large side chains of the OEGMA₃₀₀ may add to free volume and an overall lower density of polymer segments compared to NIPAM. In addition, the amide groups in PNIPAM are likely to interact due to hydrogen bonding, whereas OEGMA₃₀₀ lacks hydrogen bond donating groups thus showing a lower network density and a lower elastic modulus.

Conclusions

We aimed to investigate the spatial elastic modulus distribution of soft colloidal thermoresponsive microgels adsorbed at a solid surface as a function of the monomer composition. For this purpose, two classes of microgels composed of PNIPAM or $P(\text{MEO}_2\text{MA-co-OEGMA})$ were prepared in absence or presence of a bifunctional crosslinker. Elastic modulus maps were collected by high-resolution AFM force-indentation measurements. The studied PNIPAM microgel systems confirmed previous results, *i.e.* the presence of a crosslinker results in a strong radial elastic modulus gradient with decreasing elastic modulus from centre to edge,²³ whereas self-crosslinked PNIPAM microgels showed no elastic modulus gradient.²⁸ The elastic modulus gradients obtained for the crosslinker are likely due to the increased reactivity compared to NIPAM owing to the bivalent

structure of the crosslinker. On the other hand, self-crosslinked $P(\text{MEO}_2\text{MA-co-OEGMA})$ showed a clear elastic modulus gradient, suggesting that MEO₂MA is incorporated at higher rates compared to OEGMA. This leads to enrichment of OEGMA at the outer perimeter of the microgels and lower elastic moduli from centre to edge due to the increased excluded volume of OEGMA compared to MEO₂MA. Consequently, in absence of MEO₂MA, the homopolymerization of OEGMA leads to microgels without elastic modulus gradient and very soft networks compared to self-crosslinked PNIPAM microgels due to the absence of hydrogen bonding between the polymer segments. Upon varying the molecular weight of OEGMA the elastic modulus of $P(\text{MEO}_2\text{MA-co-OEGMA})$ can be tuned further, where increased chain lengths lead to a decreased incorporation of OEGMA and increased stiffness. This might be due to a combination of effects, such as differences in reactivity and phase behaviour upon varying the OEGMA molecular weight. Importantly, $P(\text{MEO}_2\text{MA-co-OEGMA})$ microgels synthesized with bifunctional crosslinkers showed very stiff cores, which are likely due to phase separation of MEO₂MA during the reaction as observed earlier.²¹ This overall shows that quite different network architectures can be established by mere variation of the monomer composition *via* a simple one-step precipitation reaction procedure. This may offer new prospects toward microgels and coatings with well-defined nanometer-scale material properties for advanced applications.

Conflicts of interest

There are no conflicts to declare.

Acknowledgements

The authors acknowledge funding by the German Research foundation (DFG) in the project SCHM 2748/5-1. We thank Prof. Dr. Matthias Karg (Institute of Physical Chemistry I, Heinrich-Heine-University Duesseldorf) for providing the instrumentation for the high-resolution elastic modulus mapping.

References

- 1 B. Sung, M. H. Kim and L. Abelmann, *Bioeng. Transl. Med.*, 2021, **6**, e10190, DOI: 10.1002/btm2.10190.
- 2 A. S. Caldwell, B. A. Aguado and K. S. Anseth, *Adv. Funct. Mater.*, 2020, **30**.
- 3 H. Bysell, R. Mansson, P. Hansson and M. Malmsten, *Adv. Drug Delivery Rev.*, 2011, **63**, 1172–1185.
- 4 G. Agrawal, R. Agrawal and A. Pich, *Part. Part. Syst. Charact.*, 2017, **34**, 1700132.
- 5 W. Chen, Y. Hou, Z. Tu, L. Gao and R. Haag, *J. Controlled Release*, 2017, **259**, 160–167.
- 6 M. Karg, A. Pich, T. Hellweg, T. Hoare, L. A. Lyon, J. J. Crassous, D. Suzuki, R. A. Gumerov, S. Schneider, I. I. Potemkin and W. Richtering, *Langmuir*, 2019, **35**, 6231–6255.
- 7 N. Li, P. Zhao and D. Astruc, *Angew. Chem., Int. Ed.*, 2014, **53**, 1756–1789.
- 8 J. Liang, H. Wang and M. Libera, *Biomaterials*, 2019, **204**, 25–35.
- 9 S. Schmidt, M. Zeiser, T. Hellweg, C. Duschl, A. Fery and H. Möhwald, *Adv. Funct. Mater.*, 2010, **20**, 3235–3243.
- 10 T. J. Paul, S. Rübél, M. Hildebrandt, A. K. Strzelczyk, C. Spormann, T. K. Lindhorst and S. Schmidt, *ACS Appl. Mater. Interfaces*, 2019, **11**, 26674–26683.
- 11 F. Schröer, T. J. Paul, D. Wilms, T. H. Saatkamp, N. Jäck, J. Müller, A. K. Strzelczyk and S. Schmidt, *Molecules*, 2021, **26**(2), 263, DOI: 10.3390/molecules26020263.
- 12 D. Wilms, F. Schröer, T. J. Paul and S. Schmidt, *Langmuir*, 2020, **36**(42), 12555–12562.
- 13 K. Uhlig, T. Wegener, J. He, M. Zeiser, J. Bookhold, I. Dewald, N. Godino, M. Jaeger, T. Hellweg, A. Fery and C. Duschl, *Biomacromolecules*, 2016, **17**, 1110–1116.
- 14 A. Pich and W. Richtering, in *Chemical Design of Responsive Microgels*, ed. A. Pich and W. Richtering, Springer-Verlag Berlin, Berlin, 2010, vol. 234, pp. 1–37.
- 15 T. J. Paul, A. K. Strzelczyk and S. Schmidt, *Macromol. Biosci.*, 2021, **21**(4), 2000386, DOI: 10.1002/mabi.202000386.
- 16 D. Suzuki, K. Horigome, T. Kureha, S. Matsui and T. Watanabe, *Polym. J.*, 2017, **49**, 695–702.
- 17 M. Cors, O. Wrede, A.-C. Genix, D. Anselmetti, J. Oberdisse and T. Hellweg, *Langmuir*, 2017, **33**, 6804–6811.
- 18 S. Schmidt, T. Hellweg and R. von Klitzing, *Langmuir*, 2008, **24**, 12595–12602.
- 19 T. Cai, M. Marquez and Z. Hu, *Langmuir*, 2007, **23**, 8663–8666.
- 20 K. Kratz, T. Hellweg and W. Eimer, *Polymer*, 2001, **42**, 6631–6639.
- 21 K. Gawlitza, A. Radulescu, R. von Klitzing and S. Wellert, *Polymer*, 2014, **55**, 6717–6724.
- 22 A. Burmistrova, M. Richter, C. Uzum and R. von Klitzing, *Colloid Polym. Sci.*, 2011, **289**, 613–624.
- 23 S. Backes and R. Von Klitzing, *Polymers*, 2018, **10**.
- 24 N. Welsch and L. A. Lyon, *PLoS One*, 2017, **12**, e0181369.
- 25 J. Dubbert, T. Honold, J. S. Pedersen, A. Radulescu, M. Drechsler, M. Karg and W. Richtering, *Macromolecules*, 2014, **47**, 8700–8708.
- 26 O. L. Virtanen, A. Mourran, P. T. Pinard and W. Richtering, *Soft Matter*, 2016, **12**, 3919–3928.
- 27 J. Gao and B. J. Frisken, *Langmuir*, 2003, **19**, 5217–5222.
- 28 M. F. Schulte, S. Bochenek, M. Brugnioni, A. Scotti, A. Mourran and W. Richtering, *Angew. Chem., Int. Ed.*, 2021, **60**, 2280–2287.
- 29 J. Gao and B. J. Frisken, *Langmuir*, 2003, **19**, 5212–5216.
- 30 H. Bachman, A. C. Brown, K. C. Clarke, K. S. Dhada, A. Douglas, C. E. Hansen, E. Herman, J. S. Hyatt, P. Kodlekere, Z. Y. Meng, S. Saxena, M. W. Spears, N. Welsch and L. A. Lyon, *Soft Matter*, 2015, **11**, 2018–2028.
- 31 M. A. Cooperstein and H. E. Canavan, *Biointerphases*, 2013, **8**, 19.
- 32 J.-F. Lutz, Ö. Akdemir and A. Hoth, *J. Am. Chem. Soc.*, 2006, **128**, 13046–13047.
- 33 K. Susumu, B. C. Mei and H. Mattoussi, *Nat. Protoc.*, 2009, **4**, 424–436.
- 34 O. L. J. Virtanen and W. Richtering, *Colloid Polym. Sci.*, 2014, **292**, 1743–1756.
- 35 D. Nečas and P. Klapetek, *Open Phys.*, 2012, **10**, 181–188.
- 36 E. K. Dimitriadis, F. Horkay, J. Maresca, B. Kachar and R. S. Chadwick, *Biophys. J.*, 2002, **82**, 2798–2810.
- 37 P. Carl, Radial Profile Plugin Extended, <http://questpharma.u-strasbg.fr/html/radial-profile-ext.html>, (accessed 12.12.2020, 2020).
- 38 M. Daoud, J. P. Cotton, B. Farnoux, G. Jannink, G. Sarma, H. Benoit, C. Duplessix, C. Picot and P. G. de Gennes, *Macromolecules*, 1975, **8**, 804–818.
- 39 P. G. De Gennes, *Macromolecules*, 1976, **9**, 587–593.
- 40 G. Li, I. Varga, A. Kardos, I. Dobryden and P. M. Claesson, *Langmuir*, 2021, **37**(5), 1902–1912.
- 41 M. Stieger, W. Richtering, J. S. Pedersen and P. Lindner, *J. Chem. Phys.*, 2004, **120**, 6197–6206.
- 42 S. Bergmann, O. Wrede, T. Huser and T. Hellweg, *Phys. Chem. Chem. Phys.*, 2018, **20**, 5074–5083.
- 43 D. Pussak, D. Ponader, S. Mosca, T. Pompe, L. Hartmann and S. Schmidt, *Langmuir*, 2014, **30**, 6142–6150.
- 44 A. Rubiano, C. Galitz and C. S. Simmons, *Tissue Eng., Part C*, 2019, **25**, 619–629.
- 45 M. F. Schulte, A. Scotti, M. Brugnioni, S. Bochenek, A. Mourran and W. Richtering, *Langmuir*, 2019, **35**, 14769–14781.
- 46 K. Kratz, A. Lapp, W. Eimer and T. Hellweg, *Colloids Surf., A*, 2002, **197**, 55–67.
- 47 J.-F. Lutz, *J. Polym. Sci., Part A: Polym. Chem.*, 2008, **46**, 3459–3470.

Supporting Information

Elastic modulus distribution in poly(*N*-isopopylacrylamide) and oligo(ethylene glycol methacrylate) microgels studied by AFM

Dimitri Wilms¹, Yanik Adler¹, Fabian Schröer¹, Lennart Bunnemann¹, Stephan Schmidt¹

¹ Institute for Organic Chemistry and Macromolecular Chemistry, Heinrich-Heine-University, Universitätsstr. 1 40225 Düsseldorf Germany

Hydrodynamic Radius R_h via dynamic light scattering measurements

The analysis of size and swelling behavior was done in solution of 0.5 wt% microgel sample in ultra-pure water. The measurements were conducted on a Zetasizer Nano Series Nano ZS (Malvern GmbH, Germany) at a wavelength of 633 nm and a backscattering angle of 173°. Swelling behavior was determined by measuring size at temperatures between 14 °C and 54 °C. Size was recorded at 2 °C steps with an equilibration time of 20 min.

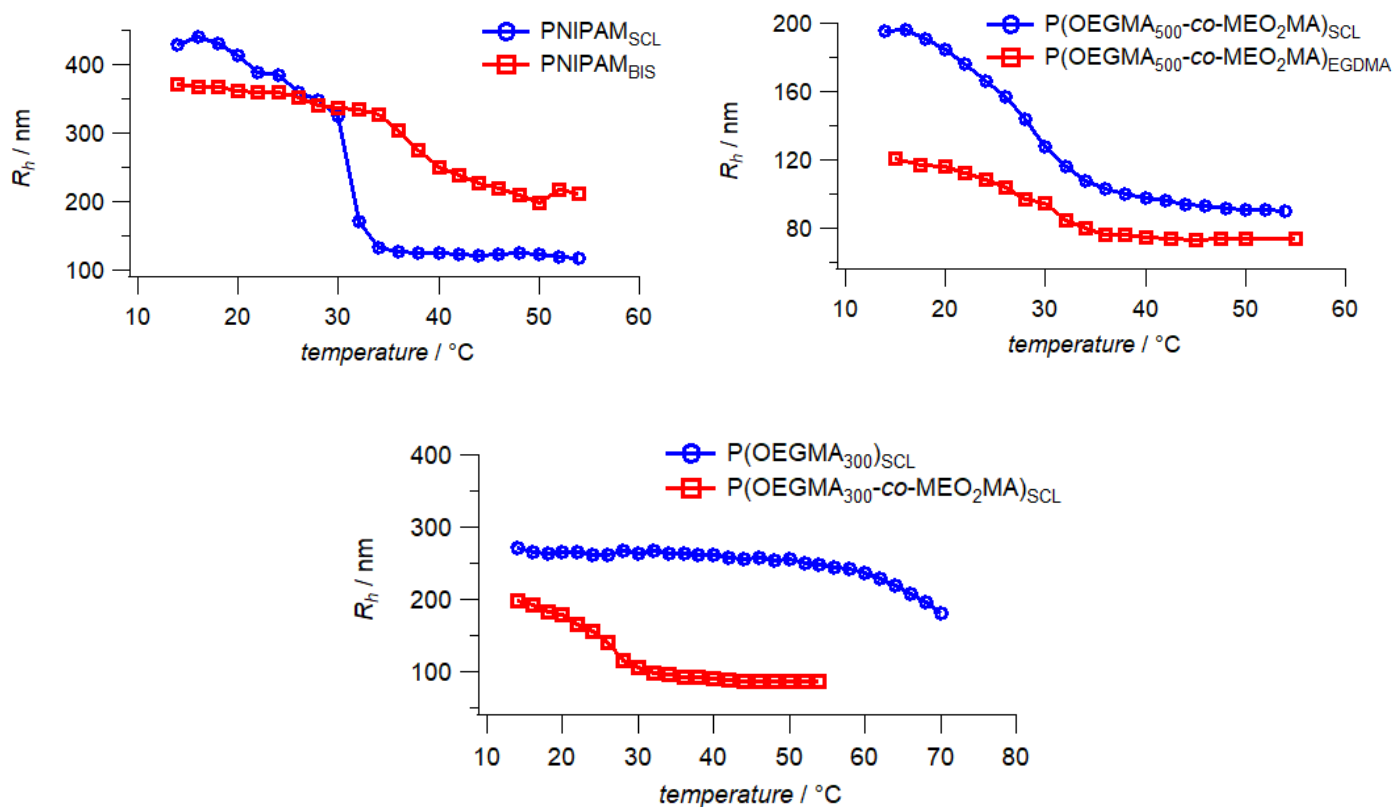


Figure S1 Summary of swelling curves of all samples.

Atomic force microscopy (AFM), elastic modulus profiles showing absolute values

AFM measurements were performed on a JPK Bruker NanoWizard IV in quantitative imaging (QI™) mode with a set point force of 5 nN and 20 s acquisition time per force curve. Cantilevers (HQ:XSC11/No Al, μ Masch, Bulgaria) with a nominal spring constant of 7 N/m were used, the force curves were acquired with a loading rate of 125 μ N/s. The AFM tip radius was obtained by imaging a porous alumina surface (PA01, μ Masch, Bulgaria) and evaluation with Gwyddion. Resulting radii were 25 ± 3 nm. Measurements were conducted in ultra-pure water at 20 °C. To submerge the coated surfaces were placed in a petri dish filled with ultra-pure water and let to equilibrate for 15 min. The obtained force-deformation maps were processed with the software provided by the AFM manufacturer to calculate the elastic modulus by fitting the approach cycle with the Hertz-Sneddon equation. Radial profiles of the elastic moduli were extracted from the resulting elastic modulus maps using the radial profile plugin for ImageJ.

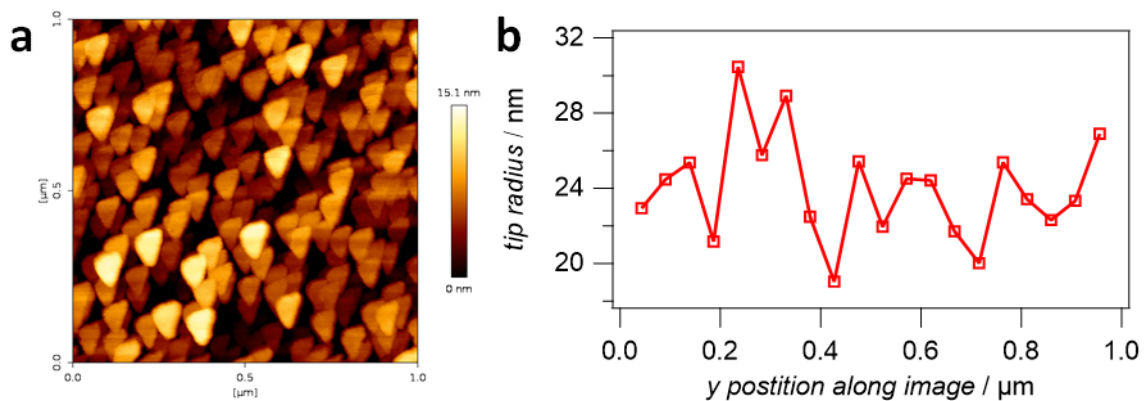


Figure S2 Tip reconstruction from porous alumina surface scan. a) Height image of the probe surface, b) calculated tip radius from separate sections of the image.

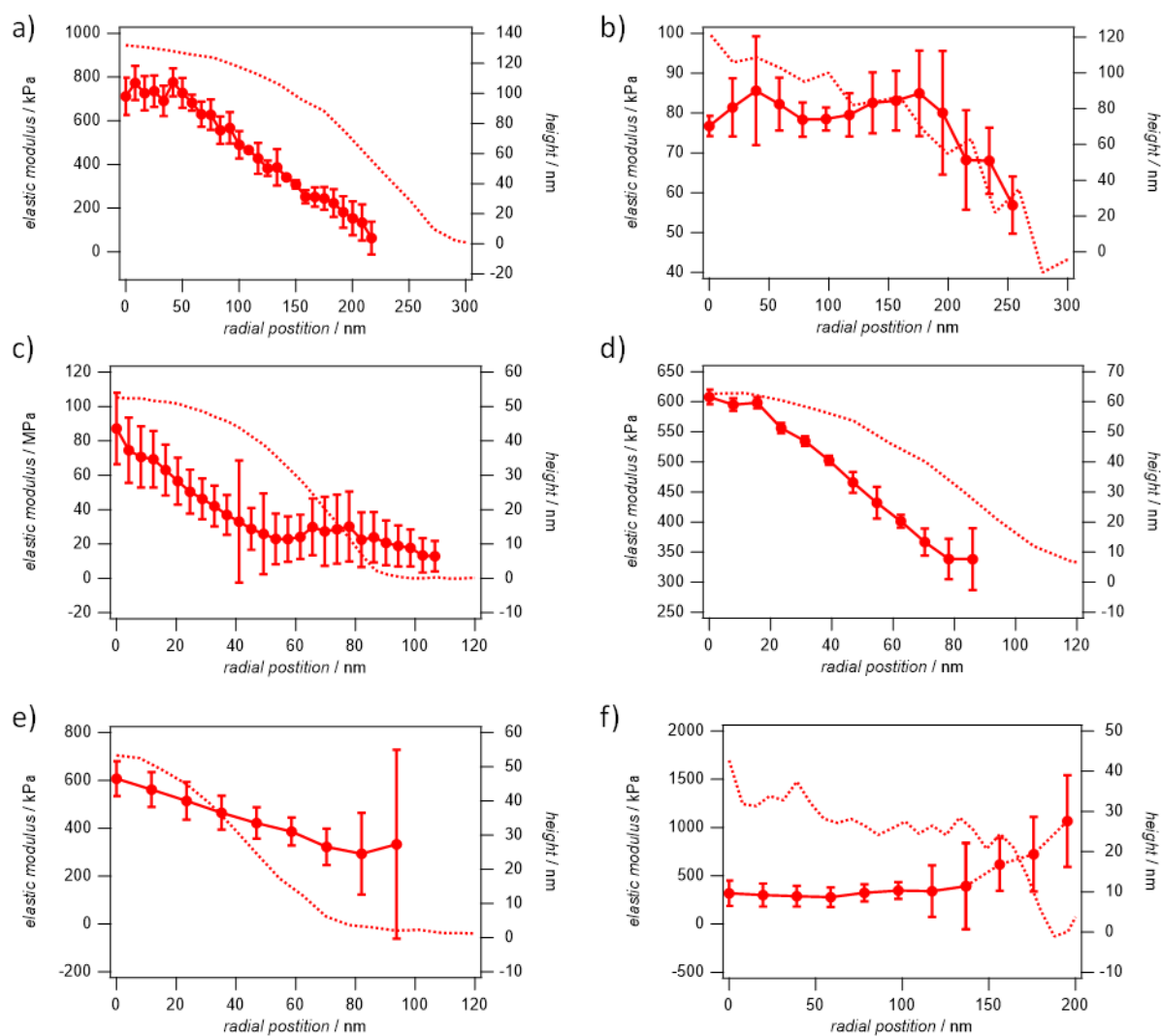


Figure S3 Summary of elastic moduli of all microgels as a function of the radial position. Plot of the elastic modulus vs. the radial position (left) calculated from at least six microgels using high-resolution elastic modulus mapping (right). The samples are ordered as follows: a) PNIPAM_{BIS}; b) PNIPAM_{SCL}; c) P(MEO₂MA-*co*-OEGMA₅₀₀)_{EGDMA}; d) P(MEO₂MA-*co*-OEGMA₅₀₀)_{SCL}; e) P(MEO₂MA-*co*-OEGMA₃₀₀)_{SCL}; f) P(OEGMA₃₀₀)_{SCL}.

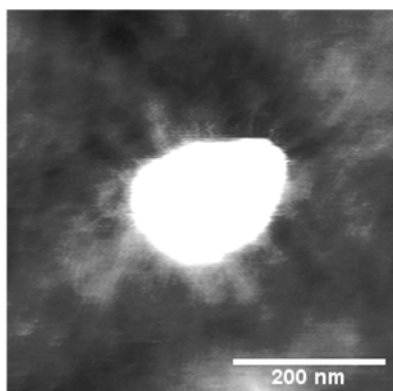
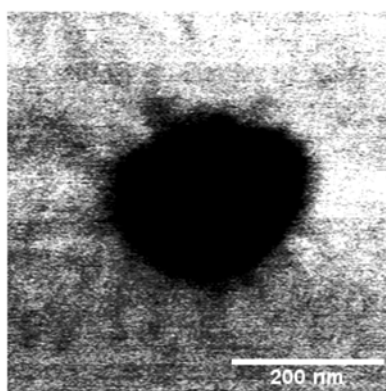
a**b**

Figure S4: a) Height image and b) phase image of $P(\text{MEO}_2\text{MA-co-OEGMA}_{500})_{\text{EGDMA}}$ microgels deposited on solid surface. The image was acquired in intermittent contact mode, the sample was submerged in ultra-pure water.

4.3. Specific binding of ligand-functionalized thermoresponsive microgels: Effect of microgel architecture, ligand density, and ligand hydrophobicity

Authors: **Dimitri Wilms**, Anselm Urach, Fabian Schröer and Stephan Schmidt

In preparation

Own contribution (first author):

Collaborative establishing of synthesis route for self-crosslinked microgels from NIPAM and OEGMA loaded with mannose. Synthesis, purification and characterization of microgels used in the experiments. Performing of aggregation studies of microgels in presence of *E. coli*. Functionalization of microgel samples with Alexa 647 and establishing a preparation method for dSTORM measurements. Collaborative performance of dSTORM measurements and data evaluation. Writing of first draft and collaborative visualization of data.

Reproduced with permission from Dimitri Wilms, Anselm Urach, Fabian Schröer and Stephan Schmidt.

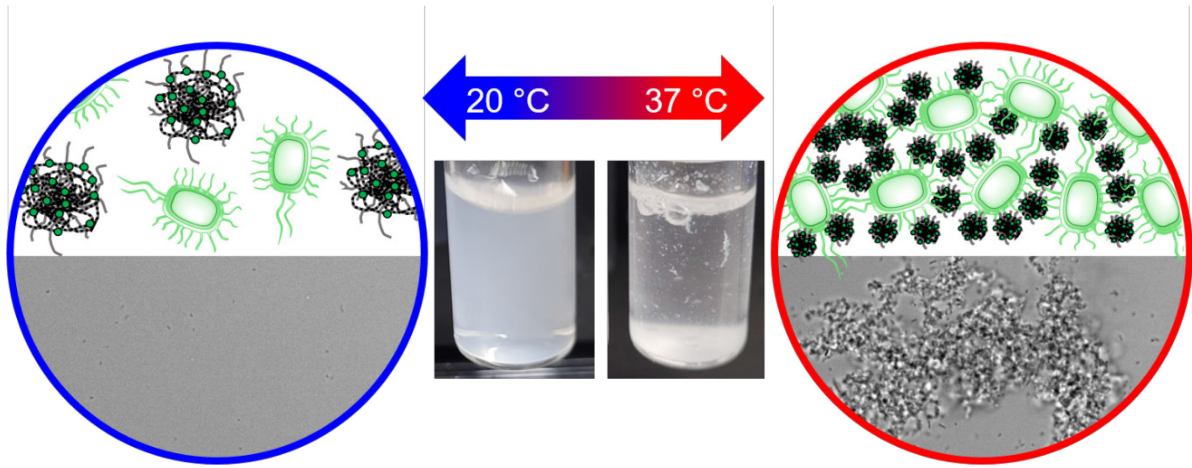
Specific binding of ligand-functionalized thermoresponsive microgels: Effect of microgel architecture, ligand density, and ligand hydrophobicity

Dimitri Wilms¹, Anselm Urach¹, Fabian Schröer¹, Stephan Schmidt¹

¹ Institute for Organic Chemistry and Macromolecular Chemistry, Heinrich-Heine-University, Universitätsstr. 1 40225 Düsseldorf Germany

Abstract

Lectin-carbohydrate binding plays an important role in pathogen adhesion prior to infection. One way to prevent invasion is to block the lectin binding sites of the pathogen and remove it from the system. This can be achieved by carbohydrate-presenting responsive microgels that can be triggered remotely to bind the target, allowing for easy separation. In this work, the bacterium *E. coli* is used as a model organism to study a catch-and-release antibiotic strategy using thermosensitive poly(*N*-isopropylacrylamide) (pNIPAM) and poly(oligo(ethylene glycol methacrylamide)) (pOEGMA) microgels functionalized with mannose. When the VPTT of the microgels exceeds 32 °C, the network collapses and the ligand density on the particle surface increases dramatically, leading to increased affinity of *E. coli* and subsequent formation of large clusters. These can be easily filtered to purify the solution. The trapped bacteria can be released by cooling the solution below the VPTT. A system that allows both catching and release are shown to be microgels synthesized without bifunctional crosslinkers. These exhibit a higher degree of swelling compared to conventional microgels and also show more homogeneous collapse behavior due to the greater uniformity of the polymer network. The results of this work show the influence of carbohydrate density and steric repulsion below and above the VPTT on the binding and release ability of carbohydrate-presenting pNIPAM and pOEGMA microgels.



1. Introduction

Lectin-carbohydrate interactions govern many processes at the cellular level for example cell-cell communication, cell development, fertilization and also pathogen invasion. The latter calls for development of new strategies to cure and prevent infections as multi resistant germs rise in numbers¹. One alternative strategy to prevent the infection of carbohydrate binding pathogens is the inhibition of lectins before they can adhere to any cell surface^{2, 3}. A fitting scaffold to bear the inhibiting carbohydrate moieties are micro- and nanoparticles, which are already relevant in pharmaceutical applications^{4, 5}. With the additional option of smart responsive polymers, the targeting of specific pathogens can be controlled not only by well-tailored functionalization but also with external stimuli to increase precision. One class of such materials are thermoresponsive polymers, mainly poly(*N*-isopropylacrylamide) (pNIPAM) and poly(oligo ethylene glycol methacrylate) (POEGMA).⁶⁻⁸ PNIPAM is a well-studied model system suitable to provide proof of principle systems and investigate pathogen interactions. Implications of cancerogenic effect of polyacrylamides raise doubts for actual applications *in vivo*^{9, 10}. A bio compatible alternative are pOEGMA microgels, which exhibit similar thermoresponsive behavior as pNIPAM and are obtained by copolymerization of OEGMA₄₇₅ and MEO₂MA via straightforward free radical polymerization¹¹. The temperature reactive behavior occurs due to entropic reasons as the hydration layer at the polymer backbone is disrupted upon temperature change. For both polymer systems used in this work this lower critical solution temperature (LCST) is at 32 °C and thus within physiological range. As microgels are a three-dimensional crosslinked network they are strictly speaking not solubilized but swollen with the medium. When the temperature is increased above 32 °C the network becomes hydrophobic and transitions from a swollen to a collapsed state as polymer-polymer interaction becomes entropically more favorable. This results in a significant change in volume, elastic modulus and surface roughness, which is directly related to steric repulsion. Even without carbohydrate functionalization the described effects lead to a switchable cell adhering system^{7, 12, 13}. As such microgels have no specificity towards the bound organism carbohydrate moieties are introduced to take advantage of the specific lectin-sugar binding and provide selectivity towards a single pathogen. The addition of sugars can be done by simply adding an additional modified carbohydrate monomer to the polymerization solution. This allows for straightforward one step synthesis of a variety of different microgel systems in environmentally friendly solution as water is used as solvent. Even without the addition of a surfactant the resulting particles have low dispersity. Microgels allow for a variable applicability as they can be used in solution or

deposited on many different substrates via drop-casting, spin-coating or adsorption from solution making them a versatile tool. It is yet unclear how the architecture of a microgel affects binding behavior. Especially the amount of crosslinker used for synthesis greatly changes the structural and elastic properties of the microgel¹⁴⁻¹⁷. Low crosslinking densities typically lead to lower elastic moduli and the complete absence of such shows to form particles with exceptional homogeneity, deformability and a very low elastic modulus. This leads to a higher swelling degree and in turn to improved switchability. The addition of a ligand increases the complexity of the system as it changes the reaction kinetics and the swelling behavior.

In this work, we show how microgels with particularly low crosslinking density, achieved by synthesis in absence of bi-functional crosslinking agent, can be used to capture and release pathogens. The effects of ligand density change upon collapsing are discussed as we expect a certain density needs to be achieved to bind and also to release the target. We further investigate the binding behavior depending on the choice of ligand in regards of hydrophobicity. Biotin is a hydrophilic molecule and upon heating is expected to orient itself toward the polymer network at higher temperatures. The interactions between lectins and carbohydrates occur naturally allowing for gentle and non-invasive capture. This has the advantage over classic antibiotics, which typically kill the pathogens by circumvention of evolutionary pressure to develop resistances.

2. Experimental

Materials

N-Isopropylacrylamide (NIPAM) (99%, Sigma-Aldrich), *N,N'*-methylenebisacrylamide (BIS) (99%, Apollo Scientific), potassium persulfate (KPS) (99.99%, Sigma-Aldrich), ammonium persulfate (APS) ($\geq 98\%$, Sigma-Aldrich), oligo(ethylene glycol) methyl ether methacrylate (OEGMA₄₇₅) (Sigma-Aldrich), di(ethylene glycol)methyl ether methacrylate (MEO₂MA) (Sigma-Aldrich), sodium dodecyl sulfate (SDS) (Sigma-Aldrich), phosphate buffered saline (PBS) (tablets, VWR), LB broth (Miller, powder microbial growth medium) (Sigma-Aldrich).

Microgel synthesis

The polymerization of mannose bearing PNIPAM microgels containing BIS was carried out in a 100 mL three-necked round bottom flask fitted with a condenser. NIPAM (6.19 mmol), BIS (0.325 mmol) and *N*-ethylacrylamide- α -*D*-mannopyranoside (ManEAM) (0.409 mmol) were dissolved in 75 mL ultra-pure water. The solution is heated to 70 °C under continuous stirring at 350 rpm and N₂ purging for at least 30 min. After the final temperature is reached the initiator APS (0.9 mmol) is dissolved in 5 mL ultra-pure water and added to the solution to start the reaction. The reaction is allowed to proceed for 2 hours and then stopped by cooling the solution down in an ice bath. Purification is achieved by repeated centrifugation at 15000 rpm and re-suspending in fresh water.

Table 1: Composition of the microgel reaction mixtures.

	monomer [mmol]	crosslinker [mmol]	Man [mmol]	SDS [mmol]	APS [mmol]
PNIPAM _{BIS} -Man	6.19 NIPAM	0.325 BIS	0.409	0.087	0.9
PNIPAM _{SCL} -Man	1.4 NIPAM	-	0.150	-	3
p(OEGMA- <i>co</i> -MEO ₂ MA) _{EGDMA} -Man	0.813 OEGMA 0.09 MEO ₂ MA	0.09 EGDMA	0.200	0.03	0.25
p(OEGMA- <i>co</i> -MEO ₂ MA) _{SCL} -Man	0.813 OEGMA 0.09 MEO ₂ MA	-	0.400	0.02	0.22

Self-crosslinked crosslinked microgels were synthesized in absence of any crosslinker via a variation of the method established by Virtanen et al¹⁸. Briefly, the polymerization is carried

out in a 50 mL one-necked round bottom flask. NIPAM (1.4 mmol), ManEAM (0.150 mmol) and the initiator APS (0.2 mmol) are dissolved in 20 mL ultra-pure water and the solution is purged with N₂ for 45 min. After sealing the flask, the solution is heated to 70 °C to start the reaction, which is carried out under N₂ atmosphere. After 16 hours the reaction is stopped by cooling down in an ice bath. Purification is achieved by repeated centrifugation at 15000 rpm and re-suspending in fresh water.

The synthesis of p(OEGMA₄₇₅-*co*-MEO₂MA)_{EGDMA}-Man microgels is carried out in a 250 mL three-necked round bottom flask fitted with a condenser. OEGMA₄₇₅ (0.813 mmol), MEO₂MA (0.09 mmol), ManEAM (0.2 mmol) and SDS (0.033 mmol) are dissolved in ultra-pure water and heated up to 70 °C under constant stirring and N₂ purging. After reaching the final temperature the initiator APS (0.25 mmol) is dissolved in 5 mL ultra-pure water and added to solution to start the reaction. After 6 hours the reaction is stopped by cooling down in an ice bath. Purification is achieved by repeated centrifugation at 15000 rpm and re-suspending in fresh water.

Self-crosslinked p(OEGMA₄₇₅-*co*-MEO₂MA)_{SCL}-Man microgels were synthesized similarly to the PNIPAM_{SCL}-Man sample. For the reaction OEGMA₄₇₅ (0.813 mmol), MEO₂MA (0.09 mmol), ManEAM (0.4 mmol) and APS (0.25 mmol) are dissolved in ultra-pure water. The reaction and purification is carried out as with PNIPAM_{SCL}-Man microgels.

Microgel characterization

Dynamic light scattering. The hydrodynamic radii at varying temperatures were acquired via DLS measurements. The Malvern Zetasizer Nano ZS (Malvern Panalytical, Kassel, Germany) is equipped with a He-Ne laser emitting light at 633 nm. Light scattering is detected at a 173° angle. For the measurements the microgel concentration was adjusted to 0.1 mg·mL⁻¹, 1 mL of this solution was placed in PMMA semi-micro cuvettes (VWR, Darmstadt, Germany). The radii were acquired at temperatures from 14 to 54 °C in 2 °C steps with 20 min of equilibration at each temperature step. The cumulants and radii were determined and calculated by the software provided by the manufacturer.

Atomic Force Microscopy

To determine dry particle volume, AFM images of dried microgel layers on solid substrate were acquired. The JPK Bruker NanoWizard II (JPK Bruker, Berlin, Germany) was used to record images in the intermediate contact mode. Cantilevers with a spring constant of 42 N·m⁻¹ (HQ:XSC11/NoAl, μ masch, Sofia, Bulgaria) were used for scanning with a line rate of 1 Hz).

The microgels are deposited on glass slides via spincoating at 2000 rpm for 30 s. The slides are cleaned by sonication in a 2 v% Helmanex III solution in ultra-pure water. After rinsing with ultra-pure water the slides are further purified in a solution of water, hydrogen peroxide and ammonia hydroxide (ratio of 5:1:1). This solution is heated to 70 °C and the slides are placed in it for 30 min. After final rinsing with ultra-pure water the microgels are applied.

Optical microscopy

The clustering measurements were carried out on an inverted fluorescent microscope (IX73, Olympus, Shinjuku, Japan) equipped with an Olympus PLN 20X Objective (Olympus, Shinjuku, Japan) and CMOS camera (DMK 33UX174L, The Imaging Source, Bremen, Germany). The microgel solution with a concentration of 0.5 mg·mL⁻¹ in PBS buffer was combined with *E.coli* bacteria suspension also in PBS at a concentration of 2 mg·mL⁻¹. Bacteria concentration is determined by measuring the optical density at 600 nm wavelength.

Stochastic optical reconstruction microscopy (dSTORM) was applied to determine carbohydrate distribution within the microgels. A Leica DMI6000 B microscope fitted with an N Plan 100x/1.25-0.60 Oil objective (Leica, Wetzlar, Germany). The microgels were deposited on glass microscope slides as described above and immersed in blinking buffer.

Mannose loading determination

To determine the amount of mannose incorporated into the microgel particles a colorimetric assay was applied. First the phenol-sulfuric acid method requires a calibration curve, which is established by a dilution series of α -D-methylmannose. For carbohydrate quantification 500 μ L of sample solution is combined with 250 μ L of a 5 w% phenol solution and 1.5 mL sulfuric acid (98%) and shaken for 30 min.

3. Results and Discussion

3.1 Synthesis of mannose functionalized PNIPAM and PEG microgels- with different architecture

The well-known precipitation polymerization procedure introduced by Pelton¹⁹ was used to prepare P(NIPAM) and P(MEO₂MA-co-OEGMA) microgels in aqueous solution. The composition of the reaction mixtures is shown in table 1. To obtain mannose functionalized microgels, the monomer *N*-ethylacrylamide- α -D-mannopyranoside (ManEAm) was added along with monomers constituting the LCST polymer backbone. The microgel architecture was

varied by conducting the synthesis in presence and absence of a dedicated crosslinker as described previously.^{8, 20, 21} Without crosslinker, the P(NIPAM) and P(MEO₂MA-co-OEGMA) networks are formed by chain transfer reactions, which leads to soft microgels with a low crosslinking degree.²² For P(NIPAM), such self-crosslinked microgels show a homogeneous distribution of polymer segments. Self-crosslinked P(MEO₂MA-co-OEGMA) microgels have higher segment density in the center because the monomers and oligomers of MEO₂MA and OEGMA have different reactivities and phase behaviors.^{15, 16, 23} In presence of 5 mol% of the bifunctional crosslinkers BIS or EGDMA, microgels with a densely crosslinked core and a fuzzy shell are formed due to the increased reactivity of the crosslinker compared to the monomers. [Platzhalter Biotin-PNIPAM Mikrogele] The resulting microgels are termed according to the monomers used and crosslinking type (“SCL” for self-crosslinked, “BIS” or “EGDMA” with dedicated crosslinker). Overall, four different mannose functionalized microgels were synthesized: 1) PNIPAM_{BIS}-Man, 2) PNIPAM_{SCL}-Man, 3) P(OEGMA-co-MEO₂MA)_{EGDMA}-Man, 4) P(OEGMA-co-MEO₂MA)_{SCL}-Man

All microgels showed an VPPT at around 30-35 °C as measured by the change in the hydrodynamic radius when changing the temperature (Figure 1, Table 2). The self-crosslinked microgels synthesized without crosslinker show the greatest change in hydrodynamic radius (R_h) and a sharper transition when crossing the VPTT. This is in accordance with expectations^{24, 25} as they show the lowest network density and also a higher network homogeneity compared to microgels containing an additional crosslinker. It can also be seen that the PEG-derived microgels show a less sharp phase transition compared to the pNIPAM microgels. The reason is that the random copolymerization of OEGMA and MEO₂MA toward PEG-derived microgels leads to varying phase transition temperatures of the different polymer segments and generally less homogeneous networks. The microgels swelling degree upon temperature change also reflects the density of crosslinks in the networks.

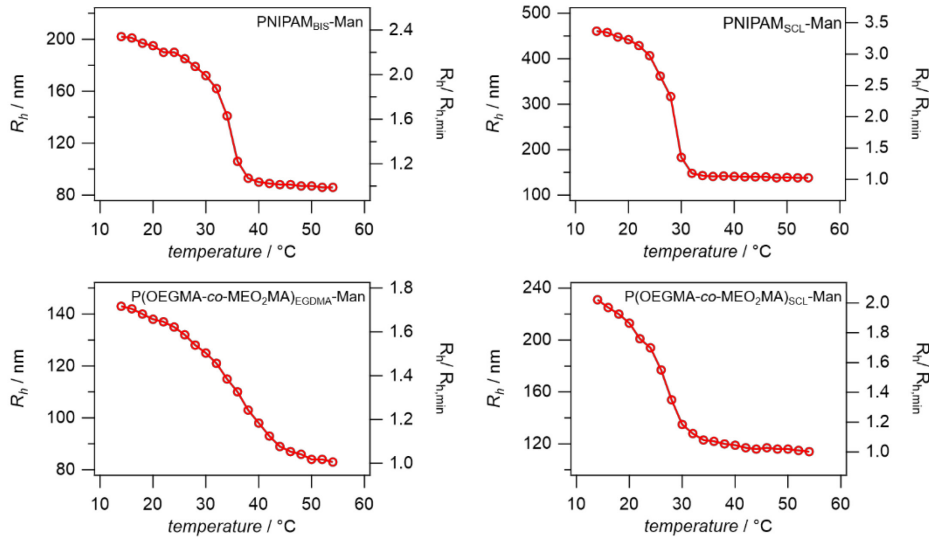


Figure 11: Hydrodynamic radius (R_h) measurements by means of DLS and the swelling degree $R_h/R_{h,min}$ of microgel samples in PBS as a function of temperature.

Table 2: Hydrodynamic radii (R_h) acquired from dynamic light scattering measurements in ultra-pure water.

	VPTT °C	R_h at 20 °C nm	R_h at 40 °C nm
PNIPAM _{BIS} -Man	33	360	220
PNIPAM _{SCL} -Man	28	410	110
p(OEGMA-co-MEO ₂ MA) _{EGDMA} -Man	35	120	75
p(OEGMA-co-MEO ₂ MA) _{SCL} -Man	27	200	87

3.2 Study of Man-specific interactions of microgels via *E. coli* binding

E. coli express the Man-binding receptor FimH at their fimbriae, which enables their binding and the colonization of host tissue.^{8, 16, 21, 26, 27} Here we used *E. coli* to evaluate the specific interactions of Man-functionalized microgels by studying the formation of aggregates between the bacteria and microgels via optical microscopy and visual inspection (Figure 2). To study the effect of microgel collapse and the concurrent increase Man density in the network, the experiments were conducted below and above the VPPT, at 20 °C and 37°C. When combining the microgel and *E.coli* suspensions at 20 °C, no clusters were formed. At 37 °C, clusters were formed except for p(OEGMA-co-MEO₂MA)_{EGDMA}-Man microgels. To test the reversibly of cluster formation, the temperature was decreased from 37 °C to 20 °C. In case of the self-

crosslinked microgels the previously formed bacteria-microgel aggregates disassemble, whereas clusters between pNIPAM_{BIS} microgels and *E. coli* were still present at 20 °C. This is broadly in line with previous studies showing that Man-functionalized pNIPAM_{BIS} microgels irreversibly bind and cluster with *E. coli* above the VPPT due to the increased Man density and statistical multivalency effects.⁸ A completely reversible binding over many cooling and heating cycles (see supporting information) was only observed for the self-crosslinked microgels indicating that their more homogeneous microgel architecture might enable such catch and release capabilities.

Importantly, the Man functionalization degree appears not to account for the capture and release capabilities of the microgels. The microgels prepared in this work have a similar Man-functionalization degree ranging from 32-60 $\mu\text{mol g}^{-1}$ (number of Man units per microgel weight, Table 3). Furthermore, from the Man-functionalization degree it is unclear why p(OEGMA-co-MEO₂MA)_{EGDMA}-Man microgels (40.0 $\mu\text{mol g}^{-1}$) did not form clusters with *E. coli* whereas pNIPAM_{BIS}-Man at a lower Man-functionalization degree (32.0 $\mu\text{mol g}^{-1}$) formed clusters.

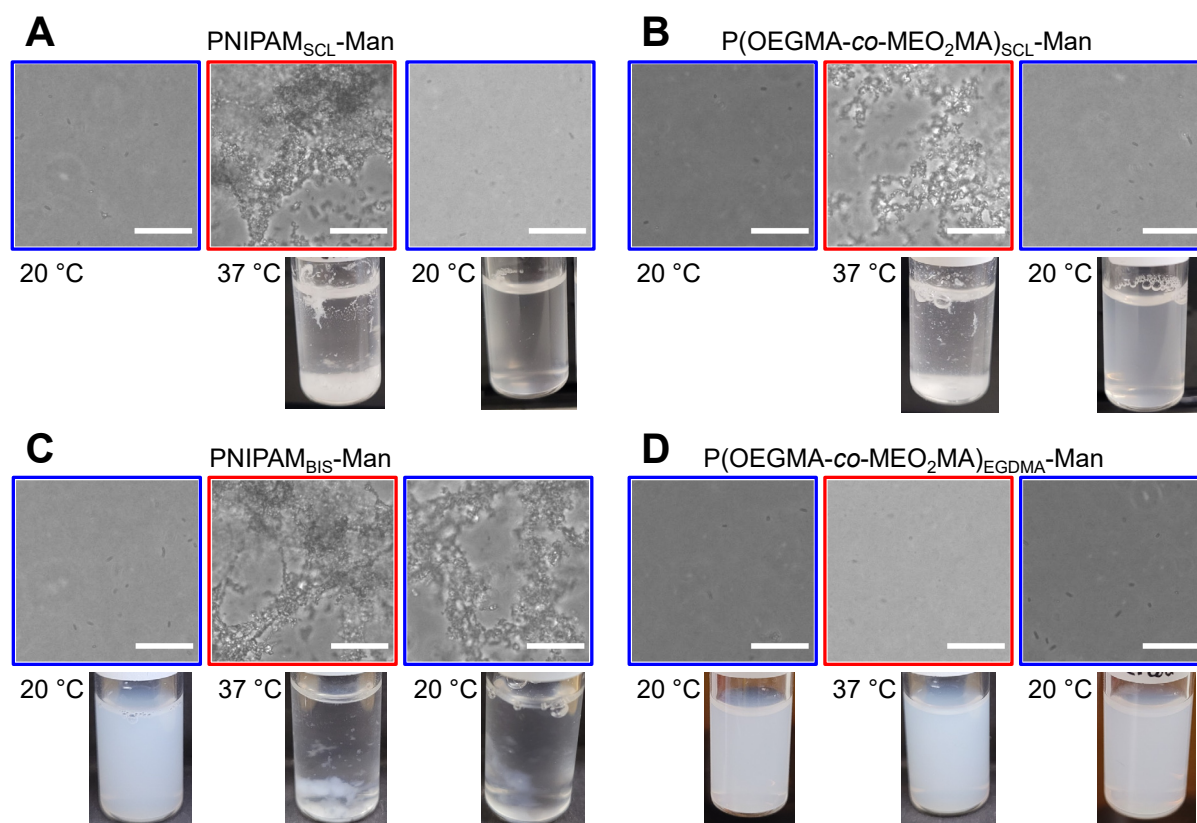


Figure 12: Aggregation studies of pNIPAM_{SCL}-Man and p(OEGMA-co-MEO₂MA)_{SCL}-Man microgels together with *E.coli* bacteria. Microgel samples with a final concentration of 0.5

mg·mL⁻¹ are mixed with bacterial suspension with a final concentration of 1 mg·mL⁻¹ and incubated at 37 °C for several hours until aggregation occurs. After cooling the sample is vortexed until aggregates are re-solubilized. Scalebars: 10 μm.

Table 3: The mannose content determined by sulfuric-acid-phenol method and bacteria catch and release ability is noted.

	Man functionalization degree	binding	release
pNIPAM _{BIS} -Man	32.0 ± 3.0 μmol·g ⁻¹	✓	✗
pNIPAM _{SCL} -Man	60.0 ± 6.8 μmol·g ⁻¹	✓	✓
p(OEGMA- <i>co</i> -MEO ₂ MA) _{EGDMA} -Man	40.0 ± 3.7 μmol·g ⁻¹	✗	n.a.
p(OEGMA- <i>co</i> -MEO ₂ MA) _{SCL} -Man	60.0 ± 4.4 μmol·g ⁻¹	✓	✓

3.3 The mannose density and architecture controls bacteria binding and release

In order to shed light on the *E. coli* capture and release behavior of the different microgels, the overall density and spatial distribution of Man units in the microgels was determined. A first task was to convert the Man functionalization degree (in μmol g⁻¹) as determined by the phenol sulfuric acid assay to the volume density of Man units in the microgel, i.e. the number of Man units per microgel volume. The microgel volume could be readily determined via DLS in the swollen (20 °C) and collapsed (37 °C) state. The volume density of Man units in the microgels could then be estimated from the Man functionalization degree (in μmol g⁻¹) and the dry volume of the microgel determined via AFM (see supporting information Figure S3) as well as assuming a density of the microgels in the dry state of 1.1 g cm⁻³.²⁸ The estimated overall Man volume density varies quite significantly between the microgel samples, showing larger values for PEG-derived compared to pNIPMA microgels and for microgels prepared with a crosslinker compared to self-crosslinked microgels. This is to be expected since the addition of a crosslinker leads to more compact networks, and previous work showed that p(OEGMA-*co*-MEO₂MA) microgels are stiffer and denser when compared to pNIPAM microgels for similar crosslinker concentrations^{16, 20, 21}. The larger swelling degree of the less dense self-crosslinked microgels enables large shifts in mannose density up to 50-fold when crossing the VPPT, whereas the microgels with an additional crosslinker showed only a 4-fold increase in Man density. This explains the reversible binding of *E. coli* for the self-crosslinked microgels upon temperature decrease, which was not seen for pNIPAM_{SCL}-Man. Importantly, the estimated

Man volume densities in Table 4 do not sufficiently explain binding and clustering of the microgels with *E. coli*. For example, pNIPAM_{SCL}-Man with the lowest Man density formed clusters with *E. coli* when collapsed, whereas for p(OEGMA-*co*-MEO₂MA)_{EGDMA}-Man with an order of magnitude larger Man density clusters no were formed.

Table 4: The estimated overall number of Man units and densities in the microgel samples as calculated from the Man functionalization degree and microgel volumes (see supporting information S4).

	est. Man units per microgel ¹	Man density ² (swollen)	Man density ² (collapsed)	Man density shift ³
pNIPAM _{BIS} -Man	106000 ± 32000	0.54	2.4	4-fold
pNIPAM _{SCL} -Man	3000 ± 1050	0.011	0.52	50-fold
p(OEGMA- <i>co</i> -MEO ₂ MA) _{EGDMA} -Man	15000 ± 4400	2.0	8.3	4-fold
p(OEGMA- <i>co</i> -MEO ₂ MA) _{SCL} -Man	40000 ± 13000	1.2	14	12-fold

¹Standard deviation calculated from the error of the phenol sulfuric acid assay and the volume variations of the dry microgels measured by AFM. ²Number of mannose units in a microgel volume of 1000 nm³; ³Increase in the Man density upon microgel collapse by heating from 20 °C to 37 °C.

Because also the Man density differences in the microgels samples do not explain the *E. coli* binding behavior we studied the spatial distribution of Man units in the microgel network by dSTORM. For labeling the Man units were first oxidized to form aldehyde groups by periodate treatment followed by coupling of a hydrazine-functionalized Alexa 647 dye. After extensive washing to remove unreacted dye from the microgel network dSTORM images were collected and processed. The resulting high-resolution images suggest that the Man units are quite homogeneously distributed within the microgel network. This is in agreement from TEM studies that showed that the distribution of various comonomers in microgel networks depends on their copolymerization parameters.²⁹ Therefore, the acrylamide-derived Man-bearing monomer ManEAM used in this work apparently had similar copolymerization rates compared backbone monomers NIPAM and OEGMA. Super resolution microscopy studies on thermoresponsive microgels so far focused not on the comonomer distribution but on analyzing but the overall network structure, e.g. by labeling the entire network or the bifunctional crosslinker.³⁰⁻³⁴

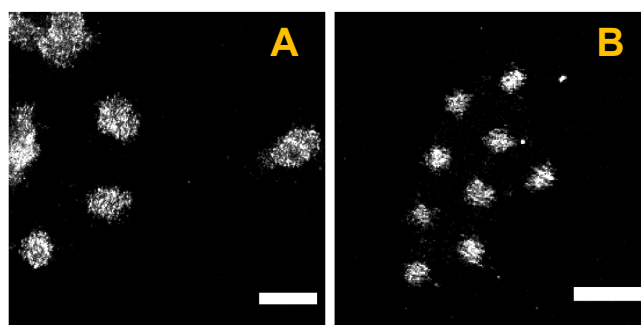


Figure 13: STORM images show a homogeneous distribution of mannose throughout the microgels. A) p(OEGMA-co-MEO₂MA)_{EGDMA}-Man, B) pNIPAM_{BIS}-Man.

The dSTORM results showed no indication of enrichment of the Man units at the center of rim of the microgels (see supporting information Figure S6). Therefore, there must be alternative explanations for the inability to bind *E. coli* of p(OEGMA-co-MEO₂MA)_{EGDMA}-Man that had a significantly larger Man-density compared to pNIPAM_{SCL}-Man. Earlier work showed that microgels synthesized from OEGMA and MEO₂MA mixtures contain a fuzzy shell that is likely enriched in long pOEGMA chains due to the lower diffusion and lower reactivity of the bulkier OEGMA monomers compared to the smaller comonomers MEO₂MA and ManEAM.¹⁶ Furthermore, the proposed pOEGMA-rich segments have a higher LCST compared segments where MEO₂MA is present in larger amount.³⁵ Therefore, these microgels are not fully collapsed at 37°C as can be seen from the swelling curve (Figure 1). This renders the Man units inaccessible for *E. coli* binding, as sketched in Figure 4. It should be noted however, that this argument is still rather speculative since the proposed OEGMA-rich fuzzy shell was not visible in dSTORM. The self-crosslinked microgels bound *E. coli* although they had a significantly lower Man density compared to p(OEGMA-co-MEO₂MA)_{EGDMA} that showed no binding. This could be explained by the loose network structure of the self-crosslinked networks, where the hydrophilic Man units might segregate to some degree from the hydrophobic segments above the VPPT, thus they are enriched at the microgel-water interface (Figure 4). This proposed enrichment of Man units at the microgel-water interface in the collapse state is less pronounced for microgels with a dedicated crosslinker leading to a lower degree of *E. coli* binding.

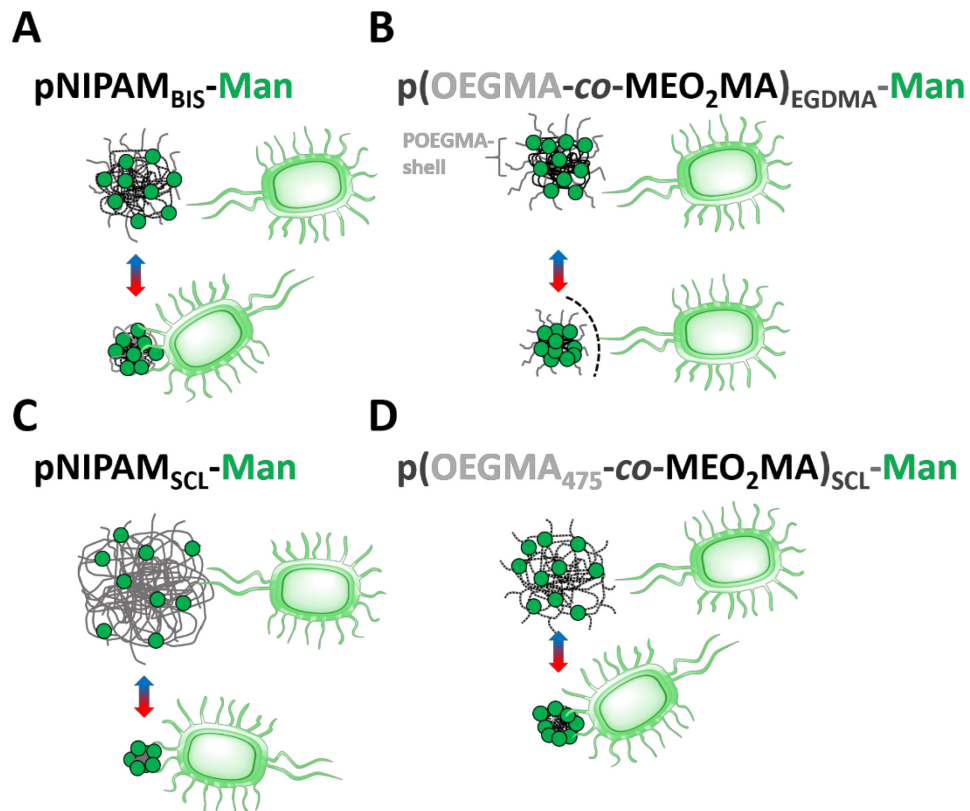


Figure 14: Sketch of microgel-*E. coli* interactions. The extended microgel network below the VPPT do not allow *E. coli* binding due to the lower Man density. $p(\text{OEGMA-co-MEO}_2\text{MA})_{\text{EGDMA}}$ microgel fail to bind also above the VPPT due to a pOEGMA-rich shell. The flexible network of self-crosslinked microgels enable enrichment of hydrophilic Man units at the microgel-water interface above the VPPT and *E. coli* binding.

4. Conclusion

We aimed to tune an established system of carbohydrate loaded lectin binding microgels to bind specific pathogens and also release them triggered remotely by changing the temperature. This was achieved by decreasing the crosslinking density and increasing the swelling degree and homogeneity of pNIPAM and pOEGMA microgels the system is enabled to successfully catch and release bacteria over several cycles by agglomeration in solution. The total amount of carbohydrate per particle is kept around 1 mol% but the number of sugars per volume changes drastically upon temperature change, as calculated it changes several orders of magnitude after the microgels collapse. Presumably a critical mannose density is reached in the collapsed state for the multivalent binding of FimH to be strong enough for successful clustering of *E.coli*. In addition, the surface structure of the polymer network becomes mostly smooth and hydrophobic above the VPTT, thus increasing ligand accessibility as the loose chain ends collapse. From dSTORM imaging individual mannose distribution is determined to be homogeneous even in particles containing bi-functional crosslinker. Above the VPTT the sugars are expected to orientate towards the outside of the particles due to their hydrophilic nature. The straightforward one-step synthesis of carbohydrate bearing microgels allows flexible functionalization for specific targeting of lectins, pathogens or cells. Together with easy deposition thermoresponsive microgels show potential for controlled, specific and gentle target binding in therapeutic or diagnostic applications.

5. References

1. Jałowiecki, Ł.; Hubeny, J.; Harnisz, M.; Płaza, G., Seasonal and Technological Shifts of the WHO Priority Multi-Resistant Pathogens in Municipal Wastewater Treatment Plant and Its Receiving Surface Water: A Case Study. *Int. J. Env. Res. Public Health* **2022**, *19* (1), 336.
2. Bernardi, A.; Jiménez-Barbero, J.; Casnati, A.; De Castro, C.; Darbre, T.; Fieschi, F.; Finne, J.; Funken, H.; Jaeger, K.-E.; Lahmann, M.; Lindhorst, T. K.; Marradi, M.; Messner, P.; Molinaro, A.; Murphy, P. V.; Nativi, C.; Oscarson, S.; Penadés, S.; Peri, F.; Pieters, R. J.; Renaudet, O.; Reymond, J.-L.; Richichi, B.; Rojo, J.; Sansone, F.; Schäffer, C.; Turnbull, W. B.; Velasco-Torrijos, T.; Vidal, S.; Vincent, S.; Wennekes, T.; Zuilhof, H.; Imberty, A., Multivalent glycoconjugates as anti-pathogenic agents. *Chem. Soc. Rev.* **2013**, *42* (11), 4709-4727.
3. Bhatia, S.; Camacho, L. C.; Haag, R., Pathogen Inhibition by Multivalent Ligand Architectures. *Journal of the American Chemical Society* **2016**, *138* (28), 8654-8666.
4. Molavi, F.; Barzegar-Jalali, M.; Hamishehkar, H., Polyester based polymeric nano and microparticles for pharmaceutical purposes: A review on formulation approaches. *J. Controlled Release* **2020**, *320*, 265-282.
5. Ahmad, M.; Rai, S. M.; Mahmood, A., Hydrogel microparticles as an emerging tool in pharmaceutical field: a review. *Adv. Polym. Tech.* **2016**, *35* (2), 121-128.
6. Karg, M.; Pich, A.; Hellweg, T.; Hoare, T.; Lyon, L. A.; Crassous, J. J.; Suzuki, D.; Gumerov, R. A.; Schneider, S.; Potemkin, II; Richtering, W., Nanogels and Microgels: From Model Colloids to Applications, Recent Developments, and Future Trends. *Langmuir* **2019**, *35* (19), 6231-6255.
7. Schmidt, S.; Zeiser, M.; Hellweg, T.; Duschl, C.; Fery, A.; Möhwald, H., Adhesion and Mechanical Properties of PNIPAM Microgel Films and Their Potential Use as Switchable Cell Culture Substrates. *Adv. Funct. Mater.* **2010**, *20* (19), 3235-3243.
8. Paul, T. J.; Rübel, S.; Hildebrandt, M.; Strzelczyk, A. K.; Spormann, C.; Lindhorst, T. K.; Schmidt, S., Thermosensitive Display of Carbohydrate Ligands on Microgels for Switchable Binding of Proteins and Bacteria. *ACS Applied Materials & Interfaces* **2019**, *11* (30), 26674-26683.
9. Amended Final Report on the Safety Assessment of Polyacrylamide and Acrylamide Residues in Cosmetics¹. *Int. J. Toxicol.* **2005**, *24* (2_suppl), 21-50.

10. Xiong, B.; Loss, R. D.; Shields, D.; Pawlik, T.; Hochreiter, R.; Zydney, A. L.; Kumar, M., Polyacrylamide degradation and its implications in environmental systems. *npj Clean Water* **2018**, *1* (1), 17.
11. Lutz, J.-F.; Akdemir, Ö.; Hoth, A., Point by Point Comparison of Two Thermosensitive Polymers Exhibiting a Similar LCST: Is the Age of Poly(NIPAM) Over? *Journal of the American Chemical Society* **2006**, *128* (40), 13046-13047.
12. Uhlig, K.; Wegener, T.; He, J.; Zeiser, M.; Bookhold, J.; Dewald, I.; Godino, N.; Jaeger, M.; Hellweg, T.; Fery, A.; Duschl, C., Patterned Thermoresponsive Microgel Coatings for Noninvasive Processing of Adherent Cells. *Biomacromolecules* **2016**, *17* (3), 1110-6.
13. Kessel, S.; Schmidt, S.; Müller, R.; Wischerhoff, E.; Laschewsky, A.; Lutz, J.-F.; Uhlig, K.; Lankenau, A.; Duschl, C.; Fery, A., Thermoresponsive PEG-Based Polymer Layers: Surface Characterization with AFM Force Measurements. *Langmuir* **2010**, *26* (5), 3462-3467.
14. Sanson, N.; Rieger, J., Synthesis of nanogels/microgels by conventional and controlled radical crosslinking copolymerization. *Polymer Chemistry* **2010**, *1* (7), 965-977.
15. Welsch, N.; Lyon, L. A., Oligo(ethylene glycol)-sidechain microgels prepared in absence of cross-linking agent: Polymerization, characterization and variation of particle deformability. *PLOS ONE* **2017**, *12* (7), e0181369.
16. Wilms, D.; Adler, Y.; Schröer, F.; Bunnemann, L.; Schmidt, S., Elastic modulus distribution in poly(N-isopopylacrylamide) and oligo(ethylene glycol methacrylate)-based microgels studied by AFM. *Soft Matter* **2021**, *17* (23), 5711-5717.
17. Gawlitza, K.; Radulescu, A.; von Klitzing, R.; Wellert, S., On the structure of biocompatible, thermoresponsive poly(ethylene glycol) microgels. *Polymer* **2014**, *55* (26), 6717-6724.
18. Virtanen, O. L. J.; Richtering, W., Kinetics and particle size control in non-stirred precipitation polymerization of N-isopropylacrylamide. *Colloid. Polym. Sci.* **2014**, *292* (8), 1743-1756.
19. Pelton, R. H.; Chibante, P., Preparation of aqueous latices with N-isopropylacrylamide. *Colloids and Surfaces* **1986**, *20* (3), 247-256.
20. Wilms, D.; Schröer, F.; Paul, T. J.; Schmidt, S., Switchable Adhesion of E. coli to Thermosensitive Carbohydrate-Presenting Microgel Layers: A Single-Cell Force Spectroscopy Study. *Langmuir* **2020**.
21. Schröer, F.; Paul, T. J.; Wilms, D.; Saatkamp, T. H.; Jäck, N.; Müller, J.; Strzelczyk, A. K.; Schmidt, S., Lectin and E. coli Binding to Carbohydrate-Functionalized Oligo(ethylene

glycol)-Based Microgels: Effect of Elastic Modulus, Crosslinker and Carbohydrate Density. *Molecules* **2021**, *26* (2).

22. Virtanen, O. L.; Mourran, A.; Pinard, P. T.; Richtering, W., Persulfate initiated ultra-low cross-linked poly(N-isopropylacrylamide) microgels possess an unusual inverted cross-linking structure. *Soft Matter* **2016**, *12* (17), 3919-28.
23. Bachman, H.; Brown, A. C.; Clarke, K. C.; Dhada, K. S.; Douglas, A.; Hansen, C. E.; Herman, E.; Hyatt, J. S.; Kodlekere, P.; Meng, Z., Ultrasoft, highly deformable microgels. *Soft Matter* **2015**, *11* (10), 2018-2028.
24. Su, W.; Zhao, K.; Wei, J.; Ngai, T., Dielectric relaxations of poly (N-isopropylacrylamide) microgels near the volume phase transition temperature: impact of cross-linking density distribution on the volume phase transition. *Soft Matter* **2014**, *10* (43), 8711-8723.
25. Füllbrandt, M.; von Klitzing, R.; Schönhals, A., The dielectric signature of poly (N-isopropylacrylamide) microgels at the volume phase transition: dependence on the crosslinking density. *Soft Matter* **2013**, *9* (17), 4464-4471.
26. Hartmann, M.; Horst, A. K.; Klemm, P.; Lindhorst, T. K., A kit for the investigation of live Escherichia coli cell adhesion to glycosylated surfaces. *Chem. Commun.* **2010**, *46* (2), 330-332.
27. Paul, T. J.; Strzelczyk, A. K.; Schmidt, S., Temperature-Controlled Adhesion to Carbohydrate Functionalized Microgel Films: An E. coli and Lectin Binding Study. *Macromol. Biosci.* **2021**, *21* (4), 2000386.
28. Sbeih, S.; Mohanty, P. S.; Morrow, M. R.; Yethiraj, A., Structural parameters of soft PNIPAM microgel particles as a function of crosslink density. *J. Colloid Interface Sci.* **2019**, *552*, 781-793.
29. Dai, Z.; Ngai, T., Microgel particles: the structure-property relationships and their biomedical applications. *J. Polym. Sci., Part A: Polym. Chem.* **2013**, *51* (14), 2995-3003.
30. Wrede, O.; Bergmann, S.; Hannappel, Y.; Hellweg, T.; Huser, T., Smart microgels investigated by super-resolution fluorescence microscopy: influence of the monomer structure on the particle morphology. *Soft Matter* **2020**, *16* (34), 8078-8084.
31. Bergmann, S.; Wrede, O.; Huser, T.; Hellweg, T., Super-resolution optical microscopy resolves network morphology of smart colloidal microgels. *Physical Chemistry Chemical Physics* **2018**, *20* (7), 5074-5083.

32. Karanastasis, A. A.; Kenath, G. S.; Sundararaman, R.; Ullal, C. K., Quantification of functional crosslinker reaction kinetics via super-resolution microscopy of swollen microgels. *Soft Matter* **2019**, *15* (45), 9336-9342.
33. Stieger, M.; Richtering, W.; Pedersen, J. S.; Lindner, P., Small-angle neutron scattering study of structural changes in temperature sensitive microgel colloids. *J. Chem. Phys.* **2004**, *120* (13), 6197-6206.
34. Conley, G. M.; Nöjd, S.; Braibanti, M.; Schurtenberger, P.; Scheffold, F., Superresolution microscopy of the volume phase transition of pNIPAM microgels. *Colloids Surf. Physicochem. Eng. Aspects* **2016**, *499*, 18-23.
35. Lutz, J.-F., Polymerization of oligo(ethylene glycol) (meth)acrylates: Toward new generations of smart biocompatible materials. *J. Polym. Sci., Part A: Polym. Chem.* **2008**, *46* (11), 3459-3470.

Supporting Information

1. Dynamic light scattering data

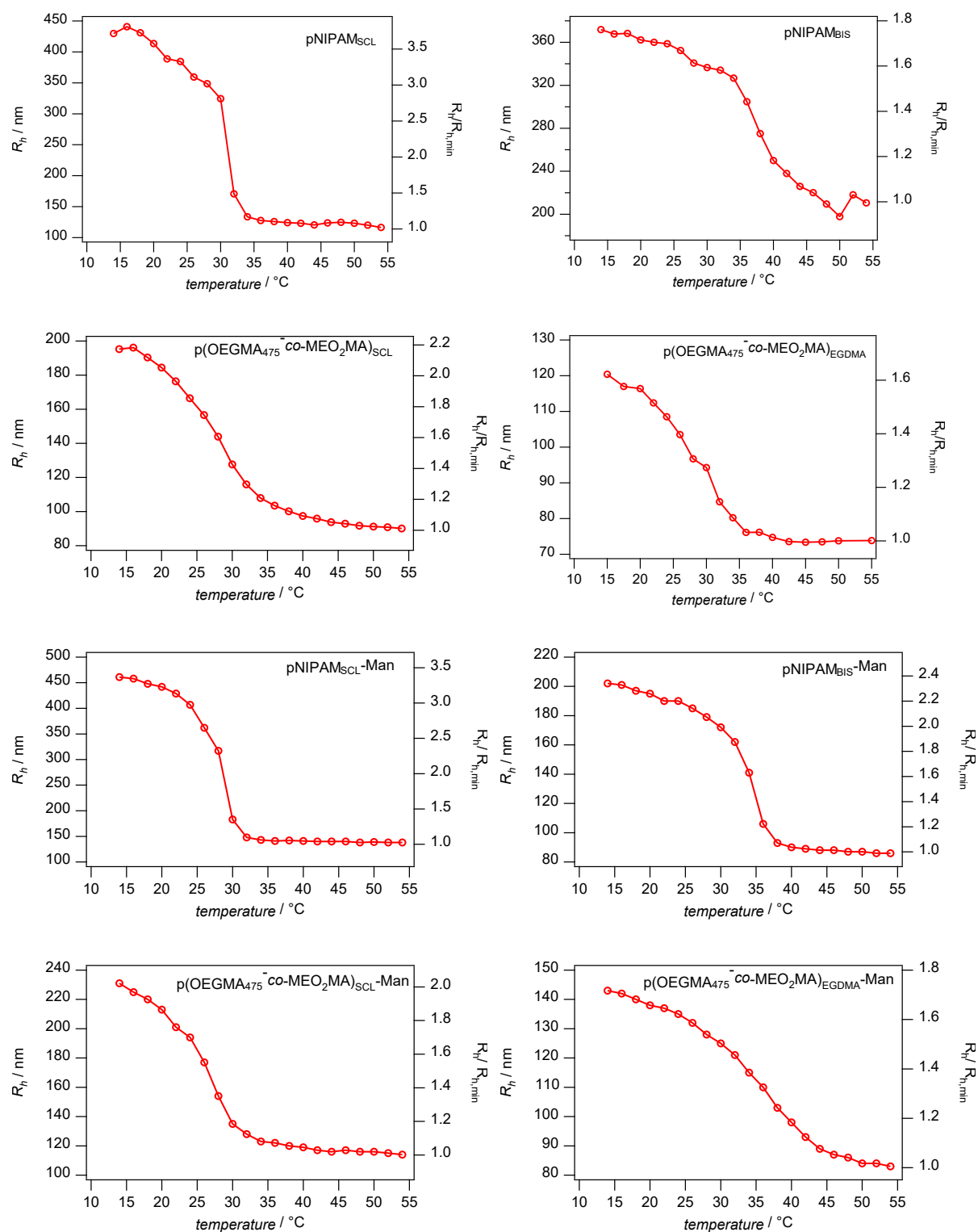


Figure S1: DLS data of microgel samples in PBS acquired at different temperatures at a concentration of $1 \text{ mg}\cdot\text{mL}^{-1}$.

2. Single cell force spectroscopy of *E. coli* adhesion to microgel monolayers

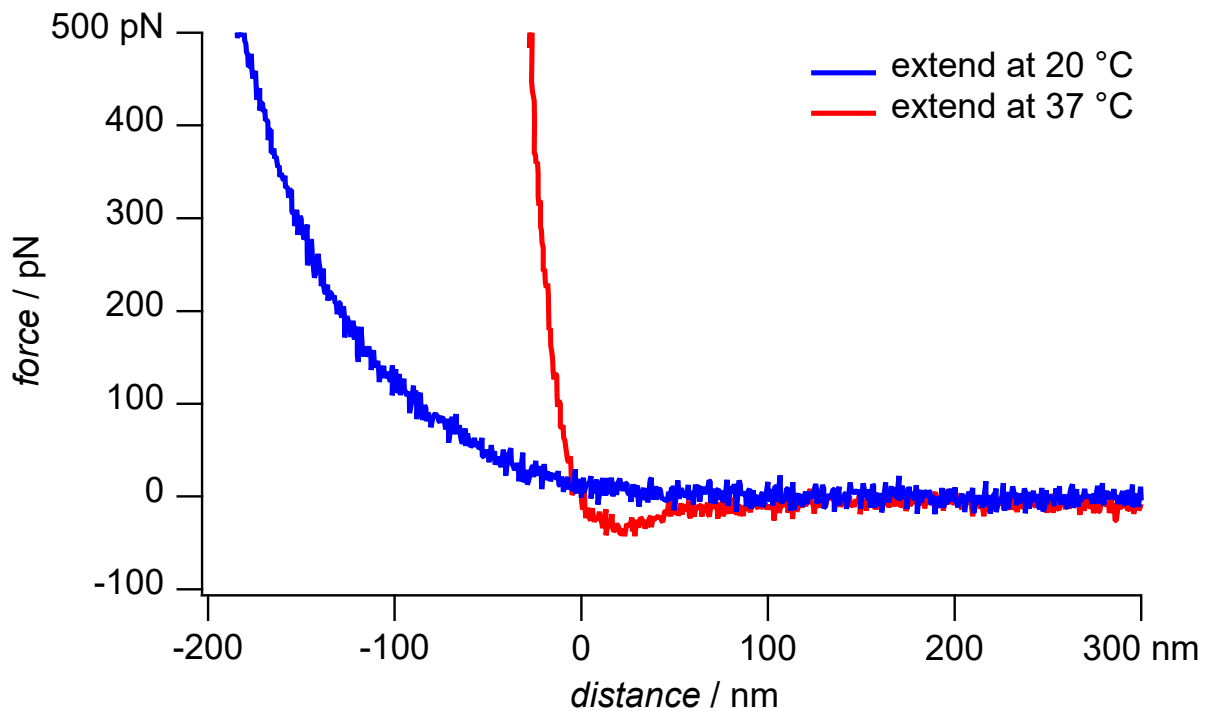


Figure S2: Exemplary force indentation curves from a single cell force spectroscopy experiment. A single *E. coli* bacterium is fixed to a cantilever and approached towards a pNIPAM_{BIS}-Man monolayer on solid substrate.

In a previous work single cell force spectroscopy experiments were performed¹¹⁸, where a single *E. coli* bacterium is fixed to a cantilever and pressed against a carbohydrate loaded microgel monolayer immobilized on hard substrate. The experiment is performed in PBS buffer at temperatures below and above the VPTT to quantify adhesion energies of bacteria to swollen and collapsed microgels. The force curves in Figure S2 are examples of an *E. coli* bacteria approached towards a layer of pNIPAM_{BIS}-Man microgels. At 37 °C a jump-to-contact is noteworthy, which does not occur at room temperature. This is partly attributed to the collapse of the particles hairy outer layer consisting of loose polymer chains and the high mannose density above VPTT on the particle surface. At room temperature this layer is preventing a fast contact between FimH and the sugar moieties.

3. AFM Images of dried particles used for volume calculation

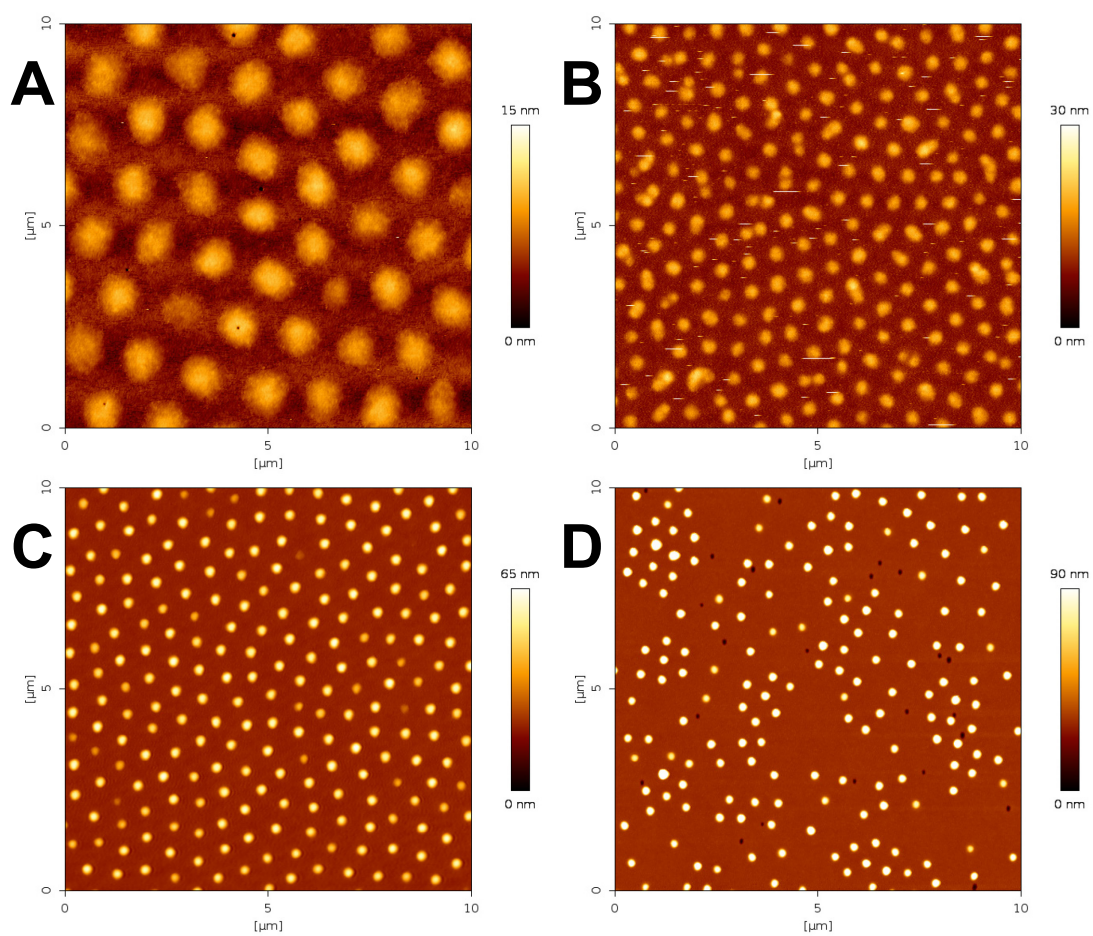


Figure S3: AFM height traces of dried microgels on glass slides: A) PNIPAM_{SCL}-Man B) PNIPAM_{BIS}-Man C) p(OEGMA_{475-co}-MEO₂MA)_{SCL}-Man D) p(OEGMA_{475-co}-MEO₂MA)_{EGDMA}-Man.

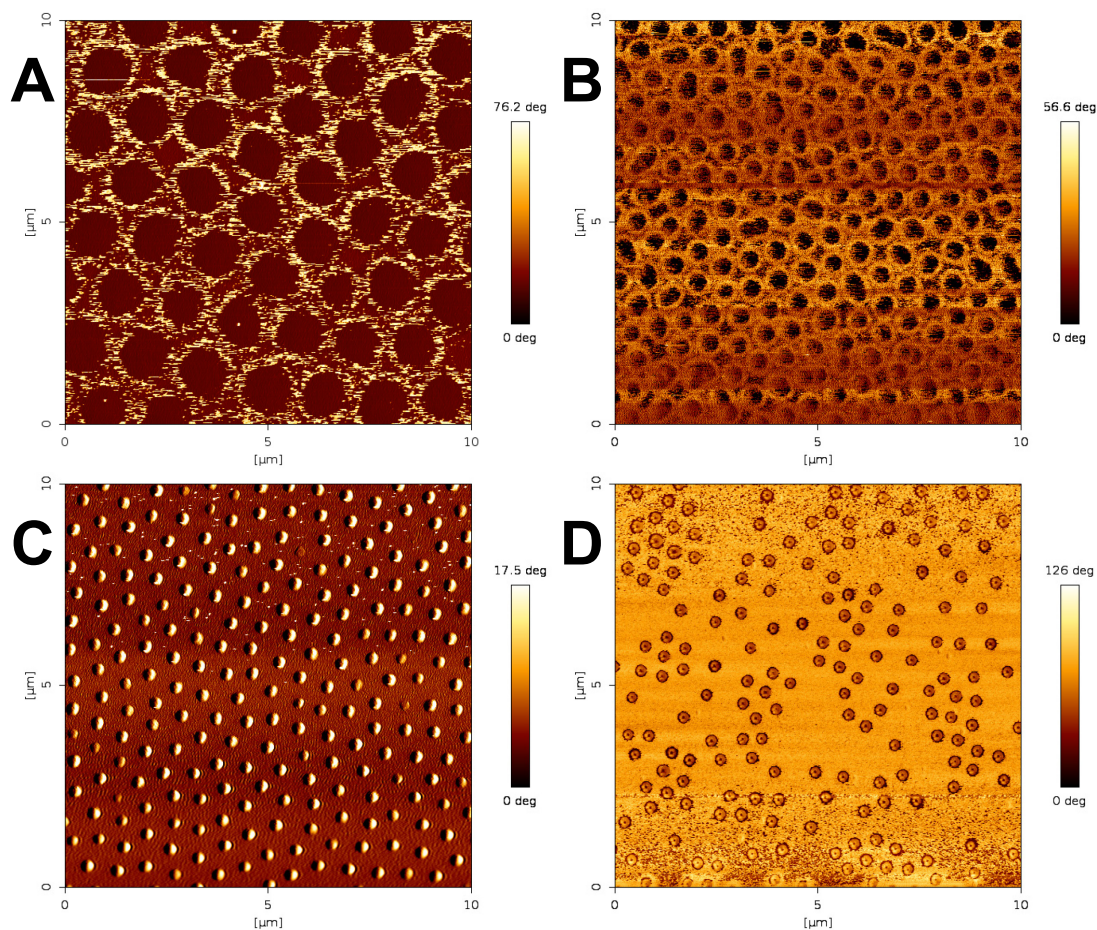


Figure S4: AFM height traces of dried microgels on glass slides: A) PNIPAM_{SCL}-Man B) PNIPAM_{BIS}-Man C) p(OEGMA₄₇₅-co-MEO₂MA)_{SCL}-Man D) p(OEGMA₄₇₅-co-MEO₂MA)_{EGDMA}-Man.

4. Determination of mannose density

To determine the mannose density per particle the dry volume was determined by AFM. The microgels were deposited on a hard glass surface by spin coating. For volume calculation the open source software Gwyddion was used.

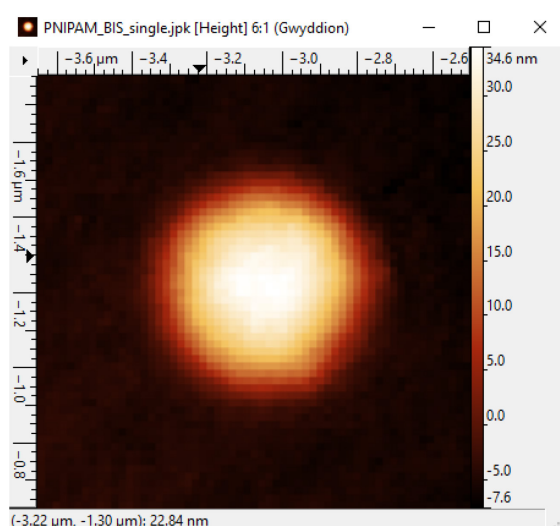


Figure S4: Exemplary AFM image of a dried microgel particle on a glass surface. Polynomial surface correction is already applied.

To calculate the volume of the adsorbed particles first the area has to be defined. This is done by setting a threshold (Figure S5) by adjusting the height until no “false pixels” on the substrate appear.

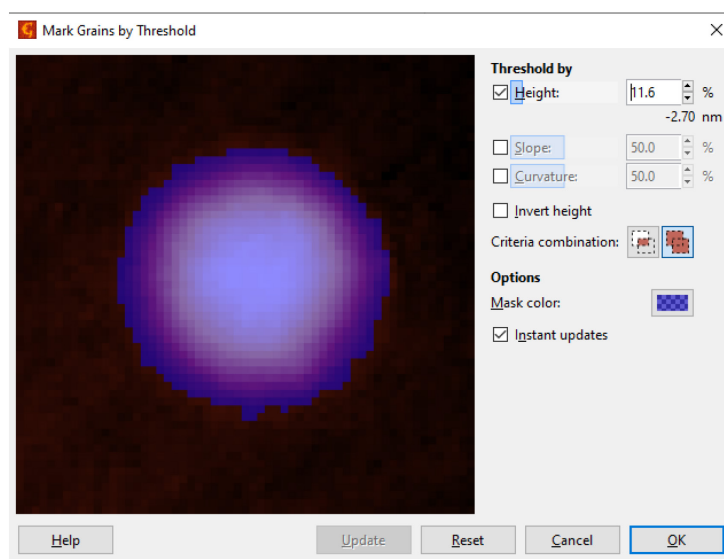


Figure S5: Example of setting up the threshold for particle volume calculation. Areas colored blue are within the threshold.

The properties of selected area *e.g.* the volume are calculated, displayed (Table S1) and used without further processing.

Table S1: Volumes of microgel particles in the swollen state V_{swollen} , calculated from DLS data and in the dry state V_{dry} , calculated from AFM images of dried particles. The absolute swelling degree q is calculated as the ratio of $V_{\text{swollen}}/V_{\text{dry}}$.

	$V_{\text{swollen}} / \mu\text{m}^3$	$V_{\text{dry}} / \mu\text{m}^3$	q
pNIPAM _{BIS} -Man	0.195	0.005	39.1
pNIPAM _{SCL} -Man	0.289	$7.35 \cdot 10^{-5}$	3928
p(OEGMA _{475-co} -MEO ₂ MA) _{EGDMA} -Man	0.007	$5.55 \cdot 10^{-4}$	13.1
p(OEGMA _{475-co} -MEO ₂ MA) _{SCL} -Man	0.034	0.001	25

Volume of dried particles, calculated from AFM images of dried particles and mannose content per gram of sample, determined by phenol-sulfuric-acid method is used to calculate the mannose density per μm^3 of each sample in the swollen and collapsed state (Table S2).

Table S2: Mannose density per μm^3 as calculated from dry particle mass.

mannose content [$\mu\text{mol} \cdot \text{g}^{-1}$]	mass per particle [g]	mannose per particle [μmol]	mannose units per particle	Mannose density (swollen) [μm^{-3}]	Mannose density (collapsed) [μm^{-3}]
32.0	$5.50 \cdot 10^{-15}$	$1.76 \cdot 10^{-13}$	106000 ± 32000	540000	2400000
60.0	$8.09 \cdot 10^{-17}$	$4.85 \cdot 10^{-15}$	3000 ± 1050	10000	520000
40.0	$6.11 \cdot 10^{-16}$	$2.44 \cdot 10^{-14}$	15000 ± 4400	2000000	8300000
60.0	$1.10 \cdot 10^{-15}$	$6.60 \cdot 10^{-14}$	40000 ± 13000	1200000	14400000

5. Stochastic Optical Reconstruction Microscopy (dSTORM)

To determine the carbohydrate distribution in the microgel particles dSTORM was implemented. Specific labeling of the mannose was done by first letting it react with NaIO_4 to generate aldehydes. Afterwards Alexa Fluor 647 hydrazide was used for coupling.

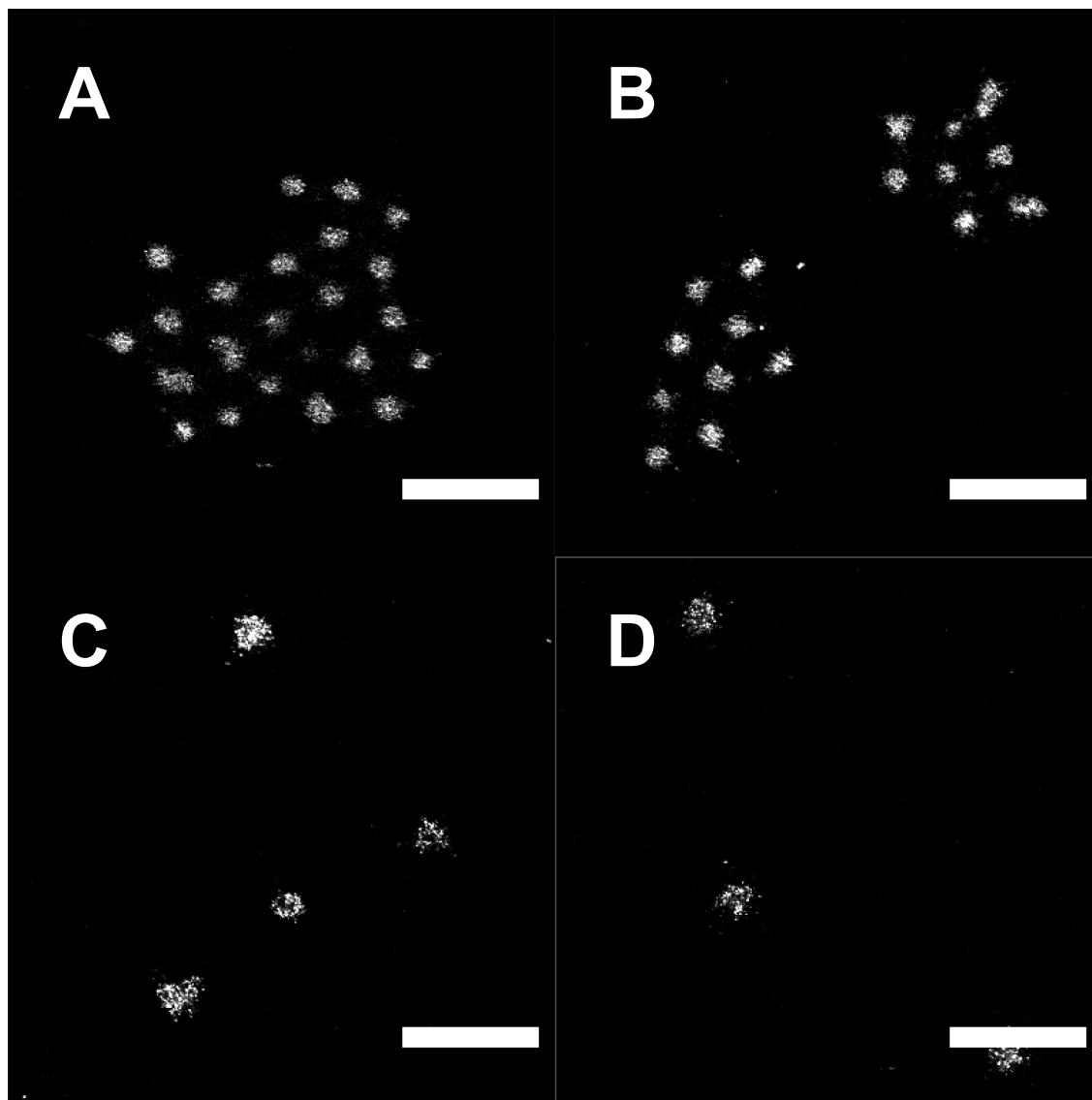


Figure S6: 2D dSTORM images of A)-B) pNIPAM_{BIS}-Man and C)-D) p(OEGMA₄₇₅-CO-MEO₂MA)_{EGDMA}-Man microgels in commercial blinking buffer at room temperature. The images show a homogeneous carbohydrate distribution.

6. *E. coli*-microgel precipitation cycle

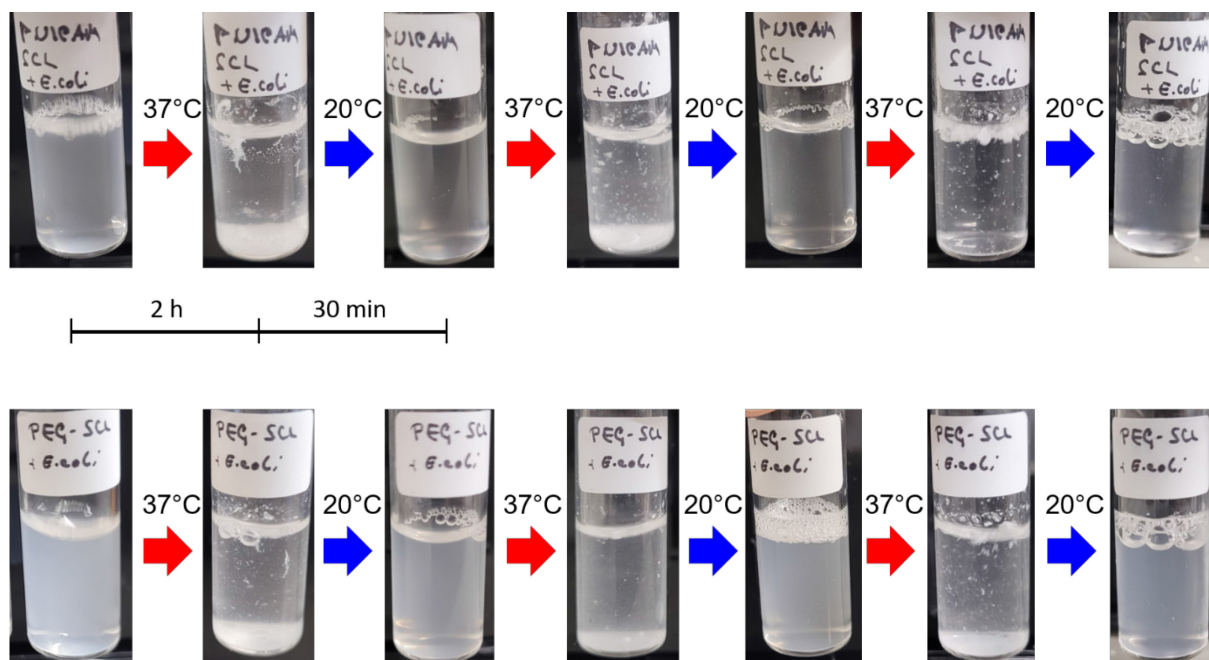


Figure S7: Aggregation studies of pNIPAM_{SCL}-Man and p(OEGMA-co-MEO₂MA)_{SCL}-Man microgels together with *E. coli* bacteria. Microgel samples with a final concentration of 0.5 mg·mL⁻¹ are mixed with bacterial suspension with a final concentration of 1 mg·mL⁻¹ and incubated at 37 °C for several hours until aggregation occurs. After cooling the sample is vortexed until aggregates are re-solubilized. This process is repeated and the binding properties of the microgels are present after several cycles are performed.

6. Citations

1. Duguid, J. P.; Smith, I. W.; Dempster, G.; Edmunds, P., Non-Flagellar Filamentous Appendages ("Fimbriae") and Haemagglutinating Activity in *Bacterium coli*. *Journal of Pathology and Bacteriology* **1955**, *70* (2), 335-48.
2. Rivier, D.; Darekar, M., Inhibitors of the adhesiveness of enteropathogenic *E. coli*. *Experientia* **1975**, *31* (6), 662-664.
3. Pearce, W. A.; Buchanan, T. M., Structure and cell membrane-binding properties of bacterial fimbriae. In *Bacterial adherence*, Springer: 1980; pp 289-344.
4. MÜLLER, W. E.; CONRAD, J.; SCHRÖDER, C.; ZAHN, R. K.; KURELEC, B.; DREESBACH, K.; UHLENBRUCK, G., Characterization of the Trimeric, Self-Recognizing Geodia cydonium Lectin I. *Eur. J. Biochem.* **1983**, *133* (2), 263-267.
5. Sharon, N.; Lis, H., Lectins: Cell-Agglutinating and Sugar-Specific Proteins: Lectins provide new tools for studying polysaccharides, glycoproteins, and cell surfaces, and for cancer research. *Science* **1972**, *177* (4053), 949-959.
6. Goldstein, I., Isolation, physicochemical characterization, and carbohydrate-binding specificity of lectins. *The lectins* **1986**.
7. Poretz, R.; Riss, H.; Timberlake, J. W.; Chien, S.-m., Purification and properties of the hemagglutinin from *Sophora japonica* seeds. *Biochemistry* **1974**, *13* (2), 250-256.
8. Ziska, P.; Kindt, A.; Franz, H., Isolation and characterization of a lectin from garden cress (*Lepidium sativum*). *Acta Histochemica* **1982**, *71* (1), 29-33.
9. Kocourek, J.; Hořejší, V., Defining a lectin. *Nature* **1981**, *290* (5803), 188-188.
10. Barondes, S. H., Bifunctional properties of lectins: lectins redefined. *Trends in biochemical sciences* **1988**, *13* (12), 480-482.
11. Naismith, J. H.; Emmerich, C.; Habash, J.; Harrop, S.; Helliwell, J.; Hunter, W.; Raftery, J.; Yariv, J., Refined structure of concanavalin A complexed with methyl α -D-mannopyranoside at 2.0 Å resolution and comparison with the saccharide-free structure. *Acta Crystallogr. Sect. D. Biol. Crystallogr.* **1994**, *50* (6), 847-858.
12. Rini, J. M.; Stanfield, R. L.; Stura, E. A.; Salinas, P. A.; Profy, A. T.; Wilson, I. A., Crystal structure of a human immunodeficiency virus type 1 neutralizing antibody, 50.1, in complex with its V3 loop peptide antigen. *Proceedings of the National Academy of Sciences* **1993**, *90* (13), 6325-6329.
13. Bourne, Y.; Rougé, P.; Cambillau, C., X-ray structure of a (α -Man (1-3) β -Man (1-4) GlcNAc)-lectin complex at 2.1-Å resolution. The role of water in sugar-lectin interaction. *J. Biol. Chem.* **1990**, *265* (30), 18161-18165.

14. Hester, G.; Kaku, H.; Goldstein, I. J.; Wright, C. S., Structure of mannose-specific snowdrop (*Galanthus nivalis*) lectin is representative of a new plant lectin family. *Nat. Struct. Biol.* **1995**, *2* (6), 472-479.
15. Sixma, T. K.; Pronk, S. E.; Kalk, K. H.; van Zanten, B. A.; Berghuis, A. M.; Hol, W. G., Lactose binding to heat-labile enterotoxin revealed by X-ray crystallography. *Nature* **1992**, *355* (6360), 561-564.
16. Holmgren, J., Actions of cholera toxin and the prevention and treatment of cholera. *Nature* **1981**, *292* (5822), 413-417.
17. Weis, W. I.; Drickamer, K.; Hendrickson, W. A., Structure of a C-type mannose-binding protein complexed with an oligosaccharide. *Nature* **1992**, *360* (6400), 127-134.
18. Kolatkar, A. R.; Weis, W. I., Structural Basis of Galactose Recognition by C-type Animal Lectins (*). *J. Biol. Chem.* **1996**, *271* (12), 6679-6685.
19. Ng, K. K.-S.; Drickamer, K.; Weis, W. I., Structural Analysis of Monosaccharide Recognition by Rat Liver Mannose-binding Protein (*). *J. Biol. Chem.* **1996**, *271* (2), 663-674.
20. Weis, W. I.; Drickamer, K., Structural basis of lectin-carbohydrate recognition. *Annual review of biochemistry* **1996**, *65* (1), 441-473.
21. Loris, R., Principles of structures of animal and plant lectins. *Biochimica et Biophysica Acta (BBA)-General Subjects* **2002**, *1572* (2-3), 198-208.
22. Lahm, H.; André, S.; Hoeflich, A.; Kaltner, H.; Siebert, H.-C.; Sordat, B.; von der Lieth, C.-W.; Wolf, E.; Gabius, H.-J., Tumor galectinology: insights into the complex network of a family of endogenous lectins. *Glycoconjugate J.* **2003**, *20* (4), 227-238.
23. Lundquist, J. J.; Toone, E. J., The cluster glycoside effect. *Chem. Rev.* **2002**, *102* (2), 555-578.
24. Rini, J. M., Lectin structure. *Annu. Rev. Biophys. Biomol. Struct.* **1995**, *24* (1), 551-577.
25. Etzler, M. E., Distribution and function of plant lectins. *The lectins: Properties, Functions, and applications in Biology and Medicine* **1986**, 371-435.
26. Rüdiger, H.; Gabius, H.-J., Plant lectins: occurrence, biochemistry, functions and applications. *Glycoconjugate J.* **2001**, *18* (8), 589-613.
27. Hirsch, A. M., Role of lectins (and rhizobial exopolysaccharides) in legume nodulation. *Curr. Opin. Plant Biol.* **1999**, *2* (4), 320-326.
28. Díaz, C. L.; Melchers, L. S.; Hooykaas, P. J.; Lugtenberg, B. J.; Kijne, J. W., Root lectin as a determinant of host-plant specificity in the *Rhizobium*-legume symbiosis. *Nature* **1989**, *338* (6216), 579-581.

29. Chrispeels, M. J.; Raikhel, N. V., Lectins, lectin genes, and their role in plant defense. *The plant cell* **1991**, *3* (1), 1.
30. Pusztai, A.; Clarke, E. M.; King, T., The nutritional toxicity of phaseolus vulgaris lectins. *Proceedings of the nutrition Society* **1979**, *38* (1), 115-121.
31. Jayne-Williams, D.; Burgess, C., Further observations on the toxicity of navy beans (*Phaseolus vulgaris*) for Japanese quail (*Coturnix coturnix japonica*). *J. Appl. Bacteriol.* **1974**, *37* (1), 149-169.
32. Liener, I. E.; Hasdai, A., The effect of the long-term feeding of raw soyflour on the pancreas of the mouse and hamster. In *Nutritional and Toxicological Significance of Enzyme Inhibitors in Foods*, Springer: 1986; pp 189-197.
33. Goldstein, I. J.; Hayes, C. E., The lectins: carbohydrate-binding proteins of plants and animals. *Adv. Carbohydr. Chem. Biochem.* **1978**, *35*, 127-340.
34. Murdock, L. L.; Huesing, J. E.; Nielsen, S. S.; Pratt, R. C.; Shade, R. E., Biological effects of plant lectins on the cowpea weevil. *Phytochemistry* **1990**, *29* (1), 85-89.
35. Beuth, J.; Ko, H.; Pulverer, G.; Uhlenbruck, G.; Pichlmaier, H., Importance of lectins for the prevention of bacterial infections and cancer metastases. *Glycoconjugate J.* **1995**, *12* (1), 1-6.
36. Edelman, G. M.; Cunningham, B. A.; Reeke, G. N.; Becker, J. W.; Waxdal, M. J.; Wang, J. L., The Covalent and Three-Dimensional Structure of Concanavalin A. *Proceedings of the National Academy of Sciences* **1972**, *69* (9), 2580-2584.
37. Shoham, M.; Kalb, A. J.; Pecht, I., Specificity of metal ion interaction with concanavalin A. *Biochemistry* **1973**, *12* (10), 1914-1917.
38. Gyles, C. L., Escherichia coli cytotoxins and enterotoxins. *Can. J. Microbiol.* **1992**, *38* (7), 734-746.
39. Haan, L. d.; Hirst, T. R., Cholera toxin: a paradigm for multi-functional engagement of cellular mechanisms. *Mol. Membr. Biol.* **2004**, *21* (2), 77-92.
40. Collier, R. J., Understanding the mode of action of diphtheria toxin: a perspective on progress during the 20th century. *Toxicon* **2001**, *39* (11), 1793-1803.
41. Tavallaie, M.; Chenal, A.; Gillet, D.; Pereira, Y.; Manich, M.; Gibert, M.; Raffestin, S.; Popoff, M. R.; Marvaud, J. C., Interaction between the two subdomains of the C-terminal part of the botulinum neurotoxin A is essential for the generation of protective antibodies. *FEBS Lett.* **2004**, *572* (1-3), 299-306.

42. Menozzi, F. D.; Mutombo, R.; Renauld, G.; Gantiez, C.; Hannah, J. H.; Leininger, E.; Brennan, M. J.; Loch, C., Heparin-inhibitable lectin activity of the filamentous hemagglutinin adhesin of *Bordetella pertussis*. *Infect. Immun.* **1994**, *62* (3), 769-778.
43. Fan, E.; Merritt, E. A.; Verlinde, C. L. M. J.; Hol, W. G. J., AB5 toxins: structures and inhibitor design. *Curr. Opin. Struct. Biol.* **2000**, *10* (6), 680-686.
44. Vierbuchen, M., Lectin Receptors. In *Cell Receptors: Morphological Characterization and Pathological Aspects*, Seifert, G., Ed. Springer Berlin Heidelberg: Berlin, Heidelberg, 1991; pp 271-361.
45. Sharon, N.; Ofek, I., Fighting Infectious Diseases with Inhibitors of Microbial Adhesion to Host Tissues. *Crit. Rev. Food Sci. Nutr.* **2002**, *42* (sup3), 267-272.
46. Ofek, I.; Mirelman, D.; Sharon, N., Adherence of *Escherichia coli* to human mucosal cells mediated by mannose receptors. *Nature* **1977**, *265* (5595), 623-625.
47. Edelman, J.; Dimilla, P.; Abbelda, S.; Richardson, P.; Steiner, M., Principles of cell adhesion. *The Integrin Cell Adhesion Molecules*, CRC Press, New York **1995**, 163.
48. Hung, C. S.; Bouckaert, J.; Hung, D.; Pinkner, J.; Widberg, C.; DeFusco, A.; Auguste, C. G.; Strouse, R.; Langermann, S.; Waksman, G., Structural basis of tropism of *Escherichia coli* to the bladder during urinary tract infection. *Mol. Microbiol.* **2002**, *44* (4), 903-915.
49. Hynes, S. O.; Teneberg, S.; Roche, N.; Wadström, T., Glycoconjugate binding of gastric and enterohepatic *Helicobacter* spp. *Infect. Immun.* **2003**, *71* (5), 2976-2980.
50. Sai Sudha, P.; Devaraj, H.; Devaraj, N., Adherence of *Shigella dysenteriae* 1 to human colonic mucin. *Curr. Microbiol.* **2001**, *42* (6), 381-387.
51. Cywes, C.; Wessels, M. R., Group A *Streptococcus* tissue invasion by CD44-mediated cell signalling. *Nature* **2001**, *414* (6864), 648-652.
52. Vierbuchen, M.; Schröder, S.; Uhlenbruck, G.; Lavina, A.; Fischer, R., Native and sialic acid masked Lewis antigen reactivity in medullary thyroid carcinoma. *Virchows Archiv* **1994**, *424* (2), 205-211.
53. Ofek, I.; Beachey, E. H., General concepts and principles of bacterial adherence in animals and man. In *Bacterial adherence*, Springer: 1980; pp 1-29.
54. Liener, I., *The lectins: properties, functions, and applications in biology and medicine*. Elsevier: 2012.
55. Zafriri, D.; Ofek, I.; Adar, R.; Pocino, M.; Sharon, N., Inhibitory activity of cranberry juice on adherence of type 1 and type P fimbriated *Escherichia coli* to eucaryotic cells. *Antimicrob. Agents Chemother.* **1989**, *33* (1), 92-98.

56. Beuth, J.; Ko, H.; Oette, K.; Pulverer, G.; Roszkowski, K.; Uhlenbruck, G., Inhibition of liver metastasis in mice by blocking hepatocyte lectins with arabinogalactan infusions and D-galactose. *J. Cancer Res. Clin. Oncol.* **1987**, *113* (1), 51-55.
57. Markwell, M. k.; Portner, A.; Schwartz, A. L., An alternative route of infection for viruses: entry by means of the asialoglycoprotein receptor of a Sendai virus mutant lacking its attachment protein. *Proceedings of the National Academy of Sciences* **1985**, *82* (4), 978-982.
58. Zell, R.; Scholtissek, C.; Ludwig, S., Genetics, Evolution, and the Zoonotic Capacity of European Swine Influenza Viruses. In *Swine Influenza*, Richt, J. A.; Webby, R. J., Eds. Springer Berlin Heidelberg: Berlin, Heidelberg, 2013; pp 29-55.
59. Beuth, J.; Stoffel, B.; Pulverer, G., Inhibition of bacterial adhesion and infections by lectin blocking. *Toward Anti-Adhesion Therapy for Microbial Diseases* **1996**, 51-56.
60. Thomas, R.; Brooks, T., Common oligosaccharide moieties inhibit the adherence of typical and atypical respiratory pathogens. *J. Med. Microbiol.* **2004**, *53* (9), 833-840.
61. Chapleur, Y., *Carbohydrate mimics*. Wiley-VCH: 1998.
62. Irvin, R. T.; Bautista, D. L., Hope for the post-antibiotic era? *Nat. Biotechnol.* **1999**, *17* (1), 20-20.
63. Mulvey, M. A.; Schilling, J. D.; Hultgren, S. J., Establishment of a persistent *Escherichia coli* reservoir during the acute phase of a bladder infection. *Infect. Immun.* **2001**, *69* (7), 4572-4579.
64. Ofek, I.; Hasty, D. L.; Sharon, N., Anti-adhesion therapy of bacterial diseases: prospects and problems. *FEMS Immunology & Medical Microbiology* **2003**, *38* (3), 181-191.
65. Aronson, M.; Medalia, O.; Schori, L.; Mirelman, D.; Sharon, N.; Ofek, I., Prevention of colonization of the urinary tract of mice with *Escherichia coli* by blocking of bacterial adherence with methyl α -D-mannopyranoside. *J. Infect. Dis.* **1979**, *139* (3), 329-332.
66. Mysore, J. V.; Wigginton, T.; Simon, P. M.; Zopf, D.; Heman-Ackah, L. M.; Dubois, A., Treatment of *Helicobacter pylori* infection in rhesus monkeys using a novel antiadhesion compound. *Gastroenterology* **1999**, *117* (6), 1316-1325.
67. Autar, R.; Khan, A. S.; Schad, M.; Hacker, J.; Liskamp, R. M.; Pieters, R. J., Adhesion inhibition of F1C-fimbriated *Escherichia coli* and *Pseudomonas aeruginosa* PAK and PAO by multivalent carbohydrate ligands. *ChemBioChem* **2003**, *4* (12), 1317-1325.
68. Sharon, N.; Ofek, I., Safe as mother's milk: carbohydrates as future anti-adhesion drugs for bacterial diseases. *Glycoconjugate J.* **2000**, *17* (7), 659-664.

69. Kelly, C. G.; Younson, J. S.; Hikmat, B. Y.; Todryk, S. M.; Czisch, M.; Haris, P. I.; Flindall, I. R.; Newby, C.; Mallet, A. I.; Ma, J. K., A synthetic peptide adhesion epitope as a novel antimicrobial agent. *Nat. Biotechnol.* **1999**, *17* (1), 42-47.
70. Lee, K. K.; Yu, L.; Macdonald, D. L.; Paranchych, W.; Hodges, R. S.; Irvin, R. T., Anti-adhesin antibodies that recognize a receptor-binding motif (adhesintope) inhibit pilus/fimbrial-mediated adherence of *Pseudomonas aeruginosa* and *Candida albicans* to asialo-GM1 receptors and human buccal epithelial cell surface receptors. *Can. J. Microbiol.* **1996**, *42* (5), 479-486.
71. Omi, H.; Okayama, N.; Shimizu, M.; Fukutomi, T.; Nakamura, A.; Imaeda, K.; Okouchi, M.; Itoh, M., Cilostazol inhibits high glucose-mediated endothelial-neutrophil adhesion by decreasing adhesion molecule expression via NO production. *Microvascular research* **2004**, *68* (2), 119-125.
72. Weinbaum, S.; Tarbell, J. M.; Damiano, E. R., The structure and function of the endothelial glycocalyx layer. *Annu. Rev. Biomed. Eng.* **2007**, *9*, 121-167.
73. Brandley, B. K.; Schnaar, R. L., Cell-surface carbohydrates in cell recognition and response. *J. Leukocyte Biol.* **1986**, *40* (1), 97-111.
74. Karlsson, K.; Angström, J.; Bergström, J.; Lanne, B., Microbial interaction with animal cell surface carbohydrates. *APMIS. Supplementum* **1992**, *27*, 71-83.
75. Töpfer-Petersen, E., Carbohydrate-based interactions on the route of a spermatozoon to fertilization. *Hum. Reprod. Update* **1999**, *5* (4), 314-329.
76. Crocker, P. R.; Feizi, T., Carbohydrate recognition systems: functional triads in cell—cell interactions. *Curr. Opin. Struct. Biol.* **1996**, *6* (5), 679-691.
77. Zan, G.; Wu, Q., Biomimetic and bioinspired synthesis of nanomaterials/nanostructures. *Adv. Mater.* **2016**, *28* (11), 2099-2147.
78. Zhao, J.; Zhao, X.; Jiang, Z.; Li, Z.; Fan, X.; Zhu, J.; Wu, H.; Su, Y.; Yang, D.; Pan, F., Biomimetic and bioinspired membranes: Preparation and application. *Prog. Polym. Sci.* **2014**, *39* (9), 1668-1720.
79. Hill, S. A.; Gerke, C.; Hartmann, L., Recent Developments in Solid-Phase Strategies towards Synthetic, Sequence-Defined Macromolecules. *Chemistry—An Asian Journal* **2018**, *13* (23), 3611-3622.
80. Sacchettini, J. C.; Baum, L. G.; Brewer, C. F., Multivalent protein— carbohydrate interactions. a new paradigm for supermolecular assembly and signal transduction. *Biochemistry* **2001**, *40* (10), 3009-3015.

81. Lee, Y. C.; Lee, R. T., Carbohydrate-Protein Interactions: Basis of Glycobiology. *Acc. Chem. Res.* **1995**, *28* (8), 321-327.
82. Breslow, R.; Belvedere, S.; Gershell, L.; Leung, D., The chelate effect in binding, catalysis, and chemotherapy. *Pure Appl. Chem.* **2000**, *72* (3), 333-342.
83. Melkko, S.; Dumelin, C. E.; Scheuermann, J.; Neri, D., On the magnitude of the chelate effect for the recognition of proteins by pharmacophores scaffolded by self-assembling oligonucleotides. *Chem. Biol.* **2006**, *13* (2), 225-231.
84. Page, M. I.; Jencks, W. P., Entropic contributions to rate accelerations in enzymic and intramolecular reactions and the chelate effect. *Proceedings of the National Academy of Sciences* **1971**, *68* (8), 1678-1683.
85. Shamout, F.; Monaco, A.; Yilmaz, G.; Becer, C. R.; Hartmann, L., Synthesis of Brush-Like Glycopolymers with Monodisperse, Sequence-Defined Side Chains and Their Interactions with Plant and Animal Lectins. *Macromol. Rapid Commun.* **2020**, *41* (1), 1900459.
86. Kiessling, L. L.; Gestwicki, J. E.; Strong, L. E., Synthetic Multivalent Ligands as Probes of Signal Transduction. *Angew. Chem. Int. Ed.* **2006**, *45* (15), 2348-2368.
87. Levine, P. M.; Carberry, T. P.; Holub, J. M.; Kirshenbaum, K., Crafting precise multivalent architectures. *MedChemComm* **2013**, *4* (3), 493-509.
88. van Heteren, J.; Pieters, R. J., Carbohydrate-protein interactions: Enhancing multivalency effects through statistical rebinding. In *Carbohydrates in Drug Discovery and Development*, Elsevier: 2020; pp 383-402.
89. Jacobi, F.; Wilms, D.; Seiler, T.; Queckbörner, T.; Tabatabai, M.; Hartmann, L.; Schmidt, S., Effect of PEGylation on Receptor Anchoring and Steric Shielding at Interfaces: An Adhesion and Surface Plasmon Resonance Study with Precision Polymers. *Biomacromolecules* **2020**, *21* (12), 4850-4856.
90. Carvalho, B. G.; Vit, F. F.; Carvalho, H. F.; Han, S. W.; de la Torre, L. G., Layer-by-Layer Biomimetic Microgels for 3D Cell Culture and Nonviral Gene Delivery. *Biomacromolecules* **2021**.
91. Liu, G.; Liu, Z.; Li, N.; Wang, X.; Zhou, F.; Liu, W., Hairy polyelectrolyte brushes-grafted thermosensitive microgels as artificial synovial fluid for simultaneous biomimetic lubrication and arthritis treatment. *ACS applied materials & interfaces* **2014**, *6* (22), 20452-20463.
92. Jiang, Y.; Chen, J.; Deng, C.; Suuronen, E. J.; Zhong, Z., Click hydrogels, microgels and nanogels: Emerging platforms for drug delivery and tissue engineering. *Biomaterials* **2014**, *35* (18), 4969-4985.

93. Yoshida, R.; Omata, K.; Yamaura, K.; Sakai, T.; Hara, Y.; Maeda, S.; Hashimoto, S., Microfabrication of Functional Polymer Gels and Their Application to Novel Biomimetic Materials. *J. Photopolym. Sci. Technol.* **2006**, *19* (4), 441-444.
94. Ebhodaghe, S. O., A scoping review on the biomedical applications of polymeric particles. *International Journal of Polymeric Materials and Polymeric Biomaterials* **2022**, 1-23.
95. Rozhkova, Y. A.; Burin, D. A.; Galkin, S. V.; Yang, H., Review of Microgels for Enhanced Oil Recovery: Properties and Cases of Application. *Gels* **2022**, *8* (2).
96. Shu, T.; Hu, L.; Hunter, H.; Balasuriya, N.; Fang, C.; Zhang, Q.; Serpe, M. J., Multi-responsive micro/nanogels for optical sensing. *Advances in Physics: X* **2022**, *7* (1), 2043185.
97. Fernandez-Nieves, A.; Wyss, H.; Mattsson, J.; Weitz, D. A., *Microgel suspensions: fundamentals and applications*. John Wiley & Sons: 2011.
98. Chu, L. Y.; Kim, J. W.; Shah, R. K.; Weitz, D. A., Monodisperse thermoresponsive microgels with tunable volume-phase transition kinetics. *Adv. Funct. Mater.* **2007**, *17* (17), 3499-3504.
99. Heskins, M.; Guillet, J. E., Solution Properties of Poly(N-isopropylacrylamide). *Journal of Macromolecular Science: Part A - Chemistry* **1968**, *2* (8), 1441-1455.
100. Lutz, J.-F.; Akdemir, Ö.; Hoth, A., Point by Point Comparison of Two Thermosensitive Polymers Exhibiting a Similar LCST: Is the Age of Poly(NIPAM) Over? *Journal of the American Chemical Society* **2006**, *128* (40), 13046-13047.
101. Schmidt, M.; Franken, A.; Wilms, D.; Fehm, T.; Neubauer, H. J.; Schmidt, S., Selective Adhesion and Switchable Release of Breast Cancer Cells via Hyaluronic Acid Functionalized Dual Stimuli-Responsive Microgel Films. *ACS Applied Bio Materials* **2021**, *4* (8), 6371-6380.
102. Rubio-Retama, J.; Zafeiropoulos, N. E.; Serafinelli, C.; Rojas-Reyna, R.; Voit, B.; Lopez Cabarcos, E.; Stamm, M., Synthesis and characterization of thermosensitive PNIPAM microgels covered with superparamagnetic γ -Fe₂O₃ nanoparticles. *Langmuir* **2007**, *23* (20), 10280-10285.
103. Hu, X.; Tong, Z.; Lyon, L. A., Control of poly (N-isopropylacrylamide) microgel network structure by precipitation polymerization near the lower critical solution temperature. *Langmuir* **2011**, *27* (7), 4142-4148.
104. Sanson, N.; Rieger, J., Synthesis of nanogels/microgels by conventional and controlled radical crosslinking copolymerization. *Polymer Chemistry* **2010**, *1* (7), 965-977.

105. Still, T.; Chen, K.; Alsayed, A. M.; Aptowicz, K. B.; Yodh, A., Synthesis of micrometer-size poly (N-isopropylacrylamide) microgel particles with homogeneous crosslinker density and diameter control. *J. Colloid Interface Sci.* **2013**, *405*, 96-102.
106. von Nessen, K.; Karg, M.; Hellweg, T., Thermoresponsive poly-(N-isopropylmethacrylamide) microgels: Tailoring particle size by interfacial tension control. *Polymer* **2013**, *54* (21), 5499-5510.
107. Zhang, Q. M.; Xu, W.; Serpe, M. J., Optical devices constructed from multiresponsive microgels. *Angew. Chem.* **2014**, *126* (19), 4927-4931.
108. Kratz, K.; Lapp, A.; Eimer, W.; Hellweg, T., Volume transition and structure of triethyleneglycol dimethacrylate, ethylenglykol dimethacrylate, and N,N'-methylene bis-acrylamide cross-linked poly(N-isopropyl acrylamide) microgels: a small angle neutron and dynamic light scattering study. *Colloids Surf. Physicochem. Eng. Aspects* **2002**, *197* (1), 55-67.
109. Zhang, H., Controlled/"living" radical precipitation polymerization: a versatile polymerization technique for advanced functional polymers. *Eur. Polym. J.* **2013**, *49* (3), 579-600.
110. Saunders, B. R.; Vincent, B., Microgel particles as model colloids: theory, properties and applications. *Adv. Colloid Interface Sci.* **1999**, *80* (1), 1-25.
111. Shah, L. A.; Farooqi, Z. H.; Naeem, H.; Shah, S. M.; Siddiq, M., Synthesis and characterization of poly (N-isopropylacrylamide) hybrid microgels with different cross-linker contents. *J. Chem. Soc. Pak.* **2013**, *35*, 1522-1529.
112. Andersson, M.; Maunu, S. L., Structural studies of poly (N-isopropylacrylamide) microgels: Effect of SDS surfactant concentration in the microgel synthesis. *J. Polym. Sci., Part B: Polym. Phys.* **2006**, *44* (23), 3305-3314.
113. Radmacher, M., Measuring the elastic properties of biological samples with the AFM. *IEEE Engineering in Medicine and Biology Magazine* **1997**, *16* (2), 47-57.
114. Zou, S.; Schönherr, H.; Vancso, G. J., Stretching and rupturing individual supramolecular polymer chains by AFM. *Angew. Chem.* **2005**, *117* (6), 978-981.
115. Helenius, J.; Heisenberg, C.-P.; Gaub, H. E.; Muller, D. J., Single-cell force spectroscopy. *J. Cell Sci.* **2008**, *121* (11), 1785-1791.
116. Bardell, D., The invention of the microscope. *Bios* **2004**, *75* (2), 78-84.
117. Falke, S.; Betzel, C., Dynamic Light Scattering (DLS). In *Radiation in Bioanalysis*, Springer: 2019; pp 173-193.

118. Wilms, D.; Schröer, F.; Paul, T. J.; Schmidt, S., Switchable Adhesion of E. coli to Thermosensitive Carbohydrate-Presenting Microgel Layers: A Single-Cell Force Spectroscopy Study. *Langmuir* **2020**.

7. List of abbreviations

$\langle \Gamma \rangle$	decay rate
μm	micro meter
AFM	atomic force microscopy
APS	ammonium peroxodisulfate
ASN	asparagin
ASP	aspartic acid
BIS	<i>N,N'</i> -Methylenebisacrylamide
ConA	Concanavalin A
CT	cholera toxin
DLS	dynamic light scattering
<i>E. coli</i>	Escherichia coli
<i>e.g.</i>	example gratia (for example)
EGDMA	ethylene glycol dimethacrylate
GLN	glutamine
kB	Boltzmann constant
KPS	potassium peroxodisulfate
LBB	lectin binding buffer
LCST	lower critical solution temperature
LED	light-emitting diode
MEO2MA	di(ethylene glycol) methyl ether methacrylate
NIPAM	<i>N</i> -isopropylacrylamide
OEGMA	oligo(ethylene glycol methylacrylate)
PBS	phosphate buffered saline
pH	pondus hydrogenii (“potential of hydrogen”)
PHA	phytohemagglutinin
PHE	phenylalanine
R_h	hydrodynamic radius
SCFS	single cell force spectroscopy
SDS	sodium dodecyl sulfate
dSTORM	Stochastic Optical Reconstruction Microscopy

T	temperature
TEM	transmission electron microscopy
TREGDMA	triethylene glycol dimethacrylate
V-50	2,2'-azobis(2-methylpropionamidine)dihydrochloride
VPTT	volume phase transition temperatures
WGA	wheat germ agglutinin
η	viscosity

8. Acknowledgements

First of all, I would like to give my special thanks to Jun. Prof. Dr. Stephan Schmidt for the opportunity to carry out my doctoral thesis in his working group at the Heinrich Heine University Düsseldorf. I am sincerely grateful for the great support and many discussions where I could learn a lot on professional and personal level. I could always contact him for advice and inspiration, which made my time in the group most valuable.

Furthermore, I would like to thank Prof. Dr. Matthias Karg for agreeing to be the second supervisor of this thesis and supporting me and our working group throughout its course.

For all the fun times and productive discussions, I want to thank the people at the working group of Prof. Dr. Laura Hartmann. The coffee sessions and lunchtime was always something to look forward to.

I also thank the students I had the opportunity to supervise, Lennart Bunnemann, Yanik Adler, Anselm Urach, Rodrigo Sperzel and Felicitas Drees. You helped me grow and contributed significantly to this work.

I want to give my greatest thanks to the people who welcomed me warmly in the working group Alberto Camaleno, Tanja Paul, Alexander Strzelczyk and Fabian Schröer. You helped me during my masters and doctoral thesis with great professional knowledge and made the time a lot more fun. And also thanks to the colleagues who joined us Melanie Schmidt, Janita Müller and Felicitas Drees. You made it a special time in the office and on trips to conferences.

My sincere and personal thanks go to my family, my parents who made this possible in the first place, who went through much greater than myself. And my sister who is hopefully as proud of me as I am of her.

The final thanks go to Verena Prust who stepped into my life just as this thesis began. You supported me the most in these sometimes easy and sometimes hard times. I could always rely on you and trust your judgement and advice. The best part of all these days was and is to come home to you.